Old Dominion University Research Foundation

NOVEMBER 19, 2001

FINAL REPORT FOR:
NASA GRANT NO. NCC-1-389

FOR THE PERIOD OF
DECEMBER 15, 1999 TO SEPTEMBER 31, 2001

"A COMPARISON OF QUASI-STATIC INDENTATION AND DROP-WEIGHT IMPACT TESTING ON CARBON-EPOXY LAMINATES"

PRINCIPAL INVESTIGATOR:
DR. R. PRABHAKARAN

RESEARCH FOUNDATION PROJECT #101491

NOVEMBER 19, 2001

FINAL REPORT FOR:
NASA GRANT NO. NCC-1-389

FOR THE PERIOD OF
DECEMBER 15, 1999 TO SEPTEMBER 31, 2001

"A COMPARISON OF QUASI-STATIC INDENTATION AND DROP-WEIGHT IMPACT TESTING ON CARBON-EPOXY LAMINATES"

PRINCIPAL INVESTIGATOR:
DR. R. PRABHAKARAN

RESEARCH FOUNDATION PROJECT #101491

FINAL REPORT

A COMPARISON OF QUASI-STATIC INDENTATION AND DROP-WEIGHT IMPACT TESTING ON CARBON-EPOXY LAMINATES

Principal Investigator: Dr. R.Prabhakaran
Mechanical Engineering

ODURF Project No. 101491

12-15-99 to 9-30-01

A Comparison of Quasi-static Indentation and Drop-weight Impact Testing on Carbon-Epoxy Laminates

1. Introduction

The project had two objectives: 1) The primary objective was to characterize damage tolerance of composite materials. To accomplish this, polymer matrix composites were to be subjected to static indentation as well as low-velocity impacts and the results analyzed. 2) A second objective was to investigate the effects of laser shock peening on the damage tolerance of aerospace materials, such as aluminum alloys, in terms of crack nucleation and crack propagation.

The impact testing was proposed to be performed using a Dynatup drop tower. The specimens were to be placed over a square opening in a steel platen and impacted with a hemispherical tup. The damage was to be characterized in the laminate specimens. The damage tolerance of aerospace alloys was to be studied by conducting fatigue tests on aluminum alloy specimens with prior shock peening treatment. The crack length was to be monitored by a microscope and the crack propagation rate, da/dN, determined.

2. Damage Tolerance of Carbon-Epoxy Composite Laminates

This part of the work was performed by Mr. Michael J. Douglas who was a Graduate Research Assistant in the Department of Mechanical Engineering. The work was motivated by a desire to model low-velocity foreign object impact events by conducting a quasi-static indentation test. This modeling is very attractive since the static test is much easier to conduct and yields much more information. In order to examine the feasibility of this idea, a series of static indentation and low velocity impact tests were carried out and compared. Square specimens of many sizes and thicknesses were utilized to cover the array of types of low velocity impact events. Laminates with a $\pi/4$ stacking sequence were employed since this is by far the most common type of engineering laminate. Three distinct flexural rigidities under two different boundary conditions were tested in order to obtain damage ranging from that due to large deflection to contact stresses and levels in between in order to examine if the static indentation- impact comparisons are valid under the spectrum of damage modes that can be experienced. Comparisons between static indentation and low velocity impact tests were based on the maximum applied transverse load. The dependent parameters examined included dent depth, back surface crack length, delamination area and to a limited extent, load-deflection behavior. Results showed that no distinct differences could be seen between the static indentation tests and the low velocity impact tests, indicating that static indentation can be used to represent a low velocity impact event.

The details regarding the experimental procedures, results, analysis of results and conclusions are contained in the Master's thesis dissertation, " A Comparison of Quasi-Static Indentation Testing to Low Velocity Impact Testing", submitted by Mr. Douglas to the Department of Mechanical Engineering, Old Dominion University, in May, 2000. A condensed version appears in NASA/TP-2000-210481, " A Comparison of Quasi-Static

Indentation to Low Velocity Impact" by A.T. Nettles and M.J. Douglas; a copy of this report is attached.

3. Effect of Shot Peening on Crack Growth and Fatigue Life in 2024 Aluminum Alloy

This part of the work was performed by Dr. Prabhakaran. The initial objective of this part of the project was to test about half a dozen 2024 aluminum alloy specimens which had been laser peened and were available. Constant amplitude fatigue tests were conducted on all these specimens and the crack growth was monitored as a function of the number of cycles. All these specimens had a semi-circular edge notch and a corner crack before being laser peened. The laser peening induced residual compressive stresses across the entire width of the specimen and the objective of the investigation was to study the effect of the residual compressive stresses on the crack re-initiation and subsequent crack growth.

After conducting the tests and processing the results, an effort was initiated to compare this group of laser-peened specimens with another group of shot-peened specimens which had been tested earlier by Dr. W.T. Matthews and whose results had been available. Further, it was also felt that the results of the two groups of specimens could be compared, in addition to crack length vs. number of fatigue cycles, on the basis of crack growth rate vs. stress intensity factor range. A compilation of all these results, with the application of proper stress intensity factor expression by Dr. J.C Newman, resulted in a very interesting study. To these results, Dr. Richard Everett added his earlier work with 4340 steel specimens. The net result was a paper, "The effects of Shot and Laser Peening on Crack Growth and Fatigue Life in 2024 Aluminum Alloy and 4340 Steel", presented at the USAF Structural Integrity Program Conference (December 5-7, 2000) in San Antonio, Texas. A copy of this paper is attached.

4. Damage Resistance and Damage Tolerance of Pultruded Composites

Pultrusion is a process that offers the advantages of a continuous production, as well as the integration of fiber impregnation and composite curing and shaping in a single step. The process has been used to produce complicated shapes which have found many applications in structures. The process is very versatile and can handle thermosetting as well as thermoplastic resins. While glass fibers have been extensively used so far, the method permits the incorporation of other reinforcements, such as carbon and kevlar, if the higher cost can be justified. This flexibility is expected to increase the appeal of pultruded composites in areas such as aerospace, in addition to civil engineering infrastructure.

Another reason to study the application of quasi-static indentation to pultruded composites is to investigate the effect of the composite architecture on the damage development and progression. While aerospace composites consist of plies of different orientations consolidated together, pultruded composites (at least those of present construction) are quite different: they consist of layers of roving fibers sandwiched between continuous strand mats. The structure of pultruded composites of various thicknesses and their mechanical properties are given in the following pages.

The damage resistance of pultruded composites under quasi-static transverse indentation was characterized and the damage tolerance of transversely indented composites under subsequent compression loading was assessed. Two specimen thicknesses were investigated. In each case, four specimens were transversely indented to failure. Five load levels were selected and sets of five specimens were loaded up to each of these load levels and then unloaded. Extensive data were gathered: load-central displacement, back surface crack length, damage area obtained from x-radiography, optical photomicrographs obtained for specimens sectioned in different orientations, etc. This information was analyzed to develop the damage initiation and progression in pultruded composites. Open hole compression tests were performed on specimens of the two thicknesses, with seven hole sizes. The specimens damaged at five load levels, during transverse indentation, were tested in compression, simulating compression after impact. From the measured compressive strengths, the concept of an 'equivalent hole diameter' for damaged specimens was explored. Extensive strain measurements were made and strain distributions in specimens were also compared.

The results from this part of the investigation have been summarized in a paper, " Damage Resistance and Damage Tolerance of Pultruded Composite Sheet Materials", which was presented at the ASTM Symposium on Composite Materials: Testing, Design, and Acceptance Criteria, in Phoenix, Arizona (March 26-27, 2001). A copy of this paper is attached to this report.

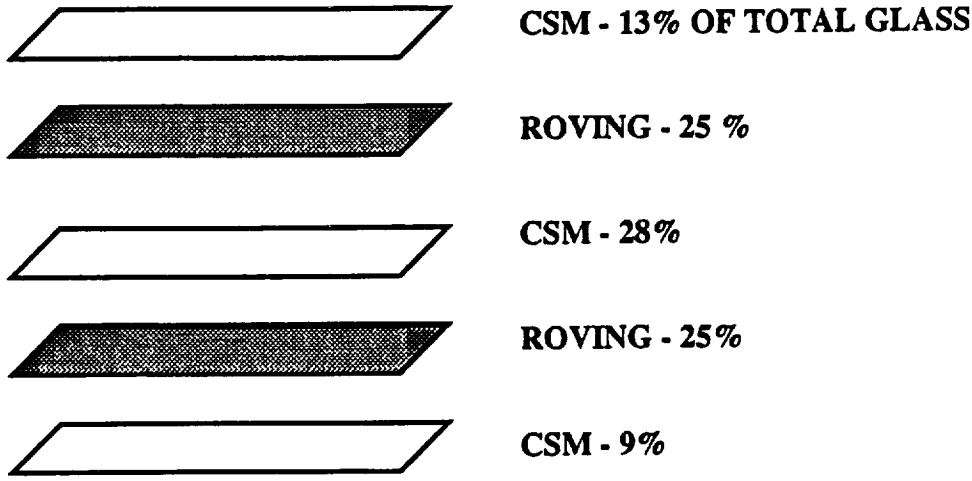

Figure : Layup of 1/8 in. thick FRP pultruded composite

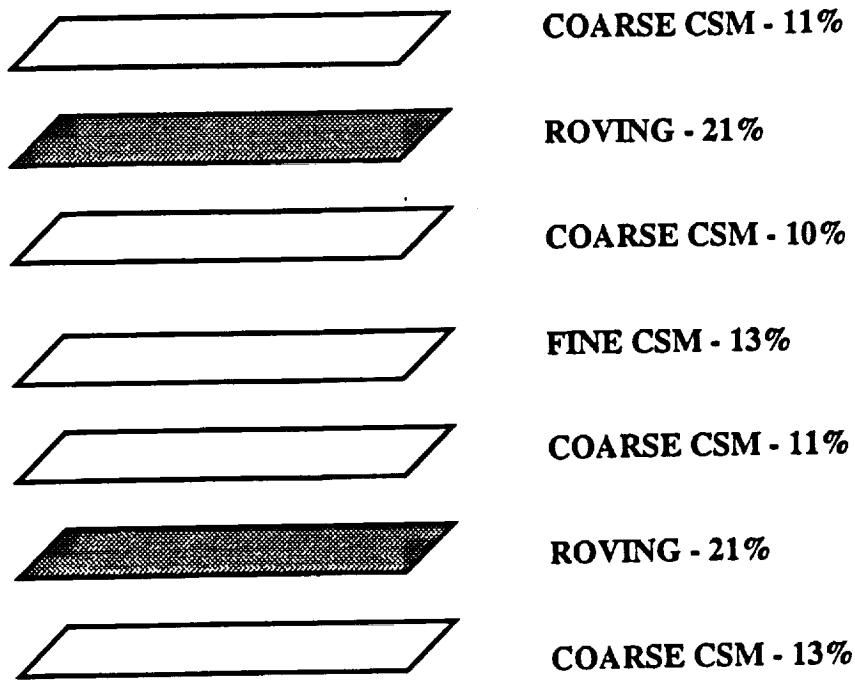

Figure **Layup of 1/4 in. thick FRP pultruded composite**

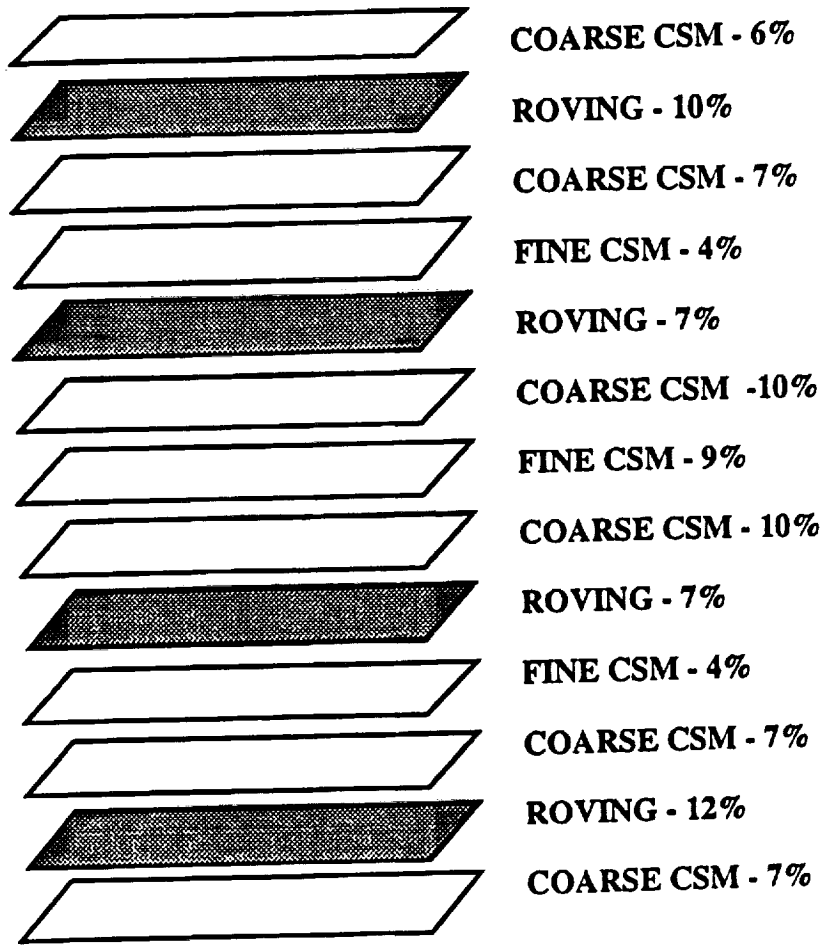

Figure **Layup of 1/2 in. thick FRP pultruded composite**

Glass	Sheet thickness (in.)		
	1/8	1/4	1/2
Total glass in composite	54	60	58
Roving as a percentage of total glass	50	42	36
CSM as a percentage of total glass	50	58	64
Coarse CSM as a percentage of total glass	—	45	46
Fine CSM as a percentage of total glass	—	13	18

Table Composition of the pultruded composite of different thicknesses by weight percent of constituent layers

Thickness (in.)	E_{11} ($x10^6$ psi)	E_{22} ($x10^6$ psi)	ν_{12}	ν_{21}	G_{12} ($x10^6$ psi)
1/8	2.76	1.37	0.28	0.14	0.45
1/4	2.63	1.18	0.34	0.17	0.55
1/2	2.34	1.17	0.29	0.19	0.29

Table In-plane elastic constants for pultruded FRP composite sheets of various thickness

NASA/TP—2000-210481

A Comparison of Quasi-Static Indentation to Low-Velocity Impact

A.T. Nettles
Marshall Space Flight Center, Marshall Space Flight Center, Alabama

M.J. Douglas
Old Dominion University, Norfolk, Virginia

National Aeronautics and
Space Administration

Marshall Space Flight Center

August 2000

TABLE OF CONTENTS

LIST OF FIGURES

LIST OF FIGURES (Continued)

LIST OF FIGURES (Continued)

LIST OF FIGURES (Continued)

LIST OF FIGURES (Continued)

LIST OF TABLES

LIST OF ACRONYMS

LaRC	Langley Research Center
LVDT	linear voltage displacement transducer
MSFC	Marshall Space Flight Center
NDE	nondestructive evaluation
TP	technical publication

TECHNICAL PUBLICATION

A COMPARISON OF QUASI-STATIC INDENTATION TO LOW-VELOCITY IMPACT

1. INTRODUCTION

Low-velocity impact events are expected to occur during the manufacturing and service life of composite parts and/or structures. Foreign body impact can occur during manufacturing, routine maintenance, or use of a laminated composite part. By dropping a 5-lb handtool less than 4 ft, an impact force anywhere between 100 to 1,500 lbf can occur, depending mainly on the transverse stiffness (flexural rigidity) of the impacted part at the site of the impact. Low-velocity impact events can occur during the service life of a composite in such forms as hail, runway debris, and collisions with other vehicles or animals. Impact events such as these can damage the integrity of the composite while leaving little or no visible damage.

There are two very distinct aspects to consider when designing composite structures/components—damage resistance and damage tolerance of composite materials. Damage resistance is the measure of a material's ability to resist damage, while damage tolerance measures the ability of a structure/component to carry service loads (or function as designed) with the presence of damage. Damage tolerance of carbon/epoxy composites is a very important aspect in the design criteria of composite structures. This is due to the relatively low strength of a carbon/epoxy laminate transverse to the fiber direction (through-the-thickness direction). The principal load-carrying mechanism in this direction is the epoxy matrix. The primary structural role of the matrix material is to provide stability to the fibers. During an impact event, the matrix will fail first, causing microcracks within a layer (lamina) and then delamination between the lamina layers. This can lead to the structure's inability to carry designed service loads, especially in compression.

This has led to much research on impact damage to laminated composite plates. Typically, laminated plates are impacted either by a "drop-weight" or "projectile" method. Drop-weight impacts usually consist of an instrumented striker (tup) that is secured to a carriage that falls along guideposts and collides with the plate. Projectile tests typically consist of firing a small spherical projectile at a composite plate with the use of a light gas gun. After an impact event has been performed, ultrasonic c-scans, x-radiography, and cross-sectional photomicroscopy are some of the common techniques used to document the damage area. Postimpact strength testing (mostly compression) is often performed to evaluate a material's or structure's damage tolerance.

It would be very beneficial to simulate an impact event using a "quasi-static" loading test. By using this test, damage initiation and propagation can be more easily detected, deflection can be directly measured with great accuracy, and maximum transverse force can be better controlled. Thus, the focus of the work in this technical publication (TP) was to examine if drop-weight impact tests and quasi-static loading tests give the same size, shape, and location of damage for a given maximum transverse load.

TECHNICAL PUBLICATION

A COMPARISON OF QUASI-STATIC INDENTATION TO LOW-VELOCITY IMPACT

1. INTRODUCTION

Low-velocity impact events are expected to occur during the manufacturing and service life of composite parts and/or structures. Foreign body impact can occur during manufacturing, routine maintenance, or use of a laminated composite part. By dropping a 5-lb handtool less than 4 ft, an impact force anywhere between 100 to 1,500 lbf can occur, depending mainly on the transverse stiffness (flexural rigidity) of the impacted part at the site of the impact. Low-velocity impact events can occur during the service life of a composite in such forms as hail, runway debris, and collisions with other vehicles or animals. Impact events such as these can damage the integrity of the composite while leaving little or no visible damage.

There are two very distinct aspects to consider when designing composite structures/components—damage resistance and damage tolerance of composite materials. Damage resistance is the measure of a material's ability to resist damage, while damage tolerance measures the ability of a structure/component to carry service loads (or function as designed) with the presence of damage. Damage tolerance of carbon/epoxy composites is a very important aspect in the design criteria of composite structures. This is due to the relatively low strength of a carbon/epoxy laminate transverse to the fiber direction (through-the-thickness direction). The principal load-carrying mechanism in this direction is the epoxy matrix. The primary structural role of the matrix material is to provide stability to the fibers. During an impact event, the matrix will fail first, causing microcracks within a layer (lamina) and then delamination between the lamina layers. This can lead to the structure's inability to carry designed service loads, especially in compression.

This has led to much research on impact damage to laminated composite plates. Typically, laminated plates are impacted either by a "drop-weight" or "projectile" method. Drop-weight impacts usually consist of an instrumented striker (tup) that is secured to a carriage that falls along guideposts and collides with the plate. Projectile tests typically consist of firing a small spherical projectile at a composite plate with the use of a light gas gun. After an impact event has been performed, ultrasonic c-scans, x-radiography, and cross-sectional photomicroscopy are some of the common techniques used to document the damage area. Postimpact strength testing (mostly compression) is often performed to evaluate a material's or structure's damage tolerance.

It would be very beneficial to simulate an impact event using a "quasi-static" loading test. By using this test, damage initiation and propagation can be more easily detected, deflection can be directly measured with great accuracy, and maximum transverse force can be better controlled. Thus, the focus of the work in this technical publication (TP) was to examine if drop-weight impact tests and quasi-static loading tests give the same size, shape, and location of damage for a given maximum transverse load.

In the present study, all tests were conducted on laminated plates made from IM7/8552 prepreg. The plates tested were quasi-isotropic with a stacking sequence of $[+45,90,-45,0]_{ns}$, with n equal to 1,2,4, and 6. This is known as a $\pi/4$ quasi-isotropic stacking sequence.

2. PREVIOUS WORK

2.1 Background

The need for a static (or more commonly referred to as quasi-static) test method for modeling low-velocity foreign object impact events would prove to be very beneficial to researchers since much more data can be obtained from a quasi-static test than from an impact test. An American Standard Testing Materials standard has been proposed for transverse quasi-static loading of composite laminates, although the standard stops short of claiming to represent low-velocity impacts.[1] Since a "low-velocity" impact event lasts approximately 6–10 ms, there is debate as to whether or not a quasi-static indentation test truly represents a low-velocity impact event.

The first order of business is to determine whether or not an impact event is considered low velocity and can thus be subjected to further analysis as a quasi-static event. It has been clearly shown that projectile-type impacts in the ballistic range are governed by dynamic events and therefore could never be represented by a quasi-static test.[2–4] Some research efforts have been focused on defining the boundary between "low-velocity" and "dynamic" impact events. One study suggested that the impactor-to-target frequency ratio governs the type of event with a low (much less than unity) ratio, implying a quasi-static event.[5] A simpler method was obtained by Swanson[6] in which a rule has been established that if the impactor mass is more than 10 times the "lumped mass" of the target, then the impact event will be quasi-static in nature. The "lumped mass" is a function of the target shape and boundary conditions but is generally about one-half the mass of the entire target. However, for most practical purposes, it is fairly clear if an impact event is "low velocity." High-velocity/large-mass impacts are of little concern since the part will be so heavily damaged by such an event that an analysis is not needed and conversely a low-velocity/low-mass impact is of little concern since no damage will form.

Once an impact event is deemed to be "low velocity," the question remains as to whether or not a static indentation test can be performed that will duplicate certain aspects of the impact. Some of these aspects include permanent indentation, maximum displacement, and most importantly, amount and type of damage formed. All of these parameters must be compared against an independent variable that will be common to both tests. It has been suggested that this independent variable be the maximum transverse load.[4,7,8]

Permanent indentation after an impact or quasi-static loading test has been examined in a few studies.[9–11] The one common feature in all of these studies is the large amount of scatter in indentation depth data, to the point of rendering this measurement useless. Nevertheless, it was decided to examine this parameter in this study to see how much scatter would exist.

For load/deflection correlation it is imperative to have an instrumented impact apparatus. The interpretation of the signals has been greatly simplified with the use of commercially available systems that filter the load signals to reduce unwanted noise. Care must be taken to ensure that the filter being used does

not mask important load events. A complete analysis of instrumented impact testing is beyond the scope of this paper, but two excellent references are noted for the reader.[12,13]

The amount of damage formed by an impact event can be measured in a number of ways. Destructively, the impacted specimen can be sectioned and examined under high magnification, or a residual property can be measured (termed "damage tolerance"). Nondestructively, ultrasonic or x-radiography can give a planar indication of the type and extent of damage. Ultimately, the amount of damage formed by an impact event is the greatest concern to the engineer investigating such an occurrence, and since the impacted part may still be useable, nondestructive techniques are preferred. Thus the major portion of this paper will deal with the resulting damage as detected via nondestructive evaluation and whether or not the damage formed for a given transverse load is similar in low-velocity impact and quasi-static testing. Specific studies that have examined this are featured in section 2.2.

2.2 Impact Versus Quasi-Static Testing

Several studies[4,7,9,14,15] show a similarity between quasi-static indentation and drop-weight impact testing, while other studies[8,16,17] have shown a limit to the applicability of using quasi-static indentation to represent impact events. It must be noted that there are many variables involved in these tests such as boundary conditions, specimen size, specimen thickness, stacking sequence, impactor size, impactor shape, and type of fiber/resin system. The amount of impact damage formed in a laminated composite has been shown to be very sensitive to stacking sequence, regardless of thickness.[18] As plies are grouped together, larger areas of delaminations tend to form. It has been conventional wisdom in the aircraft industry to disperse the ply orientations in order to increase damage resistance. For example, a stacking sequence of $[+45,0,-45,90]_{2S}$ is preferable to one of $[+45_2,0_2,-45_2,90_2]_S$ in order to increase the damage resistance of the laminate.

Jackson and Poe[4] used 48-ply specimens with dispersed plies (a layup of $[45,0,-45,90]_{6S}$) in order to examine if a low-velocity impact event was similar to a quasi-static transverse loading event. The quasi-static indentation specimens were clamped over a 10.2-cm diameter circular opening and the impacted specimens were clamped over a 12.7-cm-square opening. Although these two boundary conditions are different, it was deemed not to be of a magnitude of difference to compare the delamination area of the results. The support size-to-specimen thickness ratio was ≈20 for these tests, which indicates a stiff impact target. For fiber/resin systems of both IM7/8551–7 and AS4/3506–6, no appreciable difference between the damage diameters as seen by c-scans were evident between the quasi-static and impact tests. In these tests, as a barely visible crater became more visible, the delamination results became more similar due to the elimination of scatter.

Kwon and Sankar[7] used 24- and 32-ply laminates with dispersed plies supported over a 2-in.-diameter circular opening. These specimens had an opening-to-thickness ratio of 17 and 12.5, respectively, indicating very stiff impact targets. For a limited amount of data, the static indentation and impact tests gave approximately the same delamination radius for a given transverse load.

Despite the title of a paper by Kaczmarek and Maison,[9] little information is obtained about damage area versus transverse load for impact and static indentation testing. What little information is given indicates that static and low-velocity impact testing gave "good similarity" when based on damage area as

detected by ultrasonic c-scans. The specimens were 16 plies thick with double groupings of all orientations. The layup sequence was $[45_2,0_2,-45_2,90_2]_S$ and the specimens were supported over a 12.5- by 7.5-cm opening. This gives a specimen opening-to-thickness ratio of ≈50, which is of moderate stiffness for an impact target.

Lee and Zahuta[14] used 16-ply quasi-isotropic panels with dispersed plies clamped over a 2.2- by 5-in. opening. This gives a specimen support-to-thickness ratio of ≈45, which indicates a moderately stiff to stiff impact target. The specimens were compared on a damage width rather than on a damage area basis. The results showed a good amount of scatter in the impact results with the static indentation tests yielding a slightly higher damage width for a given transverse load. On a lost energy basis, the results between static indentation and impact testing gave vastly different results with the impact tests losing much more energy for a given damage size. This was attributed to vibrations in the drop-weight crosshead absorbing much of the energy. This has also been a concern for researchers at NASA Marshall Space Flight Center (MSFC) where "lost energy" is deemed a dubious result at best.[19]

In a study at the University of Dayton Research Institute[15] a comparison between low-velocity impact and static indentation tests was based on load/deflection curves. The specimens were 48 plies thick with dispersed plies simply supported over a 12.3-cm-diameter ring. This gives a specimen support-to-thickness ratio of 20, which indicates a stiff target. The impact curve had the typical oscillations associated with an impact event but the static indentation curve superimposed over the impact curve fairly well, with incipient damage occurring at the same load and displacement for both. As far as damage is concerned, some of the specimens were cross sectioned and examined under magnification. There was no apparent difference in the type or extent of damage to the impacted specimens and the statically indented ones.

In a study at the Massachusetts Institute of Technology,[8] a slight difference in static indentation and impact testing was found. This study used panels fabricated with 12 plies grouped in sets of two. The panels were supported in a clamped-clamped/free-free configuration with a span of 25.2 cm and a width of 13 cm. These boundary conditions create a test specimen with a support size-to-thickness ratio of 170, a much more flexible specimen than those examined in previous studies thus far. For a given transverse load, the impacted panels showed more damage area as determined from x-ray analysis than the statically indented specimens. Numbers are not given, but the differences are within ≈50 percent; not huge, but different nonetheless. A plot of force versus deflection showed a vast (>100 percent) difference between static indentation and impact testing. This study also examined sandwich panels and it was found that the static indentation and impact tests were nearly identical. This was due to the extremely rigid support condition that a honeycomb panel gives its face sheets.

Elber[16] found some differences in maximum delamination length for a given transverse load between low-velocity impact and static indentation. In this study, 8-ply quasi-isotropic plates supported over a 2-in. circular opening were used. This gives a specimen support-to-thickness ratio of ≈50, which is between a stiff and flexible impact target. Load/deflection data were given and the two match well. However, for a given transverse load, those that were loaded statically had consistently longer delaminations than those that were impacted. This difference was between 15 and 40 percent for tests at four different load levels.

The largest difference between static indentation and impact testing in the literature surveyed was found by Highsmith.[17] This study employed 20-ply specimens with a layup of $[\pm 60, 0_4, \pm 60, 0_2]_S$ supported over a 2.5-in.-diameter circular opening, which gives a specimen support to thickness ratio of ≈25, representing a stiff target. Three different transverse load levels were selected and the resulting damage was evaluated using x-ray techniques. The lowest load level chosen in this study was just at the point of damage initiation; therefore, there is so much scatter in the data that a comparison cannot be made. At the two higher load levels, the specimens that were impacted showed about half as much delamination area for a given transverse load than the impacted specimens.

2.3 Conclusions From Past Studies

A summary of the results from past studies that compared quasi-static loading to impact loading based on a given transverse load is given in table 1.

From the studies examined thus far, it appears that a quasi-static indentation test can be used to simulate a low-velocity impact event in most cases; however, a more detailed study varying more parameters is needed. Most of the studies thus far have been on fairly stiff specimens. Larger ranges of stiffness need to be tested to draw a conclusion. The one study that did show a large difference in delamination area[17] has the most group plies with four zero-degree plies grouped together. It would be a rare case for an actual engineering laminate to have this kind of grouping. Thus it will be the intent of this study to examine laminates most commonly used in structures, those of the class $[45,90,-45,0]_{nS}$.

Table 1. Conclusions from previous studies.

Reference	Specimen Support/ Thickness Ratio[1]	Layup	Conclusions
4	20	$[45,0,-45,90]_{6S}$	No difference in c-scan diameter
7	17 12.5	$[0,45,90,-45]_{4S}$ $[0,22.5,45,67.5,-45,-22.5]_{2S}$	C-scan radius approx. same for limited data
9	50	$[45_2,0_2,-45_2,90_2]_S$	C-scan area shows no difference. Very little data
14	45	$[45,0,-45,90]_{2S}$	C-scan damage width showed static cases slightly higher than impact
15	20	$[0,45,-45,90]_{6S}$	Load/deflection curves similar
8	170	$[\pm 45_2,0_2]_S$	Impact showed more damage from x rays—load/deflection curves much different.
16	50	$[0,45,-45,90]_S$	From x rays, static specimens had a 15 –40 percent longer delamination length than impact specimens
17	25	$[\pm 60, 0_4, \pm 60, 0_2]_S$	Delamination areas of static specimens twice as large as impact specimens as determined from x rays

[1] The higher the number, the more flexible the plate.

3. EXPERIMENTAL PROCEDURE

3.1 Introduction

The intent of this study was to compare quasi-static indentation testing to drop-weight impact testing based on the maximum transverse load. In order to ensure a complete analysis of the two events, testing was divided into several different categories based on boundary conditions. These two categories were then subdivided into three additional groups based on plate stiffness. To ensure the repeatability of the experimental procedure, each impact test was performed on approximately four different specimens, while the quasi-static indentation test was performed on two different specimens. A decision was made to repeat the drop-weight impact testing numerous times because of the inherent data scatter. However, the repeatability became so constant during the latter stages of the testing that the number of impacted specimens for repeatability assurance was reduced.

Finally, the rate of the quasi-static indentation test was also investigated to find if there was any time dependency involved in quasi-static indentation testing. The two rates used were 0.05 in./min and 1 in./min.

3.2 Boundary Conditions

The two main categories of tests were dependent on the boundary conditions. Specimens were either clamped on all four edges or simply supported on all four edges. For simplicity, the specimens that were clamped on all four edges will be referred to as clamped and those simply supported on all four edges will be referred to as simply supported for the remainder of this TP. This was done to determine if the boundary conditions would have a major influence on the damage introduced for the same impact force. Since an impact event does not always occur directly in the center of two ribs in a grid-stiffened aircraft component nor on top of a rib, the boundary conditions will change. For example, if an impact event occurred somewhere between the center point of a grid and on top of a rib, the actual boundary conditions would be simulated more accurately in the lab as a combination of the clamped and simply supported.

To perform the simply supported test, the specimens were placed on the machined platen shown in figure 1. The platen was machined from a 5.08-cm-thick (2-in.-thick) aluminum plate with an outside square dimension of 40.64 cm (16 in.). A total of four platens were made with the square opening, N, shown in figure 1, machined to 5.08 cm (2 in.), 60.96 cm (4 in.), 15.24 cm (6 in.), and 30.48 cm (12 in.). This was done to explore the flexural/rigidity properties of the composite panels.

In order to perform the test with clamped boundary conditions, the platen in figure 1 was modified as shown in figure 2. A series of 0.64-cm (0.25-in.) holes were drilled and tapped into the aluminum plate 3.81 cm (1.50 in.) from the edge of the opening. The bolt holes were spaced 2.54 cm (1 in.) on center. The 1.27-cm-thick (0.50-in.-thick) plate shown in figure 2 was machined from a steel plate with holes placed in the same physical location as those in the platen.

The exterior dimension, *M*, in figure 2, was dependent on the opening size of the platen. For example, the platen with the 15.24-cm (6-in.) opening required a steel plate with exterior dimension (*M*) of 25.4 cm (10 in.). The laminated composite panel was placed between the 5.08-cm-thick (2-in.-thick) aluminum platen and the 1.27-cm (0.5-in.) steel plate. Allen-head bolts were then used to secure the specimen and a uniform torque of 5.65 J (50 in.-lbf) was applied to each bolt.

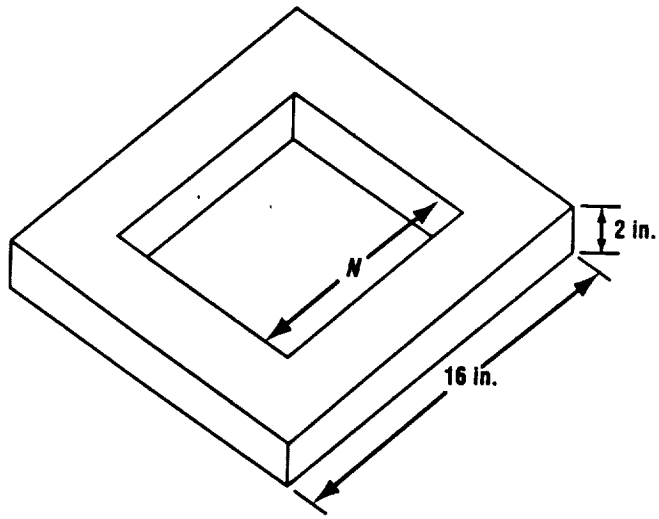

Figure 1. Test platen used for simply supported testing.

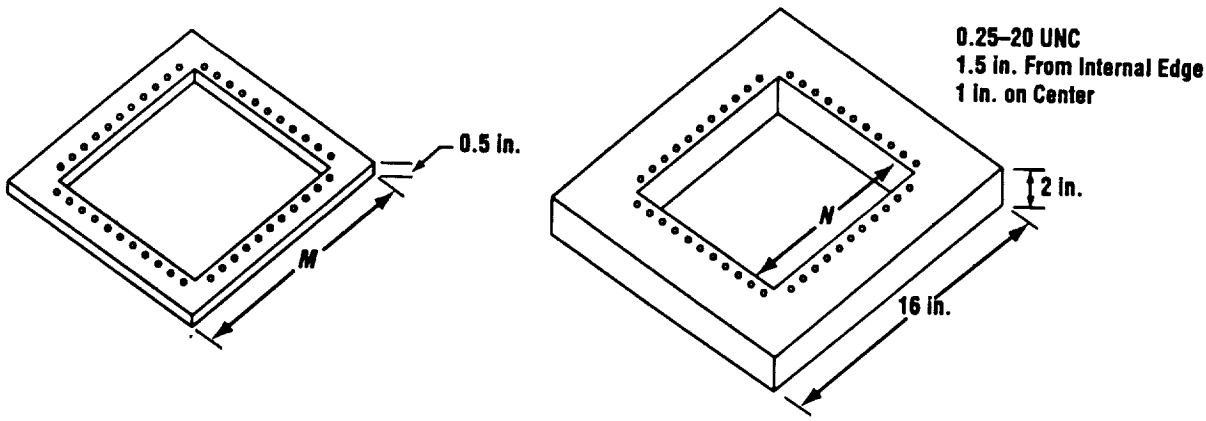

Figure 2. Modifications to test platen for clamped test.

3.3 Flexural Rigidity of Specimens

The three subgroups of tests involved the stiffness of the composite plate. It was decided that the stiffness was a function of the support opening versus the laminate plate thickness. The specimens were divided into three categories under this assumption: (1) Flex: ratio of 150, (2) medium: ratio of 50, and (3) stiff: ratio of 25.

During an impact event, this flex/stiff characteristic changes the mode of damage propagation as shown in figure 3. Figure 3 shows that for stiff laminates the contact forces caused the mode of failure, while for flexible laminates the failure propagates from the side opposite the impact site. This was characteristic of the brittle properties of the matrix materials used in advanced composites.

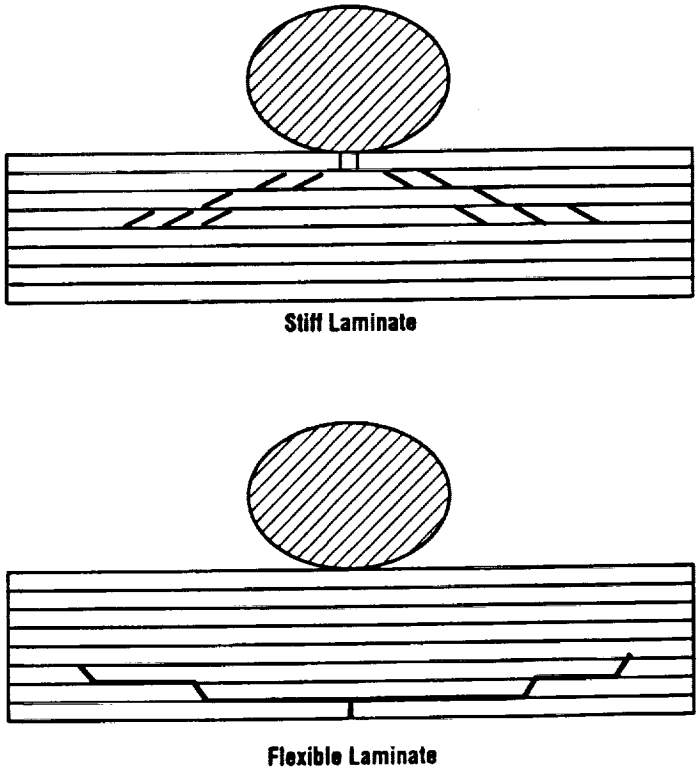

Figure 3. Impactor/laminate failure mode.

3.4 Materials

The plates used for this study were manufactured from Hexcel™ IM7/8552 prepreg. The epoxy resin, 8552, is a high-performance matrix that is used primarily in the aerospace industry for structural components. It offers exceptional toughness and damage tolerance. IM7 is an intermediate modulus carbon fiber with a tensile modulus of ≈27,580 MPa (40 msi). The manufacture's tensile strength and tensile modulus values for a unidirectional laminate of this fiber/resin system are listed in table 2.

Table 2. Material properties.

Property	Manufacturer's Value MPa (ksi)
Tensile strength	5,378 (780)
Tensile modulus	27,580 (40,000)

The quasi-isotropic laminated panels were layed up by hand, placed in a vacuum bag, and cured using the manufacturer's cure cycle shown in figure 4. The panels were fabricated into 61×91.4 cm (24×36 in.) plates. In order to obtain a large variety of flexural stiffnesses of carbon/epoxy laminates, the following four thicknesses were used: 8-, 16-, 32-, and 48-ply. The panels were fabricated utilizing the quasi-isotropic $\pi/4$ stacking sequence of $[+45,90,-45,0]_{ns}$, where n, was given the value of 1, 2, 4, and 6, respectfully.

Figure 5 is a schematic of an 8-ply laminate stacking sequence. From these panels, the test specimens were then machined into 10.16 cm (4 in.), 15.24 cm (6 in.), 20.32 cm (8 in.), and 35.56 cm (14 in.) squares. Appendix A lists all specimens, layups, and sizes. The specimens were machined using a tungsten carbide saw blade.

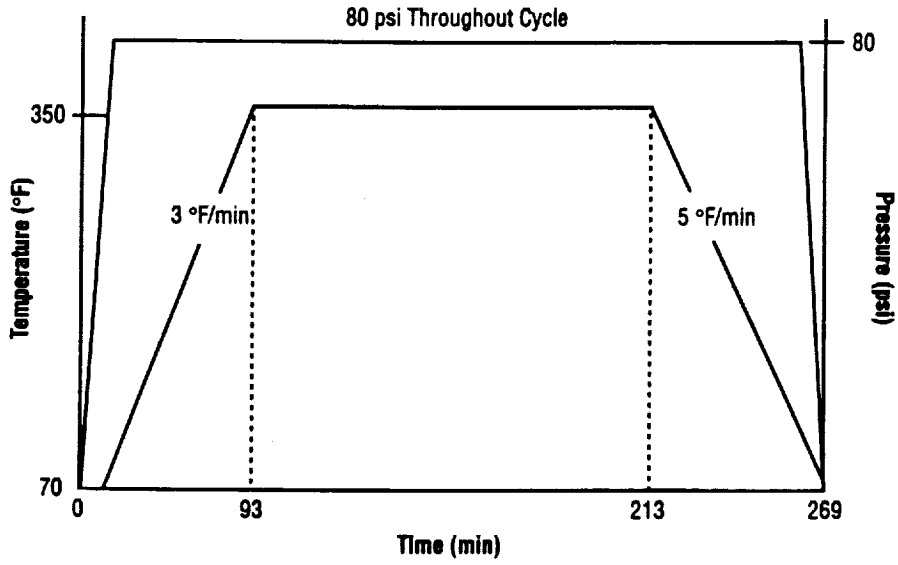

Figure 4. Typical cure cycle for IM7/8552 prepreg laminate.

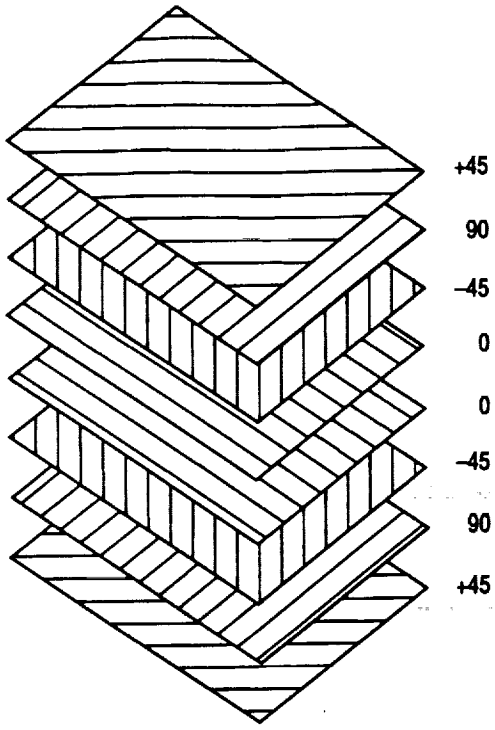

Figure 5. Schematic of an 8-ply laminate stacking sequence.

3.5 Mathematical Foundation

The impact tester measures the initial velocity by an electronic trip placed as close as possible to the surface of the impact specimen. By double-integrating the time versus load curve, deflection versus load plot was calculated. Although the computer software (GRC 930–I) performed this evaluation, the actual numbers were checked to ensure accuracy. The following equations were used:

$$F(t) = m\frac{d^2x}{dt^2}, \tag{1}$$

where

$F(t)$ is the force of the load cell (lbm*ft/sec^2)
m is the mass of the impactor (lbm)
d^2x/dt^2 is the acceleration (ft/sec^2).

From eq. (1), velocity was calculated numerically using eq. (2):

$$V(t) = \frac{-1}{m}\int F(t)dt + c_0 \ . \tag{2}$$

Using initial boundary conditions:

$$\text{at } t = 0$$
$$c_0 = V_o \,,$$

where

$V(t)$ is the velocity of the load cell (ft/sec)
c_0 is a constant of integration
V_o is the initial velocity (ft/sec).

From eq. (2), deflection was calculated numerically using eq. (3):

$$X(t) = \left(\frac{-1}{m}\iint F(t)dtdt\right) + V_0 t \,, \tag{3}$$

where

$X(t)$ is the transverse deflection of the load cell as a function of time.

These numerical integrations were performed using the software package Kaledigraph™.

3.6 Impact Testing Procedure

The impact testing was performed at MSFC using a Dynatup 8200 drop-weight impact tester. The specimens were placed on the platen shown in figures 1 and 2, depending on boundary conditions, with the desired opening size (N). Table 3 lists the opening size used, dependent on the laminate plate thickness. This divided the test into the proper flexural/rigidity ratio being examined.

Table 3. Opening and laminate thickness ratio calculations.

Flex: Ratio of 150		
Number Plies	Laminate Thickness mm (in.)	Opening Size (N) mm (in.)
8	0.102 (0.04)	152.4 (6)
16	0.204 (0.08)	304.8 (12)
Medium: Ratio of 50		
8	0.102 (0.04)	50.8 (2)
16	0.204 (0.08)	101.6 (4)
48	6.096 (0.24)	304.8 (12)
Stiff: Ratio of 25		
16	0.204 (0.08)	50.8 (2)
32	4.064 (0.16)	101.6 (4)
48	6.096 (0.24)	152.4 (6)

Specimens were then impacted with a hemispherical-tipped steel tup. The drop-height and mass of the impactor was adjusted to give the desired damage mode. The damage desired was very little visual damage to the top of the specimen while achieving a measurable crack on the bottom surface. This level of damage was chosen since the onset of visual damage is such a critical state for an impact event. If penetration is allowed, boundary conditions and rate effects will not be as noticeable and if too low of an impact level is used, damage may not form at all. Tables 4 and 5 list the height, maximum load, and mass for each subgroup that was finally chosen before proceeding to the quasi-static indentation testing. Table 4 is for the clamped boundary conditions and table 5 is for the simply supported boundary conditions. Appendix A has a complete listing of the drop-height and maximum loads for each specimen tested.

Table 4. Maximum load and drop height for the clamped boundary conditions.

Clamped			
Flex: Ratio of 150			
Number Plies	**Specimen ID No.**	**Maximum Impact Force N (lbf)**	**Drop Height cm (in.)**
8	616–15f	1,930 (434)	30.48 (12)
16	616–04f	7,108 (1,598)	121.92 (48)
Medium: Ratio of 50			
8	728–11m	1,036 (233)	12.70 (5)
16	616–28m	3,728 (838)	35.56 (14)
48	61599–04m	26,823 (6,030)	119.38 (47)
Stiff: Ratio of 25			
16	616–32s	3,100 (697)	33.02 (13)
32	616–20s	7,268 (1,634)	71.12 (28)
48	727–05s	23,100 (5,193)	63.50 (25)

Table 5. Maximum load and drop height for the simply supported boundary conditions.

Simply Supported			
Flex: Ratio of 150			
Number Plies	**Specimen ID No.**	**Maximum Impact Force N (lbf)**	**Drop Height cm (in.)**
8	727–10f	1,873 (421)	44.45 (17.50)
16	728–06f	5,400 (1,214)	148.6 (58.50)
Medium: Ratio of 50			
8	728–03m	974 (219)	5.72 (2.25)
16	727–11m	3,728 (837)	49.53 (19.50)
48	61599–02m	23,562 (5,297)	119.38 (47.00)
Stiff: Ratio of 25			
16	727–20s	2,922 (657)	52.71 (20.75)
32	727–18s	9,853 (2,215)	124.46 (49.00)
48	727–02s	22,121 (4,973)	63.18 (24.88)

Time versus load data were measured and collected using the software package GRC 930–I. Figure 6 shows a typical time versus load plot for an impact test. From this data the load displacement graphs were calculated as discussed in section 3.5.

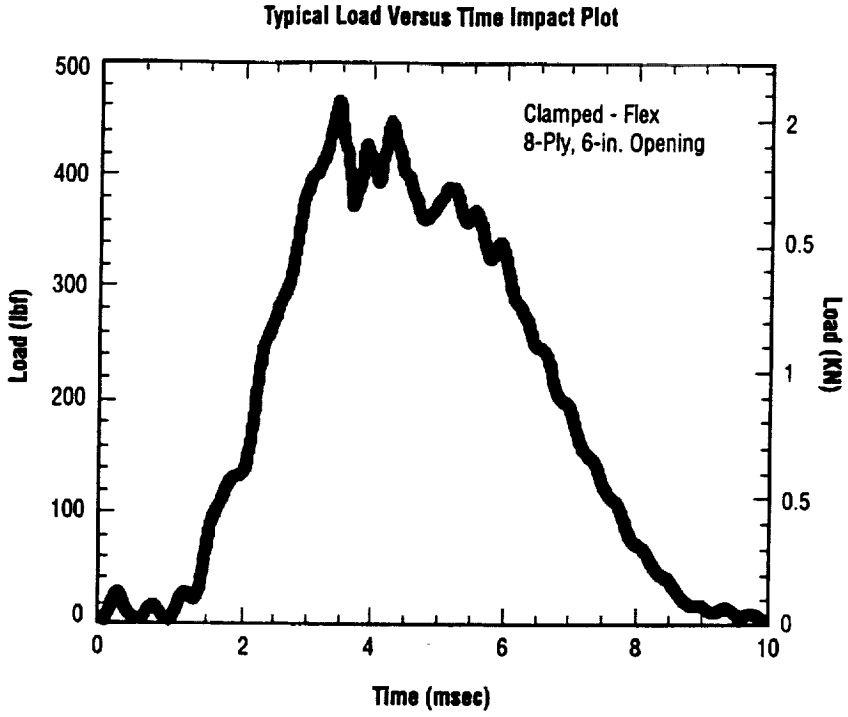

Figure 6. Typical time versus load plot.

In order to achieve the desired impact force on the 48-ply specimens, two different load cells were required. These specimens required an impact force >5,000 lbf; therefore, a 10,000-lbf load cell was used. To ensure the compatibility of the load cells, four drop-weight impact tests were performed. Both loads' cells were placed on the crosshead with an equal amount of weights placed at the same height, and then composite panels were impacted to compare maximum loads. The results of these tests are tabulated in table 6.

Table 6. 5,000- and 10,000-lb load cell comparison.

Specimen ID No.	Initial Energy J (ft-lb)	Initial Velocity M/sec (ft/sec)	Maximum Load N (lbf)	Load Cell
614E–1	15.89 (11.72)	4.3 (14.11)	5,449 (1,225)	10,000
614E–2	15.68 (11.57)	4.27 (14.02)	5,453 (1,226)	10,000
614E–3	15.82 (11.67)	4.29 (14.08)	5,351 (1,203)	5,000
614E–4	16.00 (11.80)	4.32 (14.16)	5,631 (1,266)	5,000

From these data it was concluded that both load cells were properly calibrated and giving good force values.

Figure 7 shows a typical load versus displacement plot. All load versus displacement plots for the impact test can be found in appendix B.

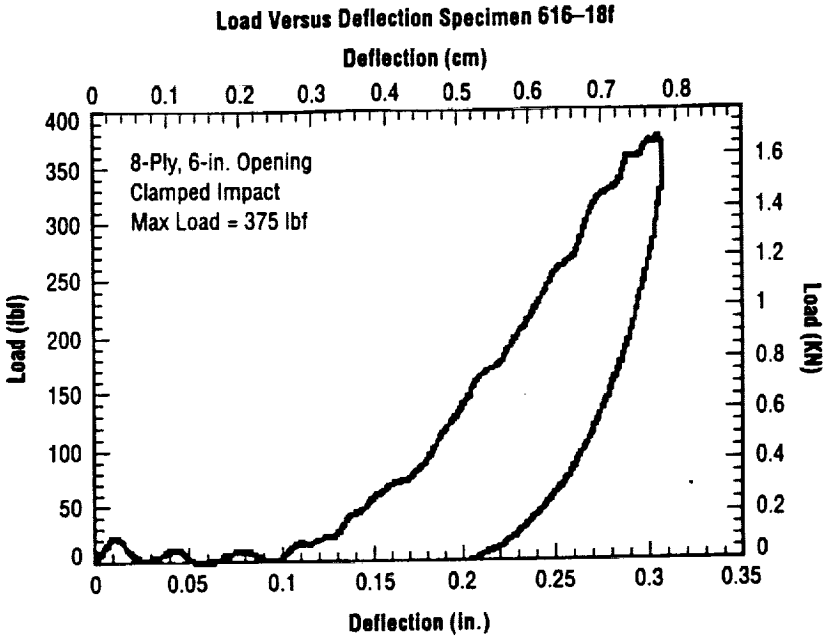

Figure 7. Typical load versus displacement plot for impact testing.

3.7 Static Indentation Testing Procedure

Once the impact testing was completed, the maximum impact force obtained for each of the different subgroups was used as the independent variable in the quasi-static indentation test. This was done primarily due to the ease of reproducing this value on a servohydraulic test frame. However, it did not turn out to be as easy as thought when the loading rate was increased to 1 in./min. Therefore, a small amount of scatter was introduced into the experimental data from the beginning. The majority of the quasi-static indentation tests were performed at NASA Langley Research Center (LaRC) on a 100-kip servohydraulic load frame. Figure 8 shows the test fixture used for all of the quasi-static indentation tests performed at LaRC. In order to perform a few tests at MSFC, a slight modification to the way the fixture was mounted in the load frame had to be accomplished. The platen shown in figure 8 was the same platen used for the impact test. For simplicity, the platen without the bolt holes is shown. The platen rested on top of the 5.08-cm-thick (2-in.-thick) aluminum uprights and could be removed without taking the fixture out of the test frame. The aluminum uprights were bolted to a 5.08-cm-thick (2-in.-thick) steel plate. The tang shown in figure 8 was also machined out of steel and was bolted to the underside of the steel plate. The impactor was placed in the upper crosshead of the servohydraulic load frame. In a limited number of tests, transverse deflection of the center point of the laminate, directly under the hemispherical tup, was measured using a linear voltage displacement transducer (LVDT). Figure 8 shows the location of the LVDT. The tests were run in stroke control at the two different load rates previously mentioned.

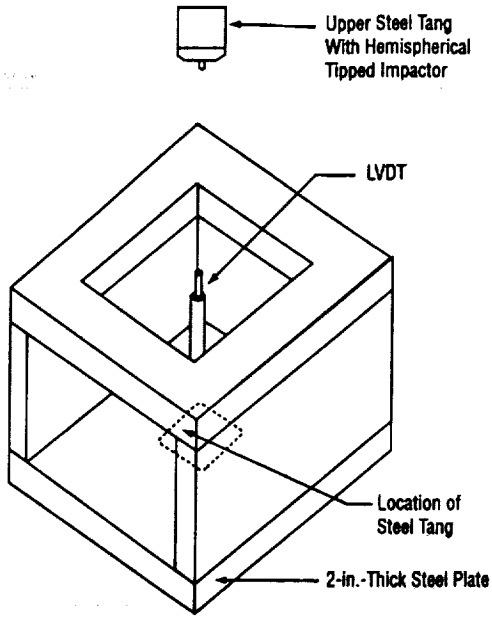

Figure 8. Test fixture for quasi-static indentation testing.

Load and transverse deflection data were collected using the WIN5000™ data acquisition system. Although the quasi-static indentation tests were repeated, it was not repeated to the magnitude of the impact testing. Each series of tests was performed twice. Since the dynamics of the quasi-static testing was not an issue, this was assumed an adequate number to ensure repeatability. Figure 9 is a typical load deflection plot for a quasi-static indentation test. Appendix C contains all of the load deflection plots from the quasi-static indentation testing.

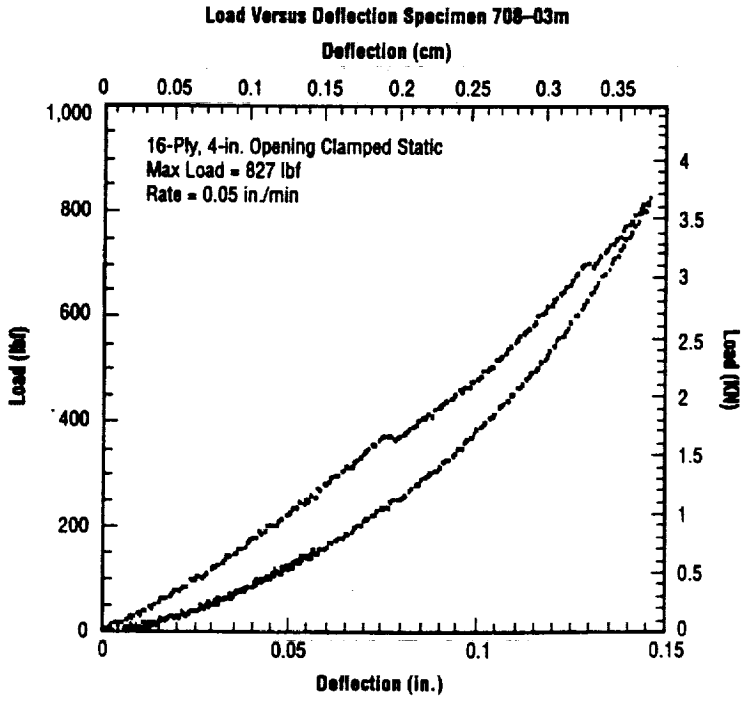

Figure 9. Typical load versus displacement plot for quasi-static indentation testing.

3.8 Nondestructive Analysis

Once the impact and quasi-static testing were completed, the specimen underwent three types of nondestructive analysis to document internal and external damage. These consisted of measuring dent depth on the impacted surface, crack lengths on the nonimpacted surface, and internal damage as determined from x-radiography.

After the specimens were impacted or subjected to quasi-static indentation testing, they were set aside for at least 24 hr so that the resulting dent would have time to relax to its equilibrium state. It was felt that this would be appropriate since a postflight inspection would be performed at least 24 hr after a flight. The dent depths were measured using a Starrett™ Model 644–44I dial depth gauge with an accuracy of 0.0254 mm (0.001 in.).

Any visible cracks on the nonimpacted surface of the specimens were measured.

After all the dent depths and crack lengths were measured, the specimens were then subjected to radiographic techniques to document the internal damage areas. The specimens were soaked on both sides with a zinc iodide penetrant solution for 24 hr and then x rayed using a Faxitron™ x-ray machine. A piece of photographic film was placed directly under the specimen to capture the image of the internal damage in the form of a negative. The exposure length and focal film distance was varied, depending on the specimens being x rayed. For example, specimens 61599–02 through 61599–05 (48-ply specimens) were exposed at 35 kV for 2 min with a focal length of 46 in. While the specimens with identification numbers 616–20 through 616–24 (32-ply specimens) were exposed at 35 kV for 1 min 15 sec at a focal length of 46 in. From the negatives, positives were made so that the planar damage area could be calculated. This was accomplished by superimposing a grid of 4 mm^2 (0.0062 $in.^2$) squares over the picture and then counting squares that were within the damage area. Figure 10 illustrates the process used. The specimen shown in figure 10 was a 16-ply clamped impact specimen, 616–04f, supported over the 30.48-cm (12-in.) opening. From this photo 192 squares were counted, which gives a planar delamination area of 768 mm^2 (1.19 $in.^2$). It should be noted that this is only a planar calculation and does not take into consideration the thickness of the specimen. The strain gauge that appears in the bottom righthand corner of figure 10 was put on the specimen after it had been impacted so the x ray could be oriented with the specimen if needed.

The planar area of delamination was the most important variable used in this study and was the main factor in determining if an impact event can be represented by a quasi-static indentation test.

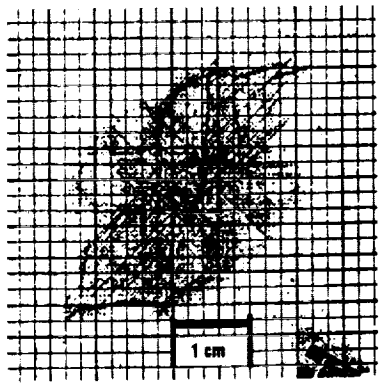

Figure 10. X-ray of impact specimen with 4 mm^2 grid superimposed.

4. RESULTS AND DISCUSSION

4.1 Introduction

Since the main purpose of the research being presented was to establish if quasi-static indentation testing was a true representation of a low-velocity impact event, this chapter will address this issue by comparing the experimental results obtained in the low-velocity impact testing to that of the quasi-static indentation testing. The impact testing will be discussed and then a comparison of the damage resistance of the material subjected to the two different events will be presented. Tables 7 and 8 list the specimens and the maximum loads used for comparison between impact and quasi-static testing. Once the specimens were tested, comparisons were made on the dent depth, crack length, and delamination area. From these comparisons, an understanding and analysis of the two types of testing procedures was achieved.

4.2 Drop-Weight Impact Testing

All of the load versus deflection plots for the drop-weight impact tests document the nonlinear characteristics inherent to large deflection of plates. This can be seen in appendix B. This nonlinear characteristic behavior makes it very difficult to accurately predict mathematically how the material will behave when subjected to a transverse load. For that reason, none of the classical laminate plate theories has been introduced for comparison in this paper.

The impact duration versus stiffness ratio plots shown in figures 11 and 12 show that the stiffness ratio has a direct effect on the duration of the impact. The impact duration increased as the stiffness ratio increased (i.e., the specimen became more "flexible") for both boundary conditions. All stiffness ratios had overlap in the duration of impact data and little difference can be noted between the two sets of boundary conditions. It is apparent from the data that the duration of impact is dependent upon much more than simply the support-to-thickness ratios of the plates, otherwise the data for ratios of 25, 50, and 150 would be clustered together in well-defined groups. The only noticeable trend between the two boundary conditions occurs on the most flexible specimens with a stiffness ratio of 150. For these data, the simply supported boundary condition gives a slightly longer duration of impact than the clamped boundary condition as long as all other parameters are held equal.

4.3 Quasi-Static Indentation Testing

Appendix C presents the load/deflection data generated for a limited number of the static indentation tests. The quasi-static test plots have very different behavior characteristics, depending on the stiffness ratio. For clarification, specimens ending in "f" indicate "flex" or a stiffness ratio of 150. Specimens ending in "m" indicate "medium" or a stiffness ratio of 50, and "s" indicates "stiff" or a stiffness ratio of 25.

For the "flex" specimens, the load/deflection curves demonstrate the extreme nonlinearity associated with large deflections of plates. The initial portion of the curve shows very little resistance to bending as a small load causes a large amount of deflection. However, as the membrane stresses begin to dominate,

Table 7. Identification numbers and maximum loads for clamped specimens.

	Type of Event	Specimen ID No.	Maximum Load N (lbf)
Flex: Support/Thickness Ratio of 150			
8-ply,	Impact	616–15f	1,930 (434)
6-in. opening	Static 0.05 in./min	708–10f	1,735 (390)
	Static 1 in./min	720–08f	1,899 (427)
16-ply,	Impact	616–04f	7,108 (1,598)
12-in. opening	Static 0.05 in./min	720–04f	6,993 (1,572)
	Static 1 in./min	720–05f	7,357 (1,654)
Medium: Support/Thickness Ratio of 50			
8-ply,	Impact	728–11m	1,036 (233)
2-in. opening	Static 0.05 in./min	722–04m	1,045 (235)
	Static 1 in./min	722–05m	939 (211)
16-ply,	Impact	616–28m	3,728 (838)
4-in. opening	Static 0.05 in./min	708–02m	3,705 (833)
	Static 1 in./min	720–06m	3,857 (867)
48-ply,	Impact	616–04m	26,823 (6,030)
12-in. opening	Static 0.05 in./min	817–01m	26,293 (5,911)
	Static 1 in./min	818–02m	28,290 (6,360)
Stiff: Support/Thickness Ratio of 25			
16-ply,	Impact	616–32s	3,100 (697)
2-in. opening	Static 0.05 in./min	722–02s	2,918 (656)
	Static 1 in./min	722–08s	2,931 (659)
32-ply,	Impact	616–20s	7,313 (1,644)
4-in. opening	Static 0.05 in./min	706–01s	7,455 (1,676)
	Static 1 in./min	708–07s	7,455 (1,676)
48-ply,	Impact	727–05s	23,100 (5,193)
6-in. opening	Static 0.05 in./min	720–01s	23,429 (5,267)
	Static 1 in./min	817–03s	23,389 (5,258)

the amount of load needed to cause a given amount of deflection increases greatly. Little damage is noted in these specimens until the maximum load is reached. This suggests a damage mode associated with large bending stresses.

The "medium" specimens all show a "kink" in the initial loading portion of the load/deflection curves associated with initial damage. Higher shear stresses are developed in the stiffer specimens, which results in delamination-type failures within the laminate. The curves are seen to be slightly nonlinear until the initial damage is formed, at which point the curves demonstrate more nonlinearity.

The "stiff" specimens also have the initial load drop along the loading curve, which appears to be of a larger magnitude than in the "medium" specimens. This follows since the stiff specimens will develop larger shear stresses which will release more energy when delamination does occur. Also of note is the change of stiffness at the very beginning of the load/deflection curve. This is associated with the contact stresses between the impactor and the plate. As the impactor first touches the plate, it begins to "dent into" the specimen, causing an indentation in the specimen. As the impactor goes deeper into the specimen, the contact stresses are spread out and the impactor stops indenting into the specimen.

Table 8. Identification numbers and maximum loads for simply supported specimens.

	Type of Event	Specimen ID No.	Maximum Load N (lbf)
Flex: Support/Thickness Ratio of 150			
8-ply,	Impact	727–10f	1,873 (421)
6-in. opening	Static 0.05 in./min	817–11f	1,859 (418)
	Static 1 in./min	817–04f	1,859 (418)
16-ply,	Impact	728–06f	5,400 (1,214)
12-in. opening	Static 0.05 in./min	818–06f	5,458 (1,227)
	Static 1 in./min	818–04f	5,667 (1,270)
Medium: Support/Thickness Ratio of 50			
8-ply,	Impact	728–03m	974 (219)
2-in. opening	Static 0.05 in./min	819–02m	907 (204)
	Static 1 in./min	819–08m	1,059 (238)
16-ply,	Impact	727–12m	3,701 (832)
4-in. opening	Static 0.05 in./min	819–016m	3,677 (827)
	Static 1 in./min	819–10m	3,777 (849)
48-ply,	Impact	61599–02m	23,562 (5,297)
12-in. opening	Static 0.05 in./min	818–07m	23,878 (5,368)
	Static 1 in./min	818–02m	28,304 (6,363)
Stiff: Support/Thickness Ratio of 25			
16-ply,	Impact	727–20s	2,922 (657)
2-in. opening	Static 0.05 in./min	819–04s	2,918 (656)
	Static 1 in./min	819–06s	2,931 (656)
32-ply,	Impact	727–18s	9,853 (2,215)
4-in. opening	Static 0.05 in./min	819–14s	9,866 (2,218)
	Static 1 in./min	819–12s	10,898 (2,450)
48-ply,	Impact	727–02s	22,121 (4,973)
6-in. opening	Static 0.05 in./min	817–08s	22,726 (5,109)
	Static 1 in./min	817–06s	21,476 (4,828)

4.4 Nondestructive Analysis

As mentioned earlier, three different types of nondestructive analysis techniques were used. All nondestructive evaluation (NDE) analysis results are tabulated in appendix D. Since visible damage that occurs from an impact event is most easily measured, all analysis will be presented with the dent depth as the independent variable.

When an impact event occurs to a laminated component, visual damage is not always apparent, although there can be severe underlying damage. It has been proposed that if a correlation between the measurable dent depth, usually the only visible damage, and underlying delamination or measurable crack length on the nonimpacted surface, then a damage resistance concern could be easily addressed. For this reason the dent depths were measured and documented for all specimens and used as the independent variable for all subsequent comparisons.

4.5 Crack Length

The specimens listed in tables 7 and 8 were used to generate the dent depth versus crack length plots shown in figures 13 and 14. Figure 13 is for the clamped boundary condition and figure 14 is for the simply supported boundary condition. For these two figures, a least-squares linear approximation was performed to find if any linear correlation between the two variables was present.

In figure 14 the data represented by the open squares were not included for the least-squares linear approximation. This was done because it fell outside of what was considered valid scatterbands. Equation (4) is the calculated linear approximation:

$$C = -0.347 + 224d \quad , \tag{4}$$

where

C is the crack length (in.)
d is the dent depth (in.).

From eq. (4) when the crack length (C) was set equal to zero and the equation solved for the dent depth (d), a value of 0.0015 in. was calculated. This would suggest that a carbon/epoxy structure/component could sustain a low-velocity impact event that produces a dent depth of 0.0015 in. and not have any measurable crack length on the nonimpacted surface.

Equation (5) is the linear approximation, calculated using the least-squares approach, as performed for figure 14:

$$C = -0.309 + 202d \quad , \tag{5}$$

where

C is the crack length (in.)
d is the dent depth (in.).

If the same analysis is performed on eq. (5) as performed on eq. (4), the value for the maximum dent depth without cracking was calculated to be 0.00153 in.

Although the two equations are in general agreement, they do not take into account the stiffness ratio of the composite plates. As previously mentioned, the stiffness ratio has a direct effect on the failure mode of the composite plates. Therefore, a correlation needs to be found that is not as generalized as this approach.

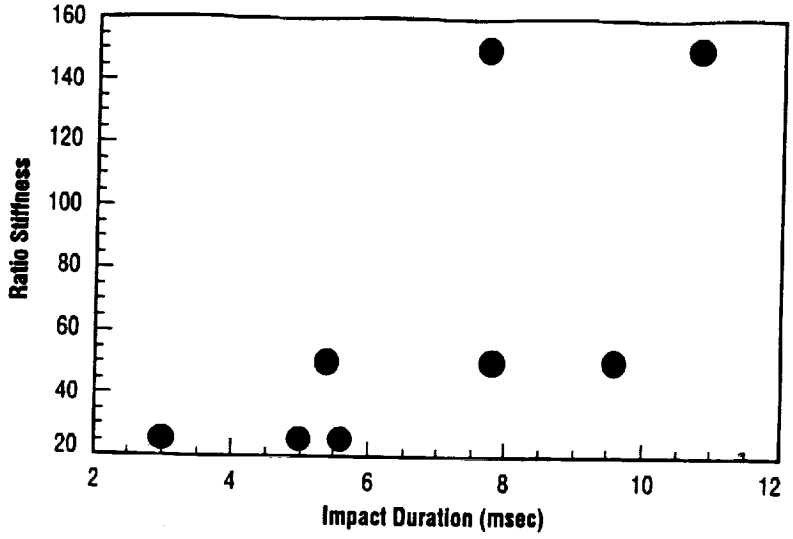

Figure 11. Impact duration versus stiffness ratio for clamped boundary conditions.

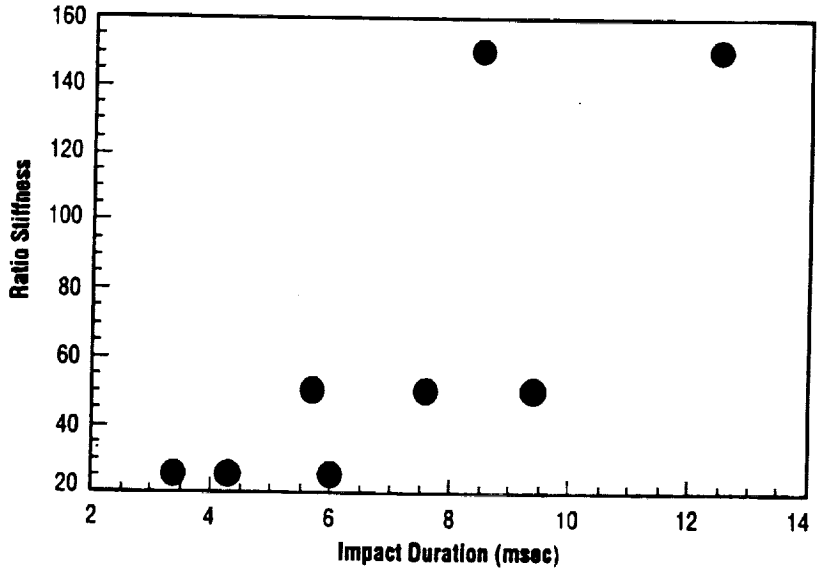

Figure 12. Impact duration versus stiffness ratio for simply supported boundary conditions.

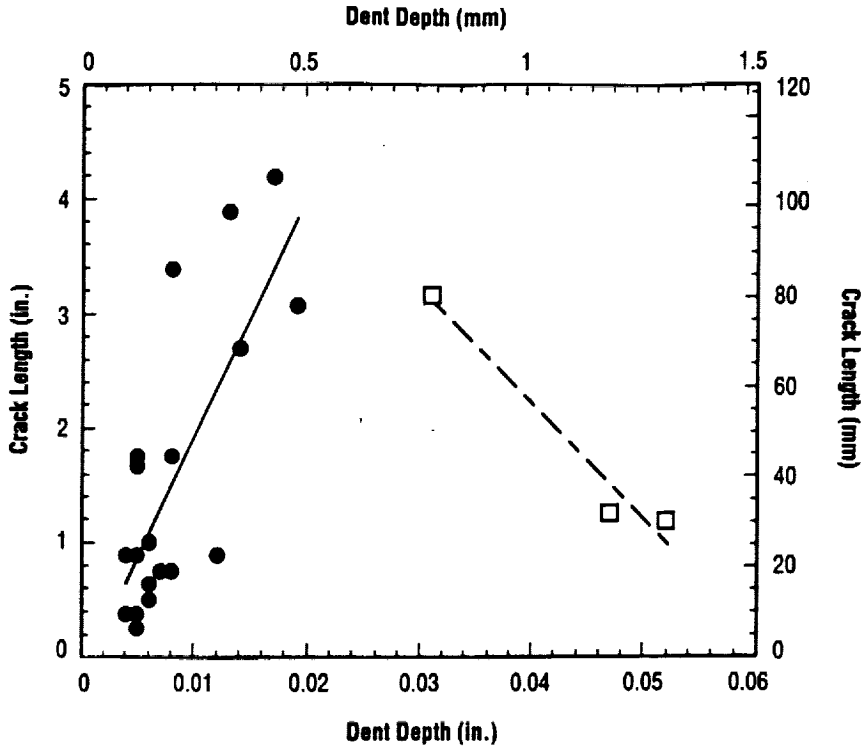

Figure 13. Crack length versus dent depth clamped boundary conditions.

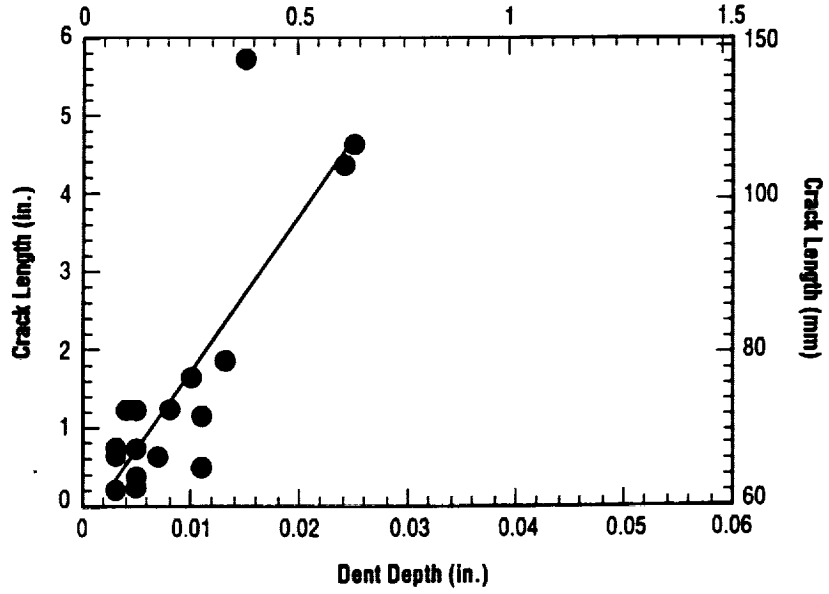

Figure 14. Crack length versus dent depth simply supported boundary conditions.

4.6 Delamination Area

For the delamination area comparisons, the same analysis will be performed as in the case of the crack lengths. Figures 15 and 16 are plots of delamination area versus dent depth for the clamped and simply supported boundary conditions, respectfully. The least-squares linear approximations are presented in eqs. (6) and (7); however, the physical interpretations of these equations take on a different approach.

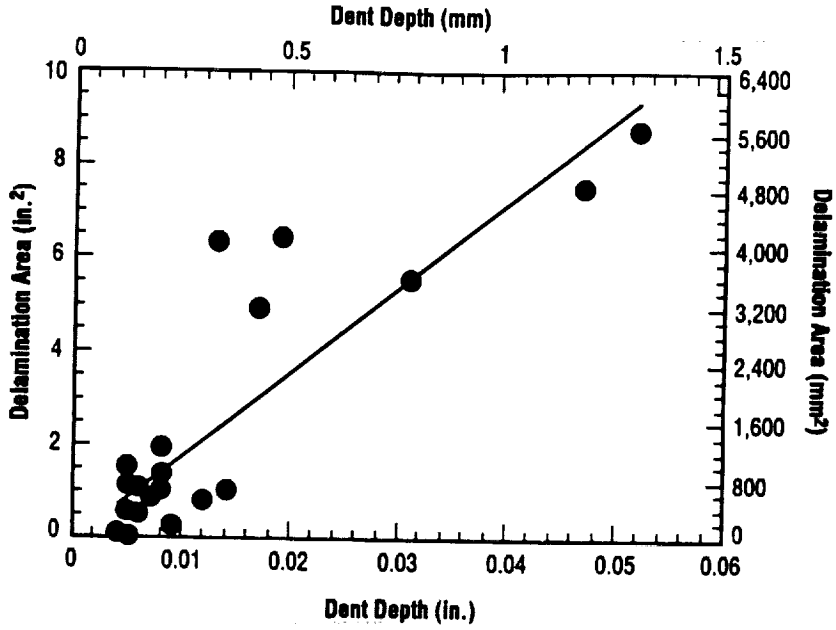

Figure 15. Delamination area versus dent depth clamped boundary conditions.

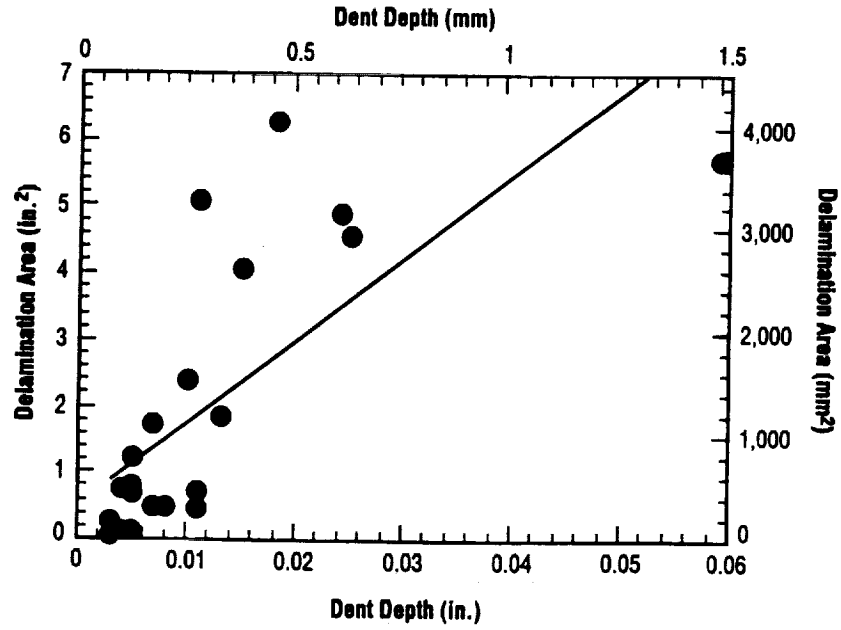

Figure 16. Delamination area versus dent depth simply supported boundary conditions.

Equation (6) is the linear approximation to the data presented in figure 15:

$$A = 0.005 + 178d \ , \tag{6}$$

where

A is the delamination area (in.^{2})
d is the dent depth (in.).

Unlike the dent depth discussion, in order to understand the physical meaning, if there is any, of eq. (6), the dent depth (d) was allowed to become zero. Doing this leads to a value of delamination area (A) equal to 0.005 in^2.

Equation (7) for figure 16 is presented as:

$$A = 0.52 + 124d \ , \tag{7}$$

where

A is the delamination area (in.^{2})
d is the dent depth (in.).

Using the same analysis as performed on eq. (6), a delamination area of 0.52 in.^{2} is found. This value is extremely large compared to the value for eq. (6). One could argue that because of the simply supported boundary conditions, this is possible. The simply supported boundary conditions allow for a larger amount of flexure to the composite plate, which in turn would produce more internal stress, alluding to large internal delaminations for the same applied load.

These data imply that after an impact event has occurred to a carbon/epoxy component/structure, underlying damage can occur with no visual evidence. Again, this analysis is overly simplified and a more indepth analysis needs to be found to better predict internal damage to laminated structures.

4.7 Comparison of Quasi-Static Indentation Testing and Drop-Weight Impact Testing

This section presents the main topic of this TP—"Does a statically applied transverse load yield the same damage as a low-velocity impact load of the same magnitude?" Using damage area as detected by x-ray analysis was deemed the most suitable method to do this since internal damage can be detected with this method. Figures 17–24 present delamination area as a function of applied transverse load for both low-velocity impacts and quasi-static loads of two rates. Each figure contains data for both clamped and simply supported specimens to test Jackson's assertion[4] that the delamination area should be independent of this parameter.

Figures 17 and 18 present data for the case of "flexible" laminates (support/thickness ratio of 150). The open symbols represent the simply supported boundary condition.

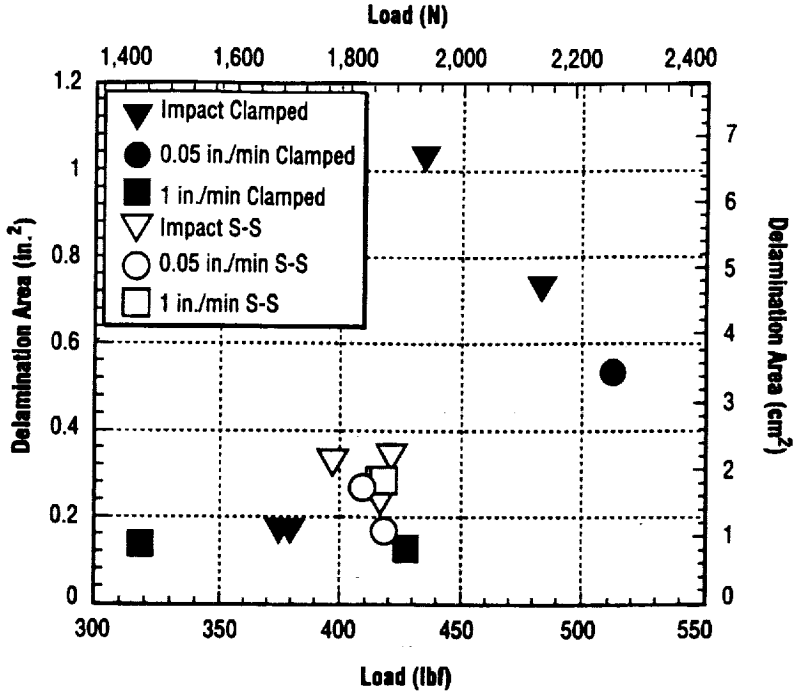

Figure 17. Delamination area versus maximum load for 8-ply specimens over 6-in. opening.

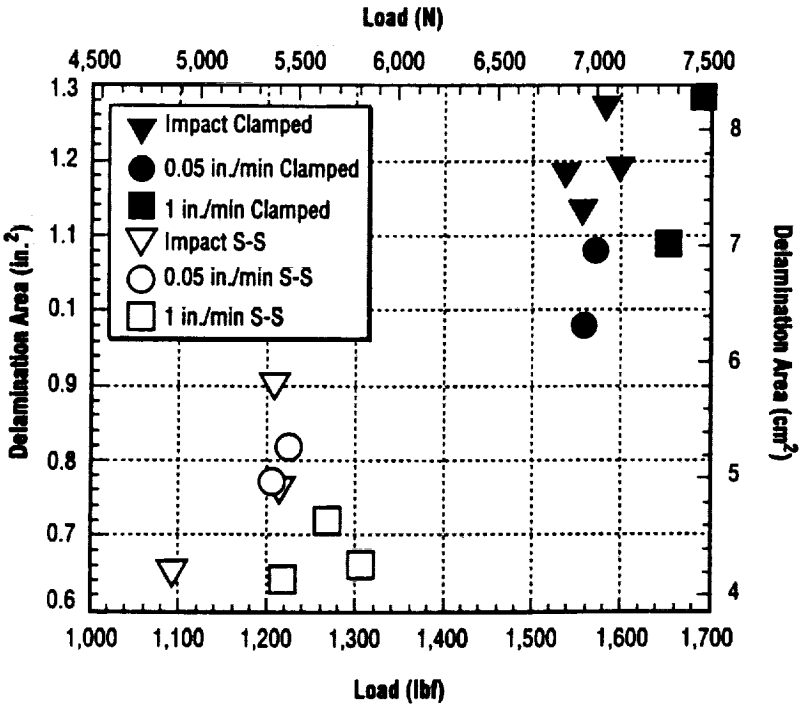

Figure 18. Delamination area versus maximum load for 16-ply specimens over 12-in. opening.

Figures 19–21 present data for the case of "medium" laminates (support/thickness ratio of 50). The open symbols represent the simply supported boundary condition.

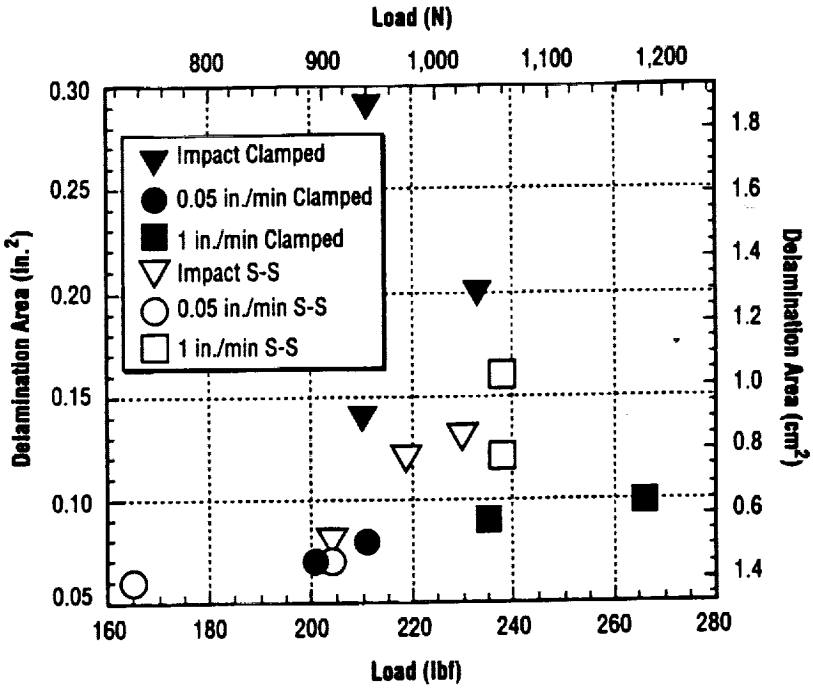

Figure 19. Delamination area versus maximum load for 8-ply specimens over 2-in. opening.

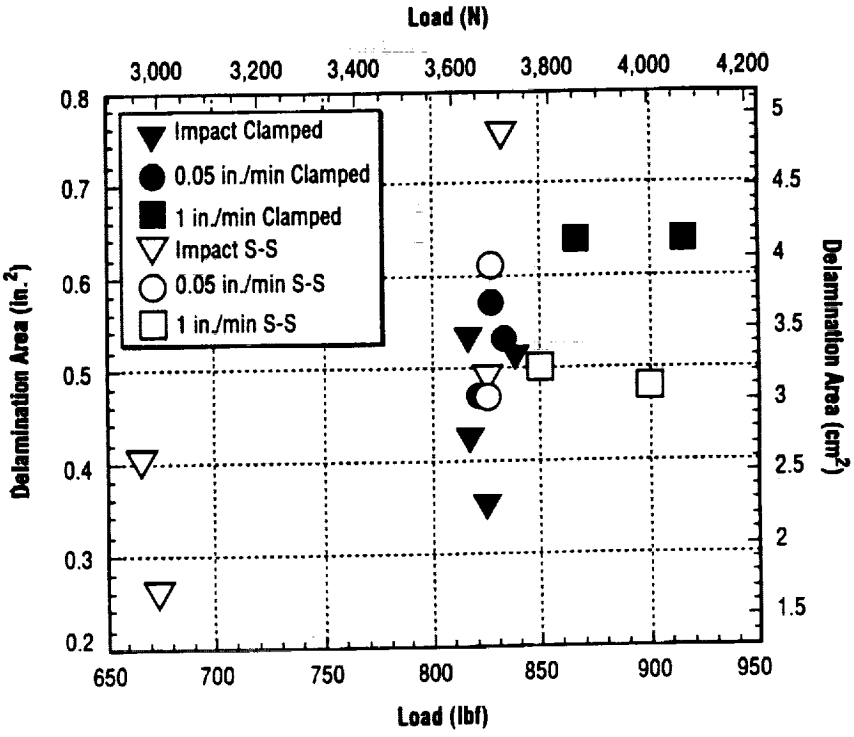

Figure 20. Delamination area versus maximum load for 16-ply specimens over 4-in. opening.

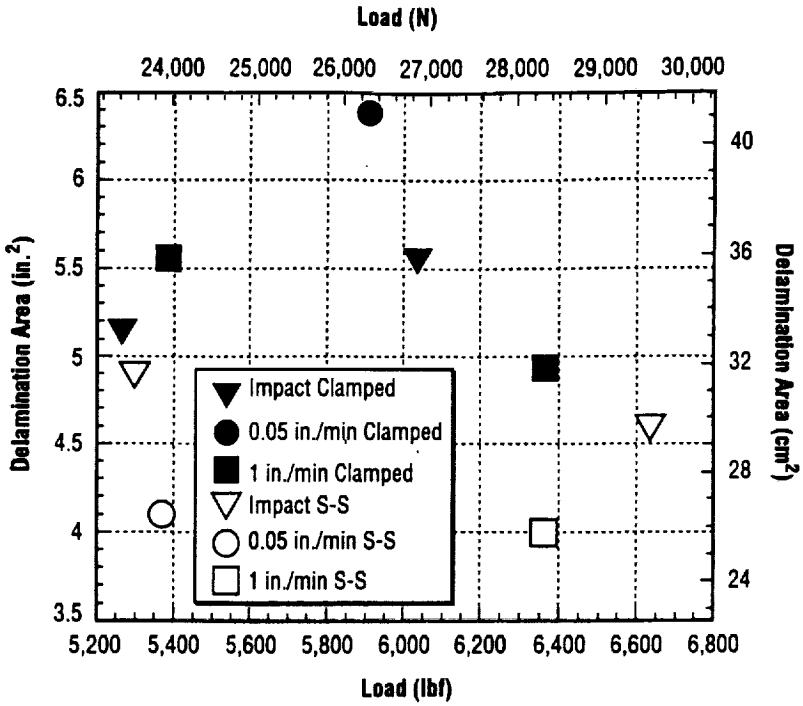

Figure 21. Delamination area versus maximum load for 48-ply specimens over 12-in. opening.

Figures 22–24 present data for the case of "stiff" laminates (support/thickness ratio of 25). The open symbols represent the simply supported boundary condition.

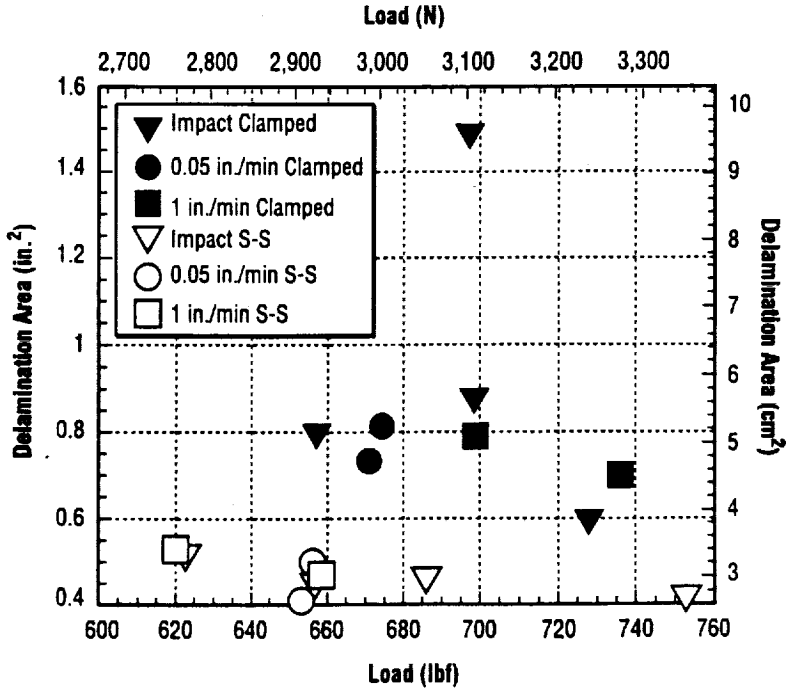

Figure 22. Delamination area versus maximum load for 16-ply specimens over 2-in. opening.

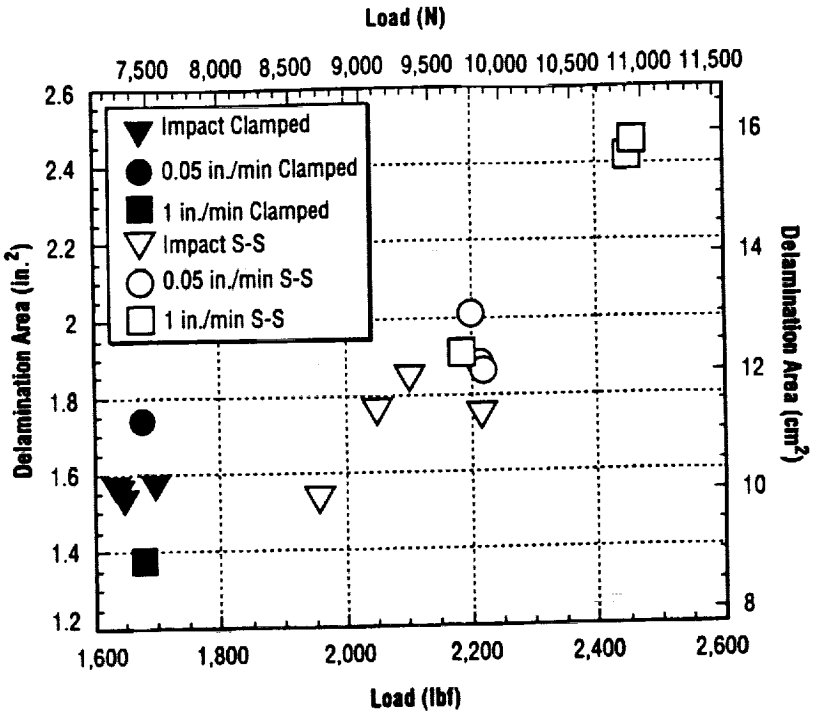

Figure 23. Delamination area versus maximum load for 32-ply specimens over 4-in. opening.

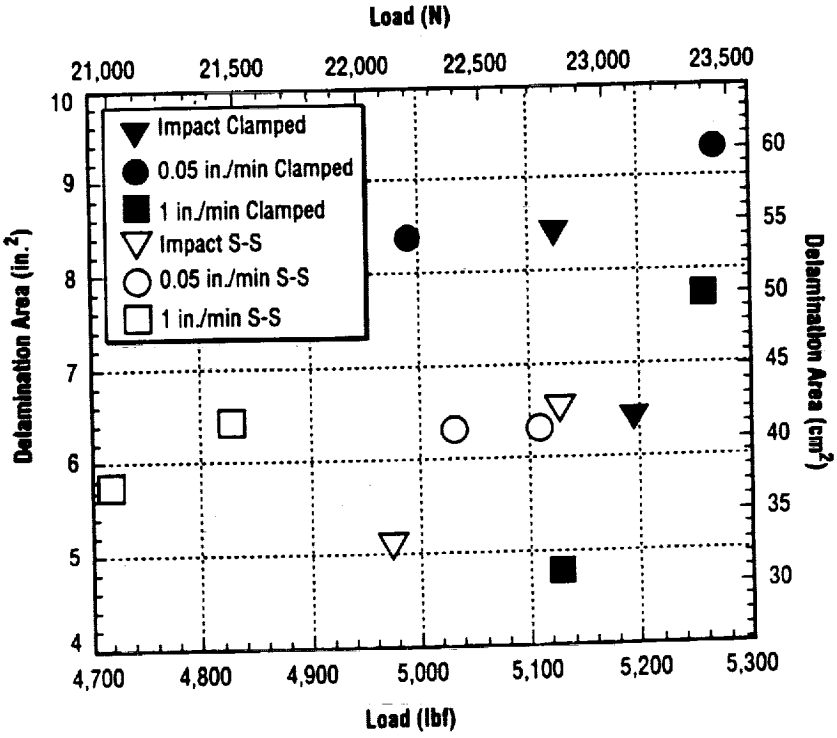

Figure 24. Delamination area versus maximum load for 48-ply specimens over 6-in. opening.

For the "flexible" laminates, there is no difference between the impacted specimens and those tested quasi-statically at either rate. The effects of the boundary conditions show no difference for the 8-ply specimens supported over the 6-in. opening, whereas a distinct difference is seen for the 16-ply specimens supported over the 12-in. opening. This difference is due to the clamped specimens being loaded to a higher level, resulting in a larger delamination area.

The "medium" specimens have no distinct trends between boundary conditions or rate of loading. The impact test results fall in well with the static indentation tests in figures 19–21. Boundary conditions also appear to have no effect on the maximum load versus delamination area.

Figures 22–24 represent the opposite extreme from the "flexible" specimens in that the contact damage is the dominant failure mode. Again, there is no discernable difference between impact and static indentation results. In figure 22, the simply supported specimens show slightly less damage for the same magnitude of maximum load than the clamped specimens; however, this difference is slight.

Overall, the low-velocity impact tests can be represented by static indentation testing at rates of 0.05 and 1 in. per minute, regardless of specimen rigidity and boundary conditions. There is enough inherent scatter in both types of tests that all data fall within this scatter. It must be kept in mind that these results are only valid for laminates of the $\pi/4$ type and laminates with different layups or clumped plies may yield different results.

Another check of the validity of using static indentation tests to represent impact tests, a comparison of the load/deflection data, can be made.

Figures 25–31 show static indentation load/deflection data superimposed over impact load/deflection data. The static data are represented by filled symbols, while the impact data are represented by open symbols. Static load/deflection data were not available for all of the static tests since a faulty LVDT was used; thus, only the valid data are presented.

On the loading portion of the curves, the data agree well. However, for the unloading portion of the curves, the impact data consistently indicate that more energy was lost during the event since there is a much larger hysteresis in the impact curves. However, from the delamination area data, it was anticipated that the energy lost should be about the same. It has always been suspected that most of the energy lost in this type of impact testing is lost due to vibrations within the impact apparatus, not in damage to the specimen. When the falling crosshead and tup impact the composite plate, the head will tend to rebound at an angle that is not parallel to the guideposts. Thus, a sideways force is exerted on the guideposts which causes them to vibrate and interfere with the "natural" rebound of the impactor.

Figures 25, 27, and 30 represent this erroneous "loss of energy" data quite well. Figure 25 is a flexible specimen and the loading portions of the curves agree well for both the static and impact cases. However, for unloading, the impact data show a much larger deflection than the static data for a given load on the rebound. Furthermore, the maximum displacement does not coincide with the maximum load, rather it is seen to occur during the unloading portion of the curve and is quite a bit larger than the displacement at the maximum load for two of the four impact specimens. Figures 27 and 30 also demonstrate this behavoir and are data for medium and stiff plates, respectfully, so this phenomena is not a function of how rigid the target is.

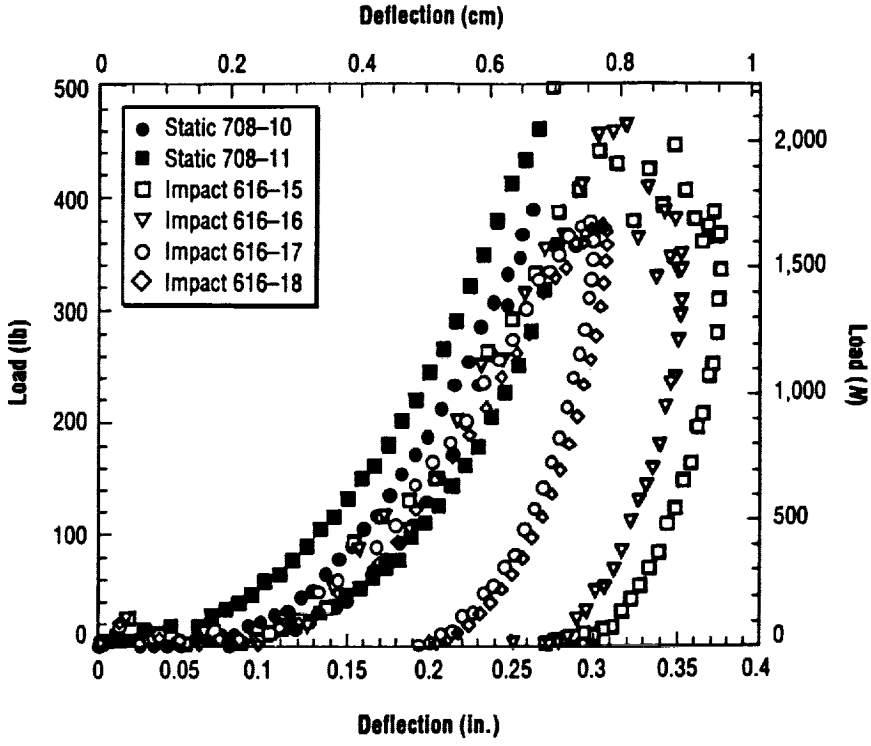

Figure 25. Static indentation data superimposed over impact data for 8-ply clamped specimens over a 6-in. opening.

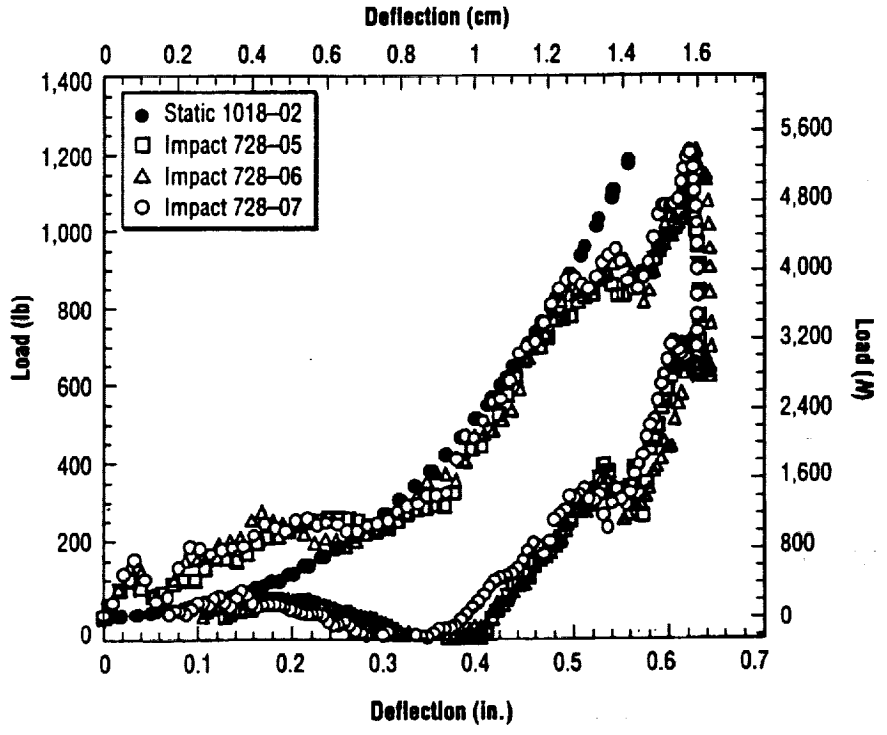

Figure 26. Static indentation data superimposed over impact data for 16-ply simply supported specimens over a 12-in. opening.

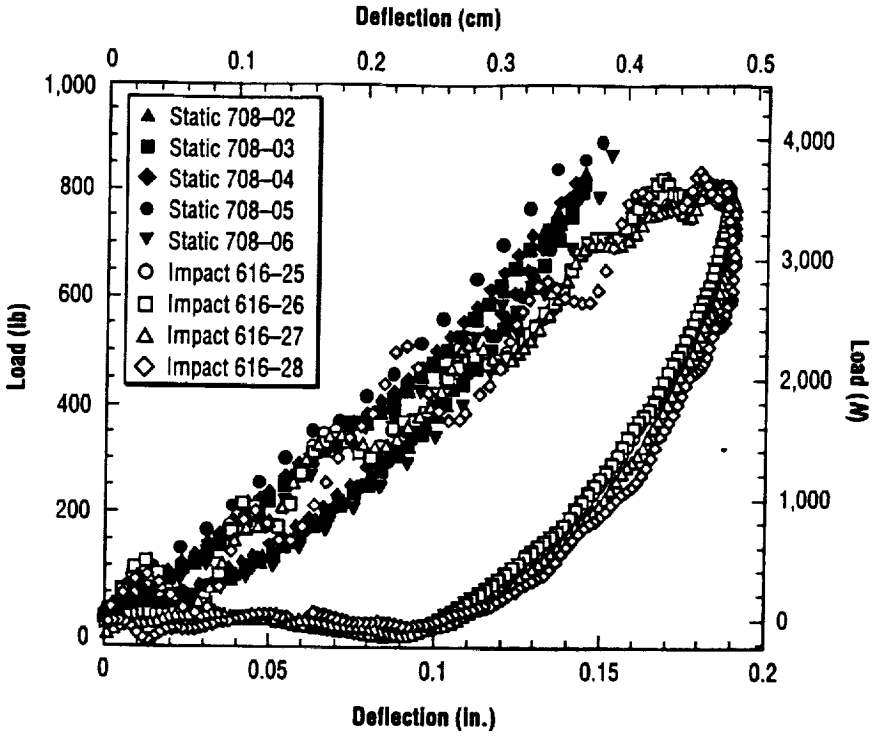

Figure 27. Static indentation data superimposed over impact data for 16-ply clamped specimens over a 4-in. opening.

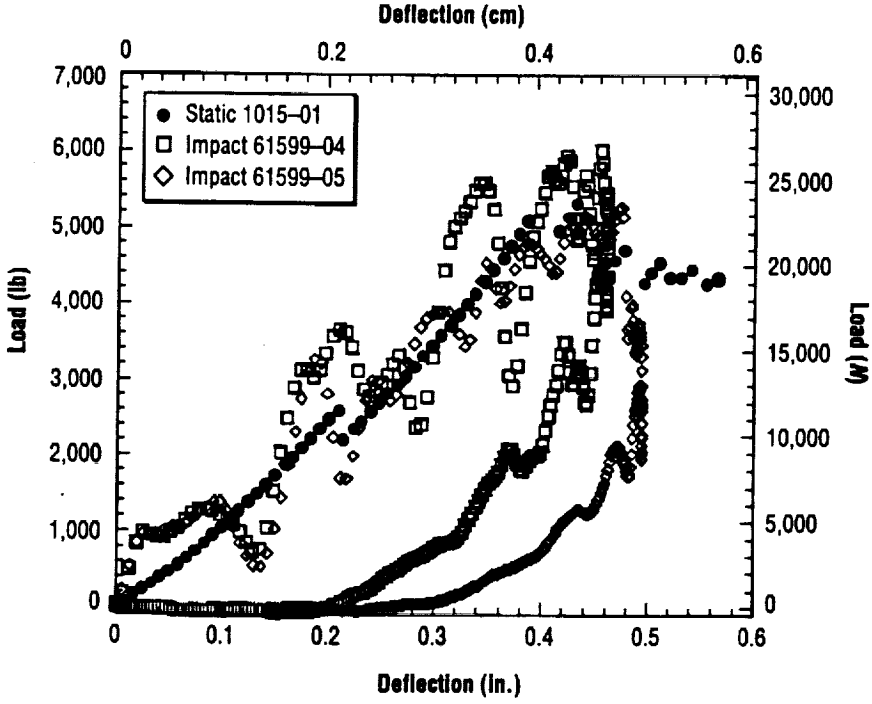

Figure 28. Static indentation data superimposed over impact data for 48-ply clamped specimens over a 12-in. opening.

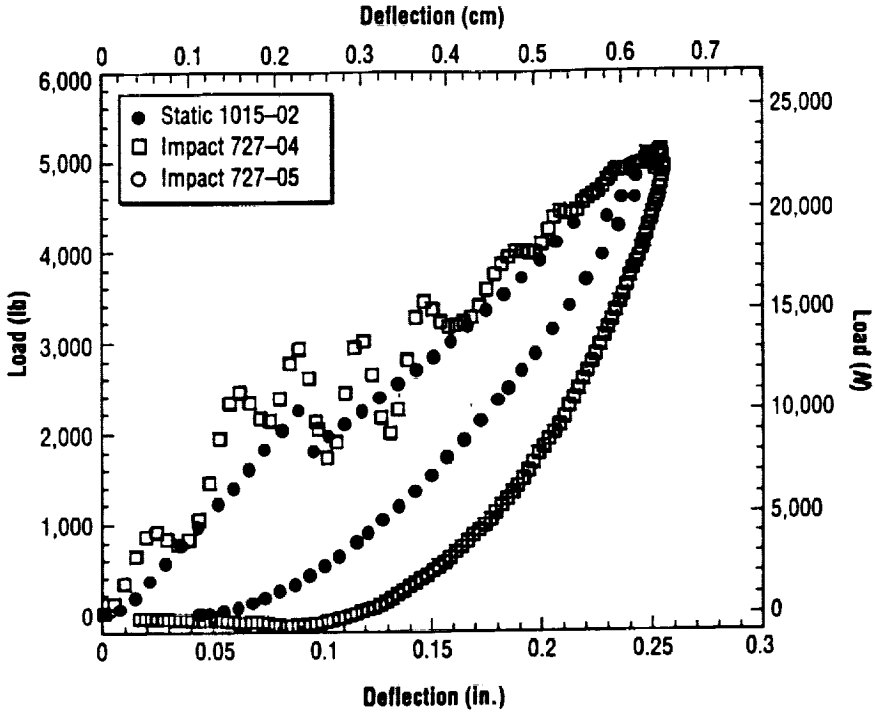

Figure 29. Static indentation data superimposed over impact data for 48-ply clamped specimens over a 6-in. opening.

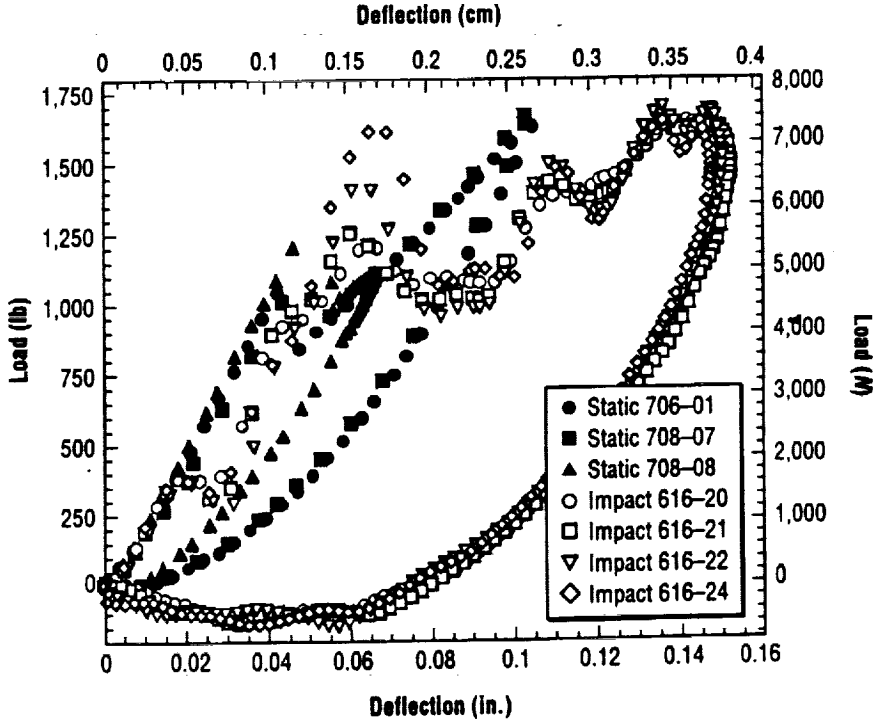

Figure 30. Static indentation data superimposed over impact data for 32-ply clamped specimens over a 4-in. opening.

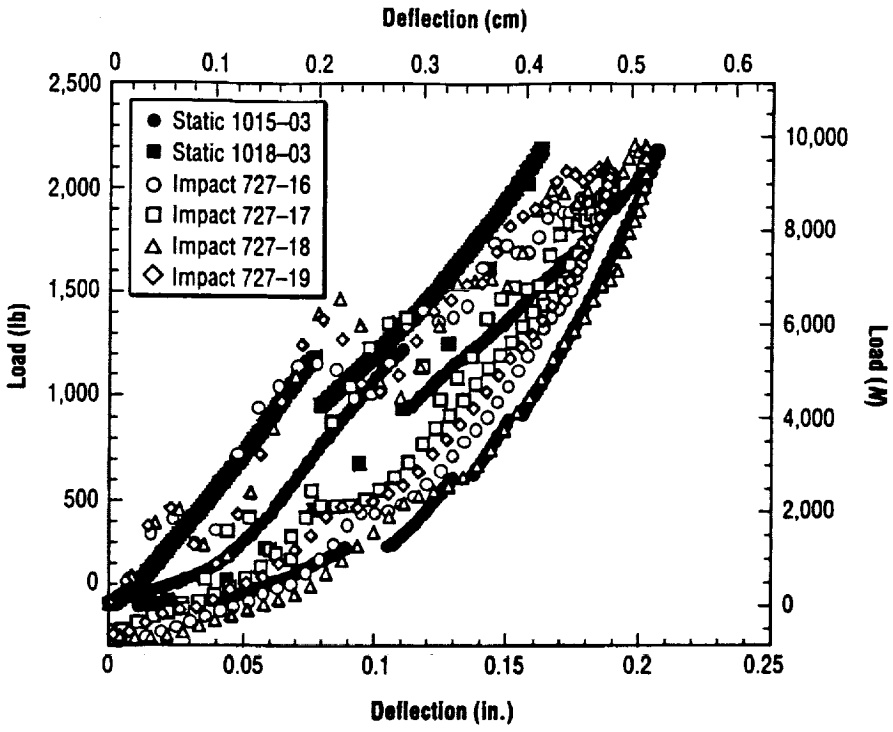

Figure 31. Static indentation data superimposed over impact data for 32-ply simply supported specimens over a 4-in.opening.

An argument may be made that this is due to the inertial effects of the plate, that after the "collision" of the impactor and plate, the plate continues to move downward due to its own inertia. This argument would indicate that heavier plates would show more difference in load/deflection data for static indentation and impact since heavier plates will have more inertia. However, figure 29 is a 48-ply plate over a 6-in. opening whereas figure 25 is an 8-ply plate over the same size opening, yet the lighter plate shows more of a difference.

Figure 26 does not have unloading data for the static case, but the loading portions of the curves agree quite well.

Figure 28 is unique in that during the static indentation test, the maximum load, as determined from the impact tests, could not be reached since the impactor began penetrating through the plate before this load was obtained.

5. CONCLUSIONS

Major conclusions of this study are as follows:

1. Static indentation tests can be used to represent low-velocity impact events when the damage is compared by maximum transverse force. This is true of plates that experience flexural-type damage, contact-type damage, and a combination of the two. Layups other than those of the $\pi/4$ type may not yield these same results.

2. Duration of an impact event is dependent upon the transverse stiffness of the plate. The stiffer the plate, the shorter the duration of impact. Boundary conditions have little effect on this behavior.

3. Much nonlinear behavior is observed in the load/deflection curves for flexible laminates. As the laminate becomes stiffer, more linearity is seen and a distinct drop in load due to delamination becomes more pronounced.

4. Load/deflection plots of static indentation and low-velocity impact are similar.

5. Dent depth results produce a great deal of scatter, which makes any conclusions concerning this parameter difficult.

APPENDIX A—IMPACT SPECIMEN IDENTIFICATION NUMBERS

Tables 9–14 show clamped and simply supported data for impact specimens.

Table 9. Clamped flex.

8 Ply on 6-in. Platen					
Specimen ID No.	Drop Height cm (in.)	Maximum Load N (lbf)	Impact Energy J (ft-lbf)	Impact Velocity m/sec (ft/sec)	Maximum Deflection cm (in.)
616–15f	30 (12)	1,930 (434)	7.5 (5.6)	2.42 (7.95)	No data
616–16f	25 (10)	2,148 (483)	6.4 (4.7)	2.22 (7.29)	0.90 (0.35)
616–17f	15 (6)	1,673 (376)	3.7 (2.8)	1.71 (5.60)	0.76 (0.30)
616–18f	15 (6)	1,668 (375)	3.8 (2.8)	1.71 (5.60)	0.78 (0.31)

16 Ply on 12-in. Platen					
Specimen ID No.	Drop Height cm (in.)	Maximum Load N (lbf)	Impact Energy J (ft-lbf)	Impact Velocity m/sec (ft/sec)	Maximum Deflection cm (in.)
616–01f	122 (48)	6,841 (1,538)	30.1 (22.2)	4.86 (15.94)	1.49 (0.59)
616–02f	122 (48)	6,921 (1,556)	29.7 (30.1)	4.82 (15.81)	1.49 (0.59)
616–03f	122 (48)	7,037 (1,582)	30.3 (22.3)	4.86 (15.96)	1.47 (0.58)
616–04f	122 (48)	7,108 (1,598)	30.3 (22.3)	4.87 (15.97)	1.44 (0.57)

Table 10. Clamped medium.

8 Ply on 2-in. Platen					
Specimen ID No.	Drop Height cm (in.)	Maximum Load N (lbf)	Impact Energy J (ft-lbf)	Impact Velocity m/sec (ft/sec)	Maximum Deflection cm (in.)
616–37m	12.7 (5)	1,045 (235)	3.3 (2.4)	2.10 (6.89)	0.31 (0.12)
616–38m	12.7 (5)	939 (211)	2.3 (1.7)	1.76 (5.78)	No data
728–09m	12.7 (5)	936 (210)	3.0 (2.2)	1.61 (5.28)	No data
728–11m	12.7 (5)	1,036 (233)	2.9 (2.1)	1.57 (5.14)	0.46 (0.18)

16 Ply on 4-in. Platen					
Specimen ID No.	Drop Height cm (in.)	Maximum Load N (lbf)	Impact Energy J (ft-lbf)	Impact Velocity m/sec (ft/sec)	Maximum Deflection cm (in.)
616–25m	35.6 (14)	3,634 (817)	8.6 (6.4)	2.61 (8.55)	0.48 (0.19)
616–26m	35.6 (14)	3,629 (816)	8.7 (6.4)	2.61 (8.57)	0.48 (0.19)
616–27m	35.6 (14)	3,665 (824)	8.7 (6.4)	2.61 (8.55)	0.48 (0.19)
616–28m	35.6 (14)	3,728 (838)	8.9 (6.5)	2.60 (8.53)	0.48 (0.19)

48 Ply on 12-in. Platen					
Specimen ID No.	Drop Height cm (in.)	Maximum Load N (lbf)	Impact Energy J (ft-lbf)	Impact Velocity m/sec (ft/sec)	Maximum Deflection cm (in.)
61599–04m	119 (47)	26,823 (6,030)	155 (115)	4.71 (15.46)	1.26 (0.50)
61599–05m	119 (47)	23,420 (5,265)	157 (115)	4.73 (15.52)	1.17 (0.46)

Table 11. Clamped stiff.

16 Ply on 2-in. Platen					
Specimen ID No.	Drop Height cm (in.)	Maximum Load N (lbf)	Impact Energy J (ft-lbf)	Impact Velocity m/sec (ft/sec)	Maximum Deflection cm (in.)
616–29s	34.3 (13.5)	3,239 (728)	8.4 (6.2)	2.57 (8.43)	0.43 (0.17)
616–30s	26.7 (10.5)	2,922 (657)	6.4 (4.7)	2.23 (7.33)	0.34 (0.13)
616–31s	33.0 (13.0)	3,105 (698)	8.1 (6.0)	2.52 (8.27)	0.42 (0.17)
616–32s	33.0 (13.0)	3,100 (697)	8.0 (5.9)	2.51 (8.24)	0.41 (0.16)

32 Ply on 4-in. Platen					
Specimen ID No.	Drop Height cm (in.)	Maximum Load N (lbf)	Impact Energy J (ft-lbf)	Impact Velocity m/sec (ft/sec)	Maximum Deflection cm (in.)
616–20s	71.1 (28)	7,313 (1,644)	17.2 (12.7)	3.67 (12.05)	0.38 (0.15)
616–21s	71.1 (28)	7,268 (1,634)	17.4 (12.8)	3.69 (12.12)	0.39 (0.15)
616–22s	71.1 (28)	7,544 (1,696)	17.1 (12.6)	3.66 (12.00)	0.38 (0.15)
616–24s	71.1 (28)	7,322 (1,646)	17.5 (12.9)	3.70 (12.14)	No Data

48 Ply on 6-in. Platen					
Specimen ID No.	Drop Height cm (in.)	Maximum Load N (lbf)	Impact Energy J (ft-lbf)	Impact Velocity m/sec (ft/sec)	Maximum Deflection cm (in.)
727–04s	63.5 (25)	22,788 (5,123)	80.7 (59.5)	3.40 (11.15)	0.65 (0.26)
727–05s	63.5 (25)	23,100 (5,193)	80.7 (59.5)	3.40 (11.15)	0.64 (0.25)

Table 12. Simply supported flex.

8 Ply on 6-in. Platen					
Specimen ID No.	Drop Height cm (in.)	Maximum Load N (lbf)	Impact Energy J (ft-lbf)	Impact Velocity m/sec (ft/sec)	Maximum Deflection cm (in.)
727-06f	44.4 (17.5)	1,850 (416)	10.2 (7.5)	2.9 (9.6)	No data
727-07f	44.4 (17.5)	1,766 (397)	9.6 (7.1)	2.9 (9.3)	1.18 (0.47)
727-08f	44.4 (17.5)	1,850 (416)	10.2 (7.5)	2.9 (9.6)	1.23 (0.48)
727-09f	44.4 (17.5)	1,873 (421)	10.1 (7.5)	2.9 (9.6)	1.34 (0.53)
727-10f	44.4 (17.5)	1,873 (421)	9.7 (7.1)	2.9 (9.4)	1.24 (0.49)

16 Ply on 12-in. Platen					
Specimen ID No.	Drop Height cm (in.)	Maximum Load N (lbf)	Impact Energy J (ft-lbf)	Impact Velocity m/sec (ft/sec)	Maximum Deflection cm (in.)
728-05f	132 (52.0)	4,862 (1,093)	29.7 (21.9)	4.8 (15.8)	1.61 (0.63)
728-06f	149 (58.5)	5,400 (1,214)	32.2 (23.8)	5.0 (16.5)	1.64 (0.64)
728-07f	149 (58.5)	5,373 (1,208)	31.6 (23.3)	5.0 (16.3)	No data

Table 13. Simply supported medium.

8 Ply on 2-in. Platen					
Specimen ID No.	Drop Height cm (in.)	Maximum Load N (lbf)	Impact Energy J (ft-lbf)	Impact Velocity m/sec (ft/sec)	Maximum Deflection cm (in.)
728–02m	7.6 (3.0)	1,023 (230)	1.8 (1.3)	1.23 (4.04)	0.29 (0.11)
728–03m	5.7 (2.3)	974 (219)	1.3 (0.9)	1.03 (3.38)	0.23 (0.09)
728–04m	4.5 (1.8)	907 (204)	1.1 (0.8)	0.96 (3.16)	No data

16 Ply on 4-in. Platen					
Specimen ID No.	Drop Height cm (in.)	Maximum Load N (lbf)	Impact Energy J (ft-lbf)	Impact Velocity m/sec (ft/sec)	Maximum Deflection cm (in.)
727–11m	49.5 (19.5)	3,723 (837)	11.9 (8.8)	3.18 (10.43)	0.63 (0.25)
727–12m	46.4 (18.3)	3,701 (832)	10.6 (7.8)	2.30 (9.83)	0.58 (0.23)
727–13m	39.4 (15.5)	3,670 (825)	8.3 (6.1)	2.65 (8.71)	0.52 (0.20)
727–14m	24.1 (9.5)	2,998 (674)	5.6 (4.1)	2.18 (7.15)	0.44 (0.17)
727–15m	24.1 (9.5)	2,963 (666)	5.3 (3.9)	2.13 (6.99)	0.34 (0.17)

48 Ply on 12-in. Platen					
Specimen ID No.	Drop Height cm (in.)	Maximum Load N (lbf)	Impact Energy J (ft-lbf)	Impact Velocity m/sec (ft/sec)	Maximum Deflection cm (in.)
61599–02m	119 (47)	23,562 (5,297)	158 (116)	4.75 (15.57)	1.42 (0.56)
61599–03m	119 (47)	29,492 (6,630)	159 (116)	4.75 (15.58)	1.42 (0.56)

Table 14. Simply supported stiff.

16 Ply on 2-in. Platen					
Specimen ID No.	Drop Height cm (in.)	Maximum Load N (lbf)	Impact Energy J (ft-lbf)	Impact Velocity m/sec (ft/sec)	Maximum Deflection cm (in.)
727–20s	52.7 (20.8)	2,922 (657)	4.5 (3.3)	1.95 (6.40)	0.28 (0.11)
727–21s	20.3 (8.0)	2,771 (623)	4.5 (3.3)	1.96 (6.42)	0.28 (0.11)
727–22s	16.5 (6.5)	3,350 (753)	3.9 (2.8)	1.81 (5.95)	0.27 (0.11)
728–01s	16.5 (6.5)	3,051 (686)	3.9 (2.9)	1.82 (5.97)	0.27 (0.10)

32 Ply on 4-in. Platen					
Specimen ID No.	Drop Height cm (in.)	Maximum Load N (lbf)	Impact Energy J (ft-lbf)	Impact Velocity m/sec (ft/sec)	Maximum Deflection cm (in.)
727–16s	104 (41.0)	8,696 (1,955)	22.2 (12.7)	4.35 (14.27)	0.46 (0.18)
727–17s	112 (44.3)	9,101 (2,047)	24.0 (12.8)	4.52 (14.82)	0.48 (0.19)
727–18s	125 (49.0)	9,853 (2,215)	27.1 (12.6)	4.80 (15.74)	0.51 (0.20)
727–19s	125 (49.0)	9,346 (2,101)	24.1 (12.9)	4.53 (14.86)	0.48 (0.19)

48 Ply on 6-in. Platen					
Specimen ID No.	Drop Height cm (in.)	Maximum Load N (lbf)	Impact Energy J (ft-lbf)	Impact Velocity m/sec (ft/sec)	Maximum Deflection cm (in.)
727–02s	63.2 (24.9)	22,121 (4,973)	79.2 (58.4)	3.36 (11.04)	0.70 (0.27)
727–03s	63.2 (24.9)	22,810 (5,128)	82.6 (60.9)	3.39 (11.12)	No data

APPENDIX B—LOAD VERSUS DEFLECTION PLOTS FOR IMPACT SPECIMENS

Impact specimen load versus deflection plots are displayed in figures 32–82.

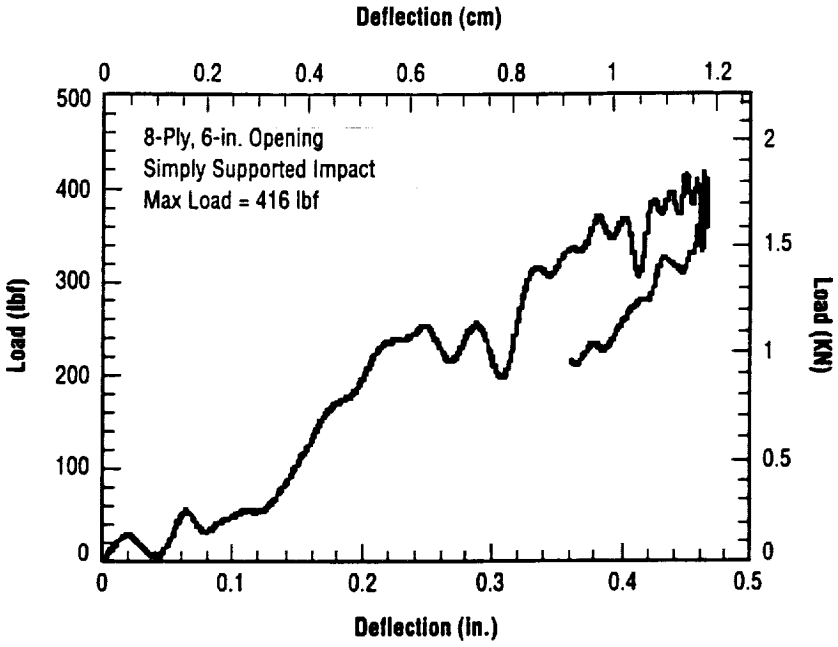

Figure 32. Load versus deflection specimen 727–06f.

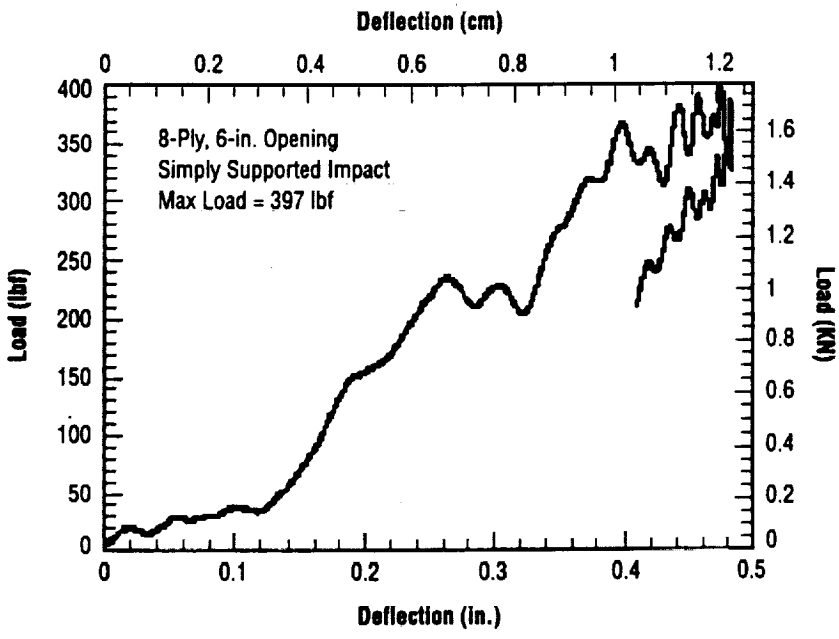

Figure 33. Load versus deflection specimen 727–07f.

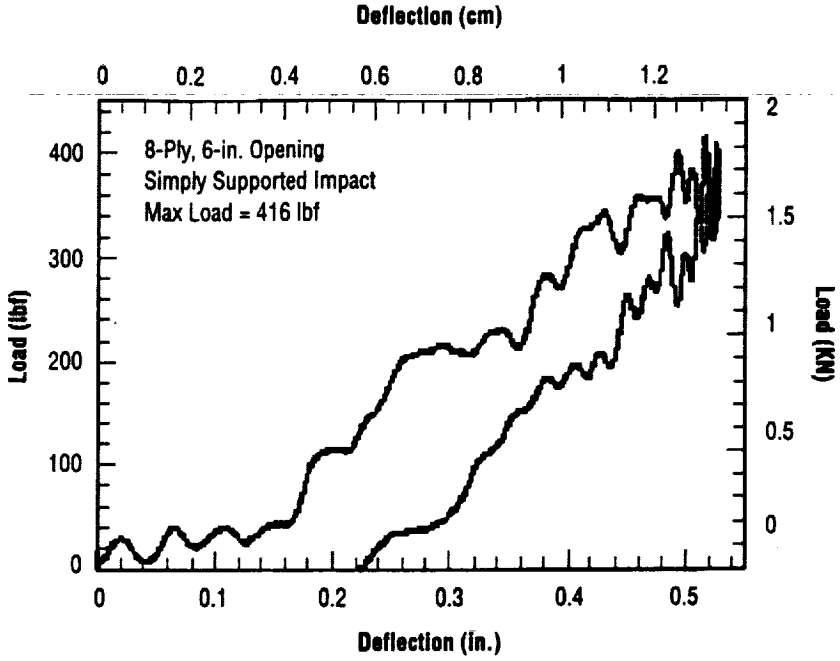

Figure 34. Load versus deflection specimen 727–08f.

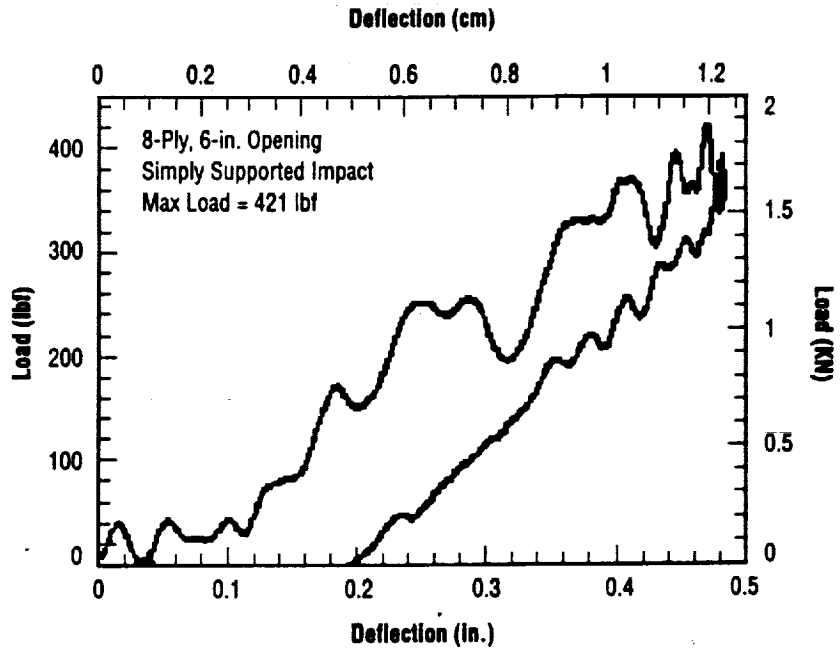

Figure 35. Load versus deflection specimen 727–09f.

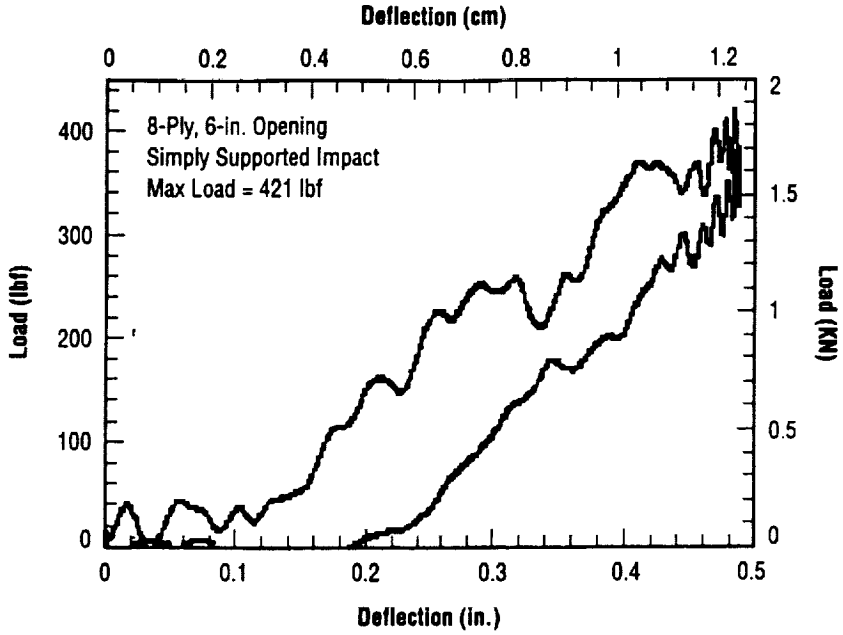

Figure 36. Load versus deflection specimen 727–10f.

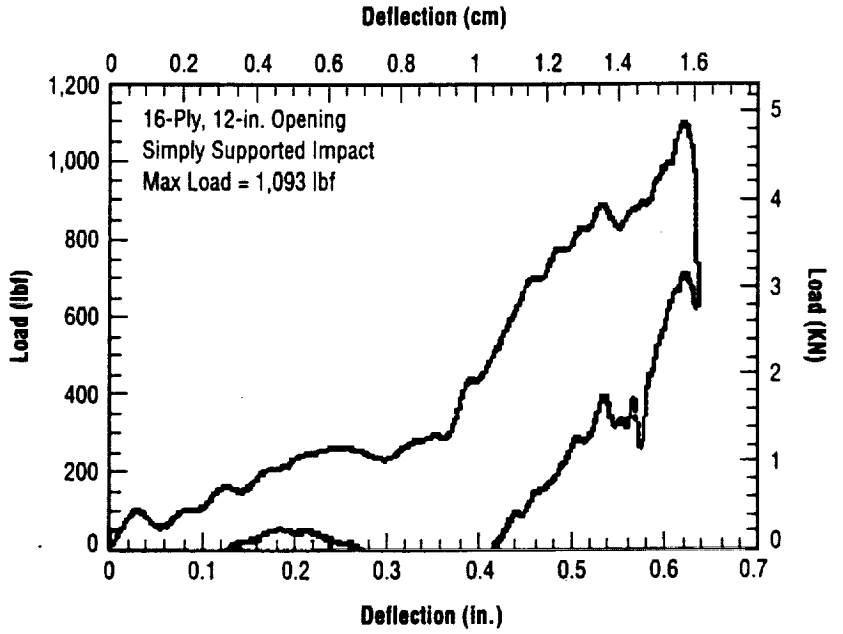

Figure 37. Load versus deflection specimen 728–05f.

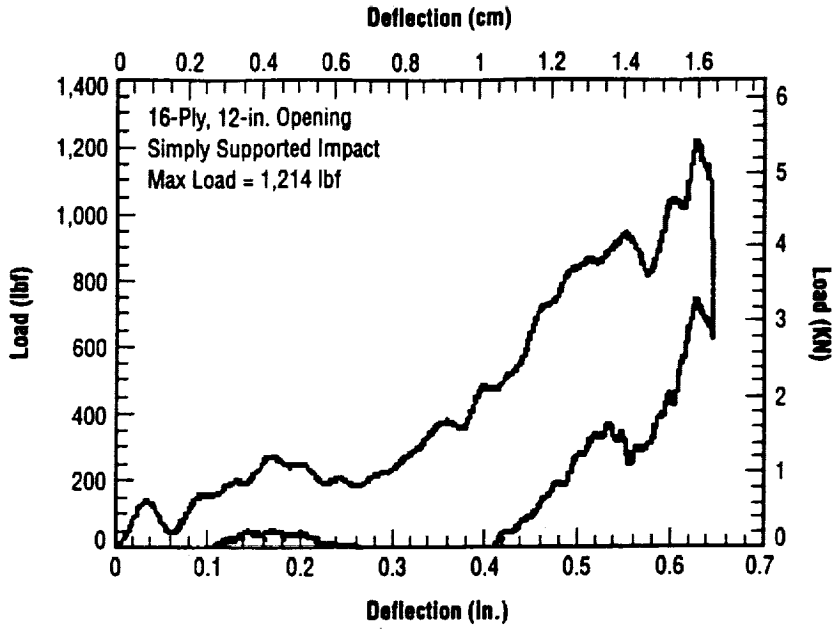

Figure 38. Load versus deflection specimen 728–06f.

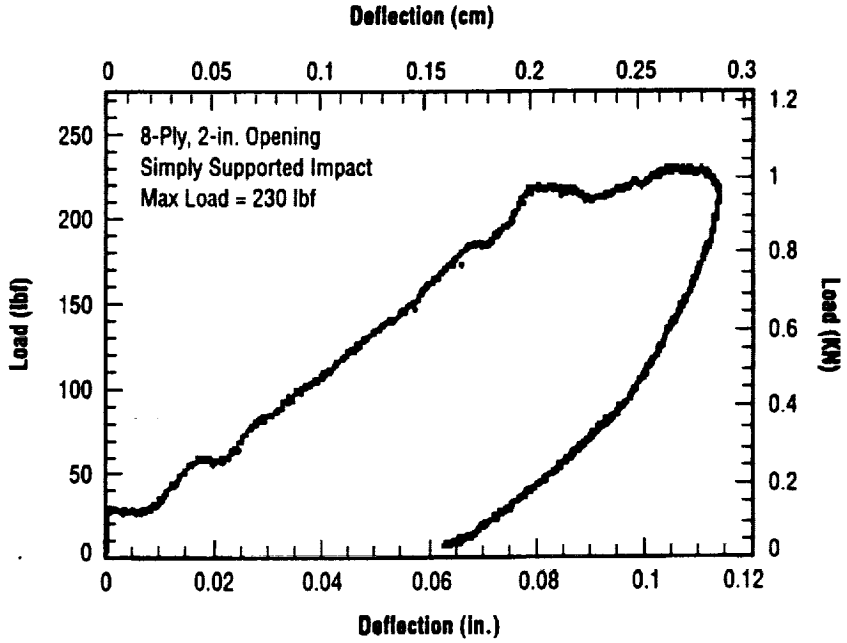

Figure 39. Load versus deflection specimen 728–02m.

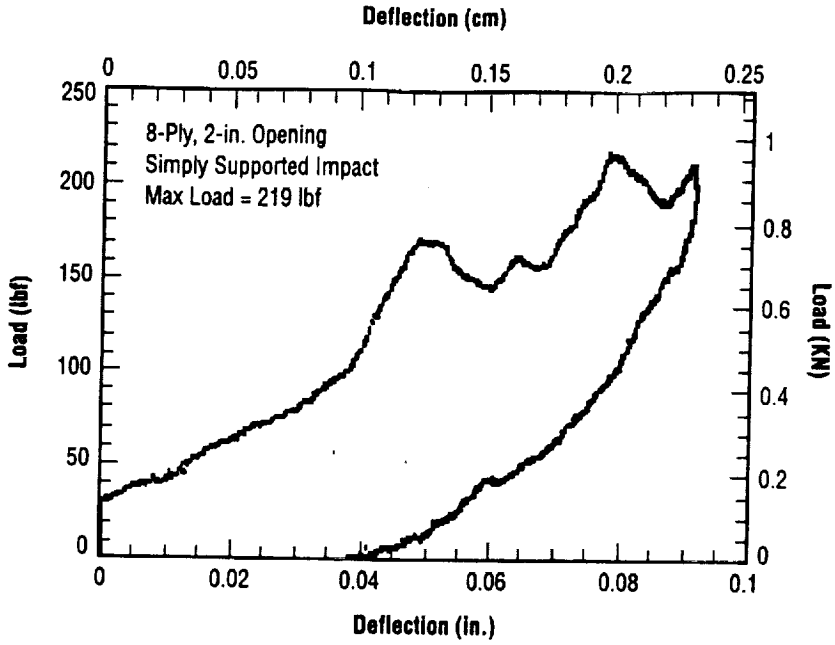

Figure 40. Load versus deflection specimen 728–03m.

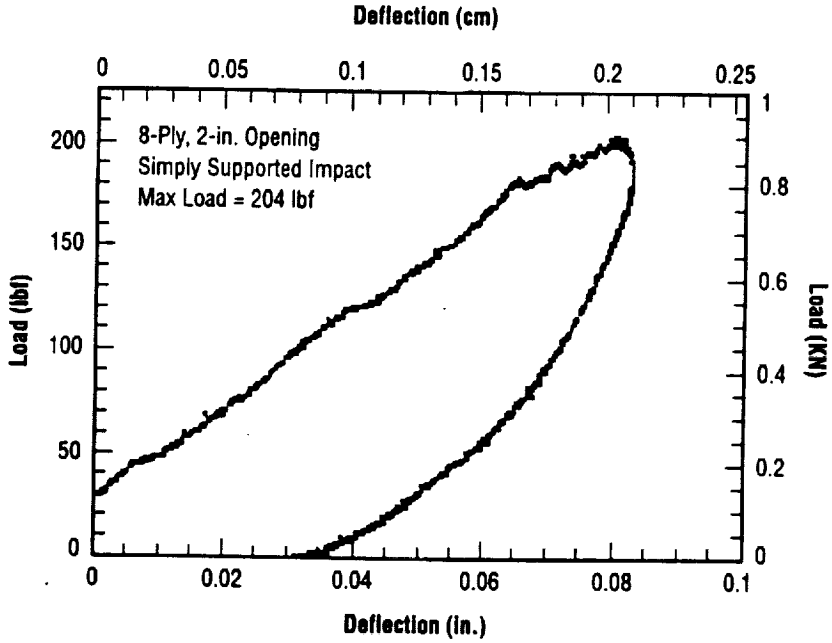

Figure 41. Load versus deflection specimen 728–04m.

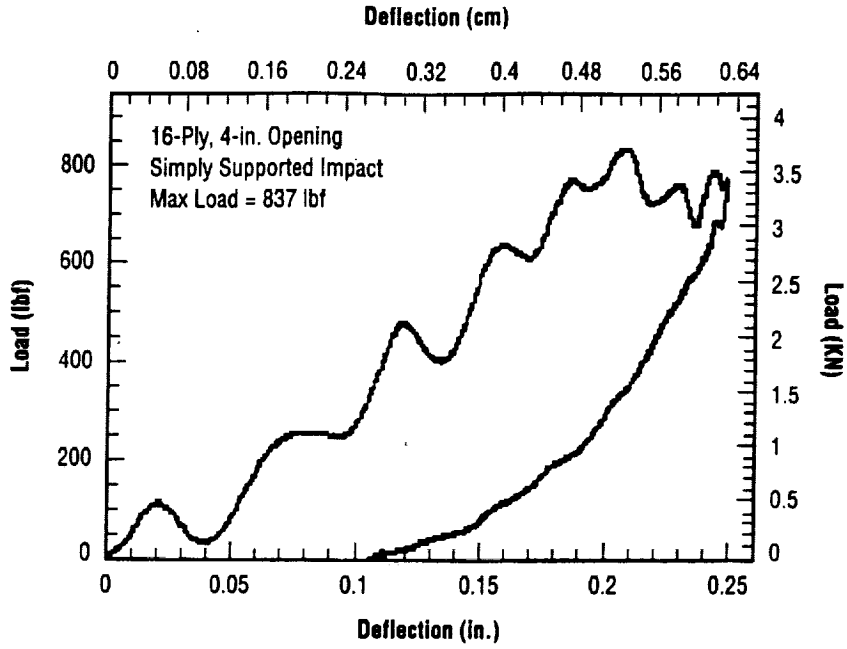

Figure 42. Load versus deflection specimen 727–11m.

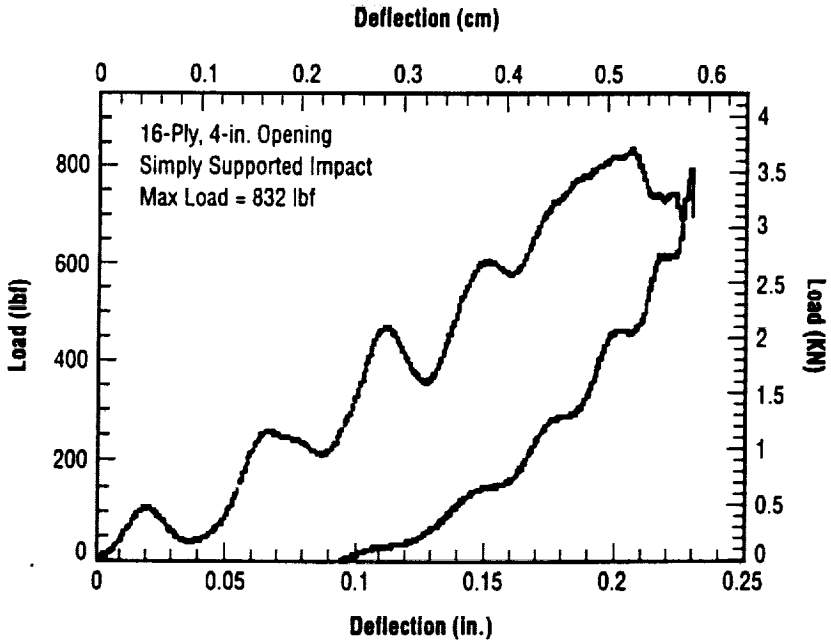

Figure 43. Load versus deflection specimen 727–12m.

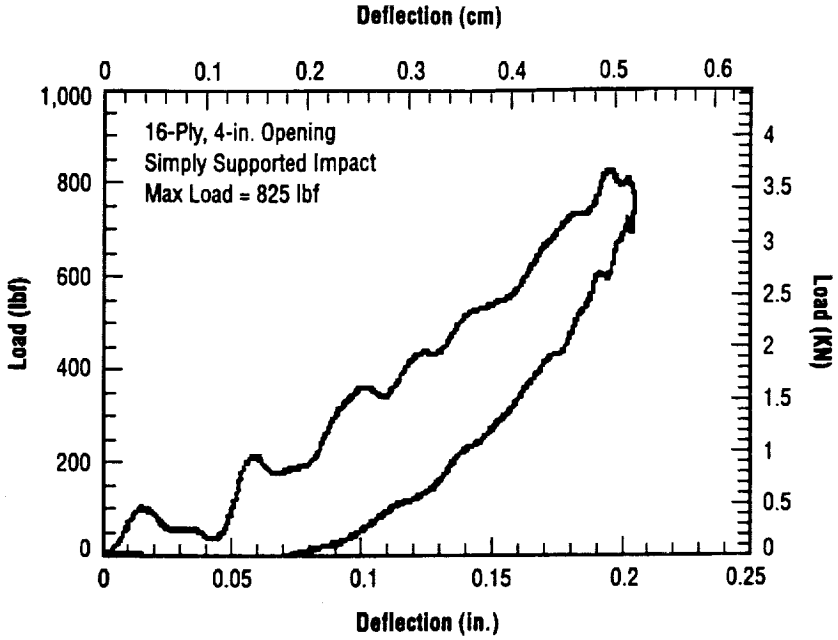

Figure 44. Load versus deflection specimen 727–13m.

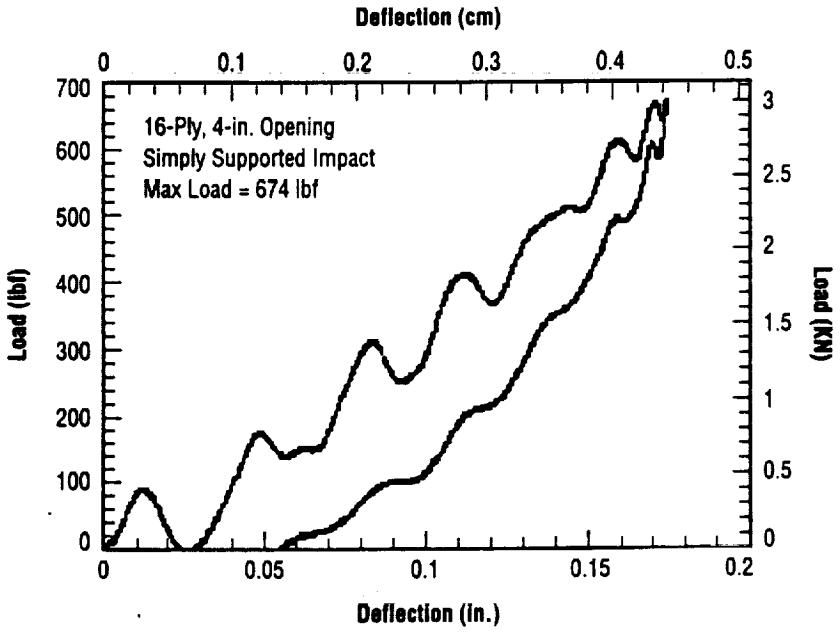

Figure 45. Load versus deflection specimen 727–14m.

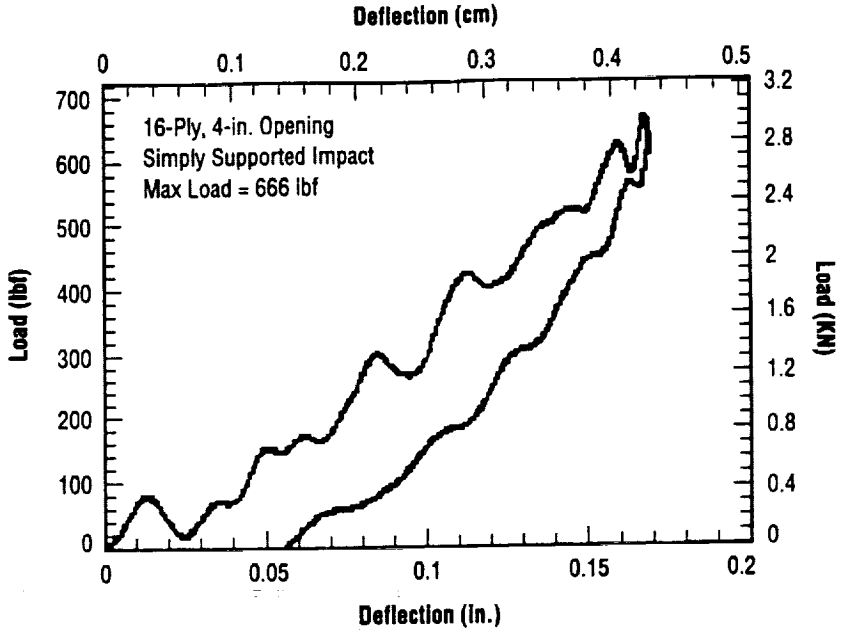

Figure 46. Load versus deflection specimen 727–15m.

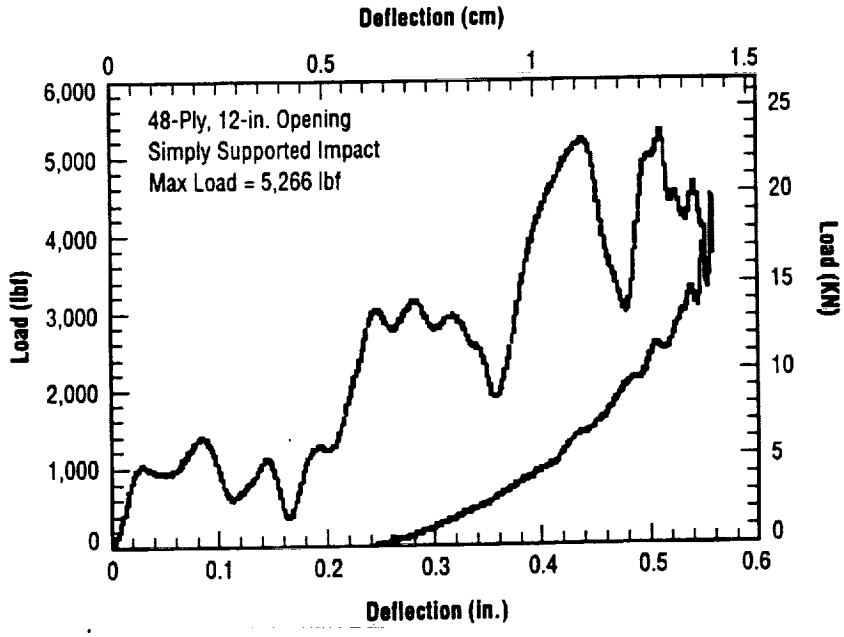

Figure 47. Load versus deflection specimen 61599–02m.

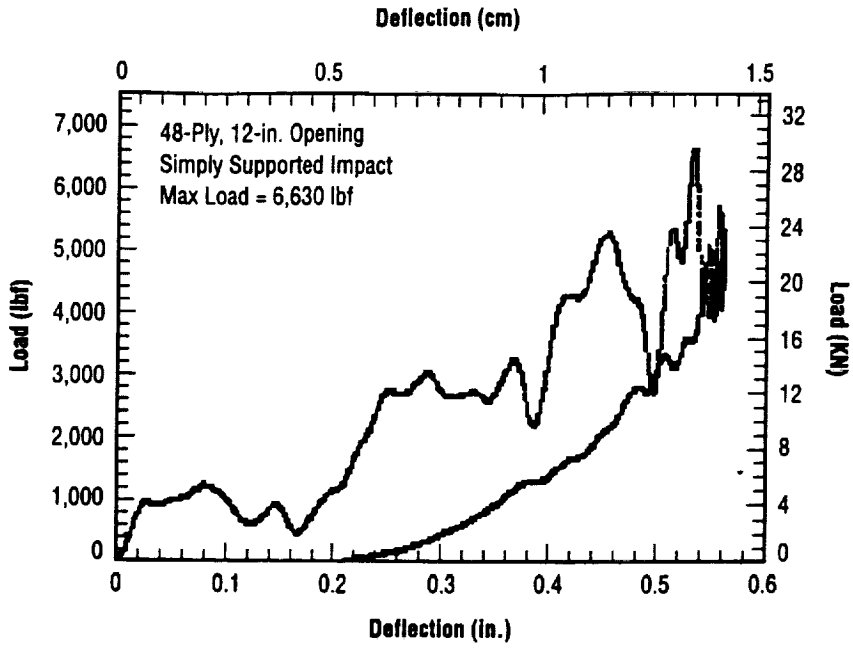

Figure 48. Load versus deflection specimen 61599–03m.

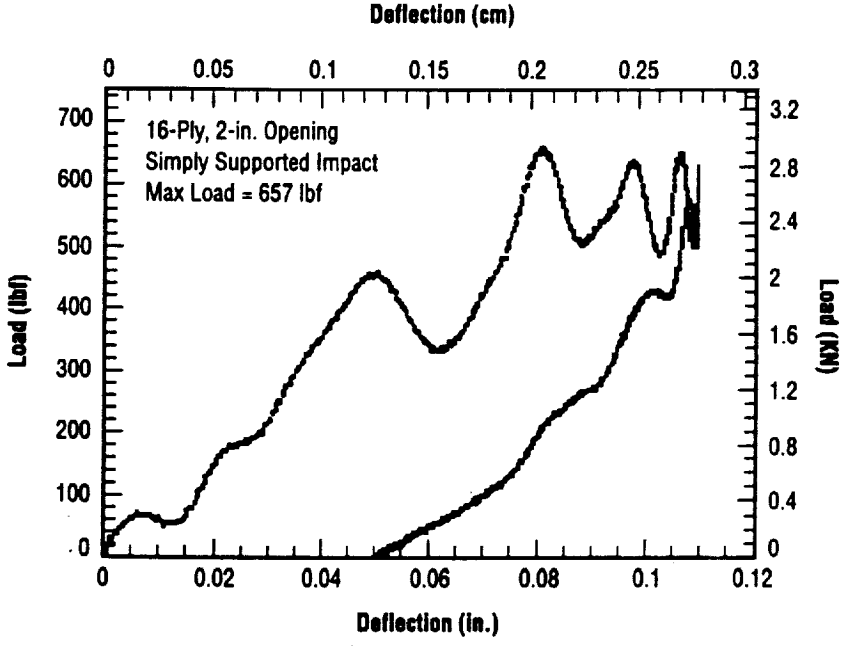

Figure 49. Load versus deflection specimen 727–20s.

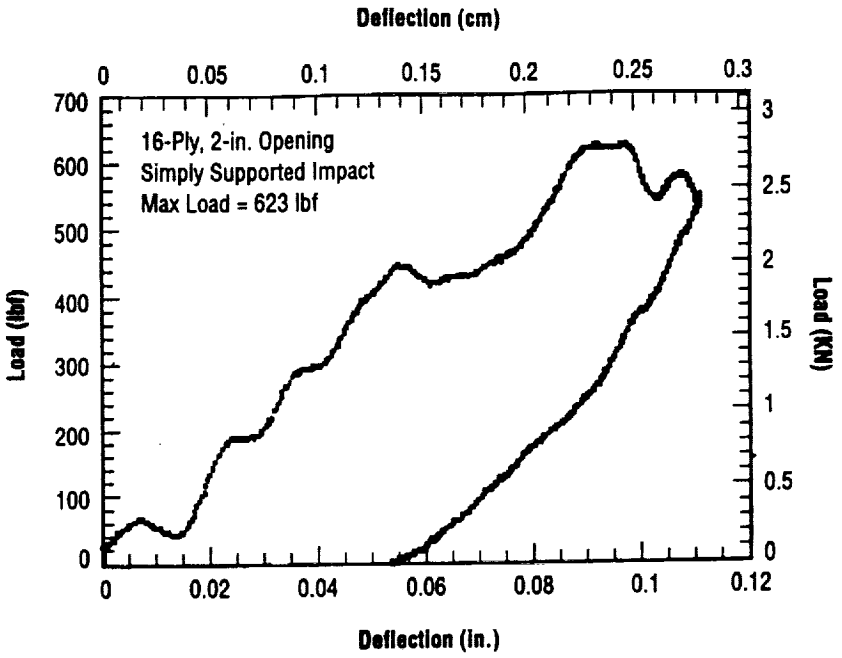

Figure 50. Load versus deflection specimen 727–21s.

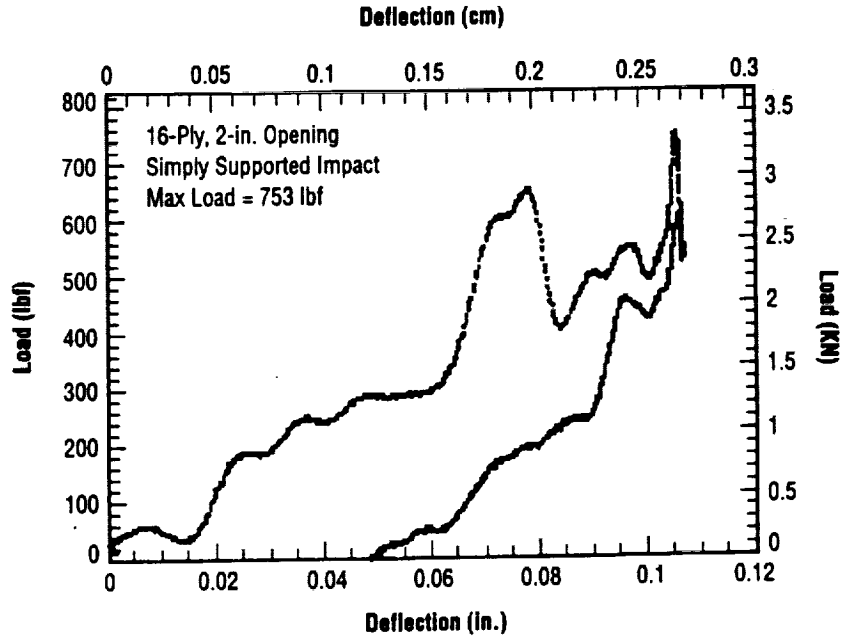

Figure 51. Load versus deflection specimen 727–22s.

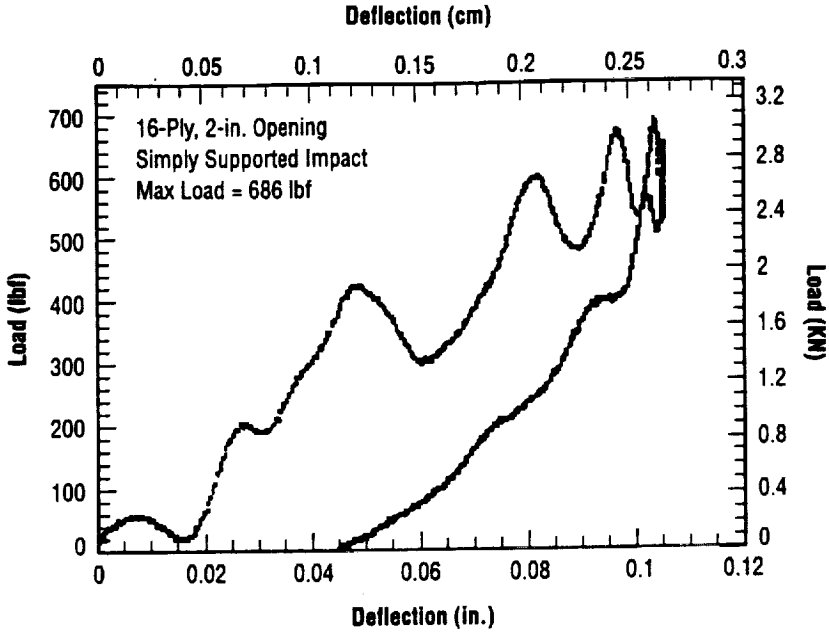

Figure 52. Load versus deflection specimen 728–01s.

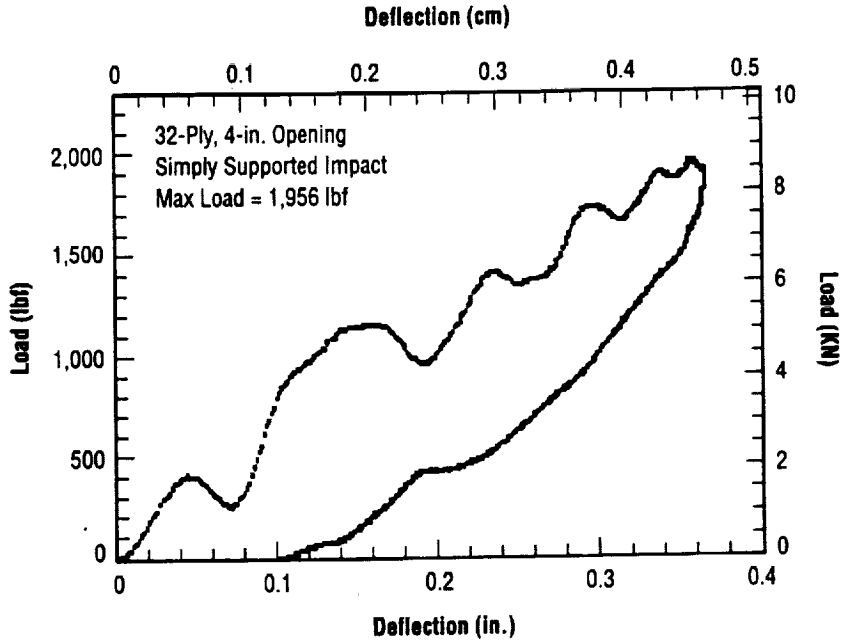

Figure 53. Load versus deflection specimen 727–16s.

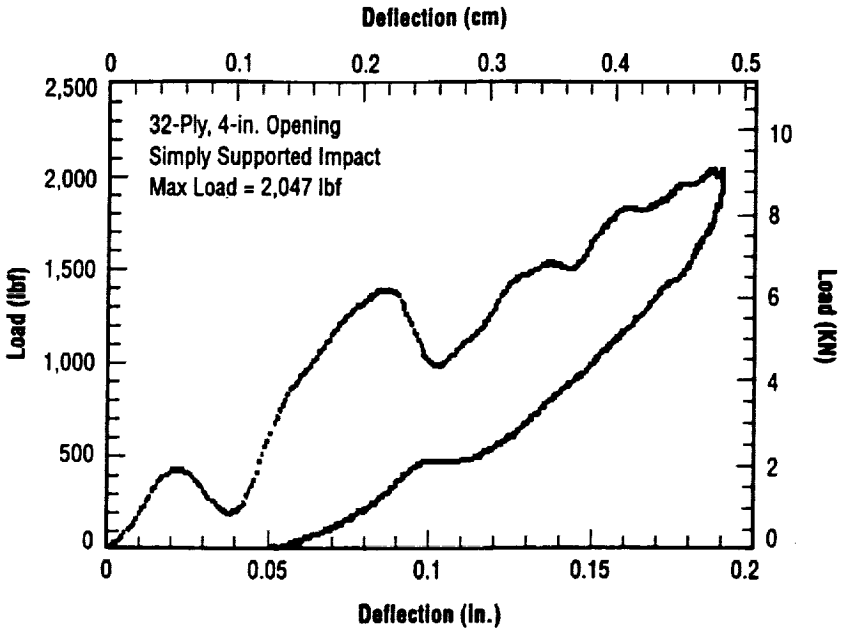

Figure 54. Load versus deflection specimen 727–17s.

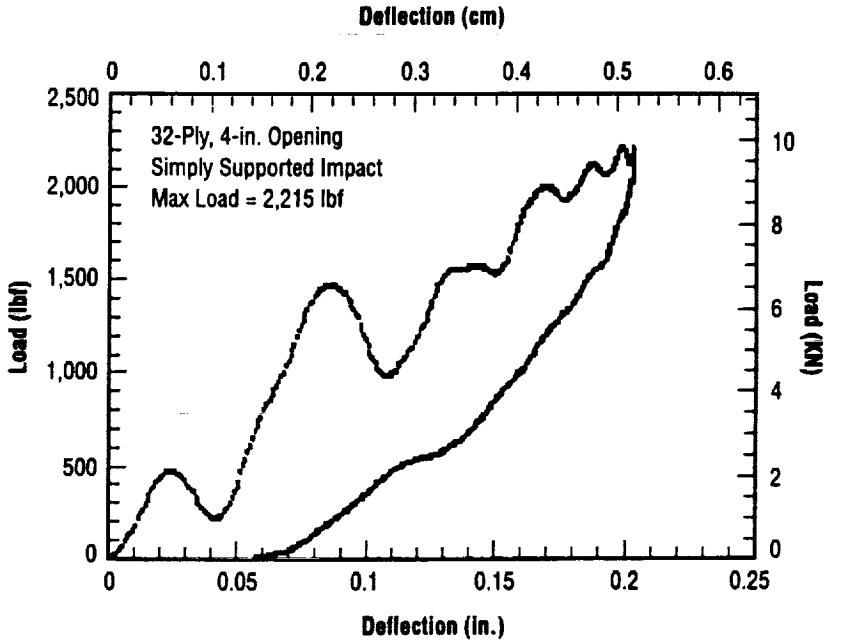

Figure 55. Load versus deflection specimen 727–18s.

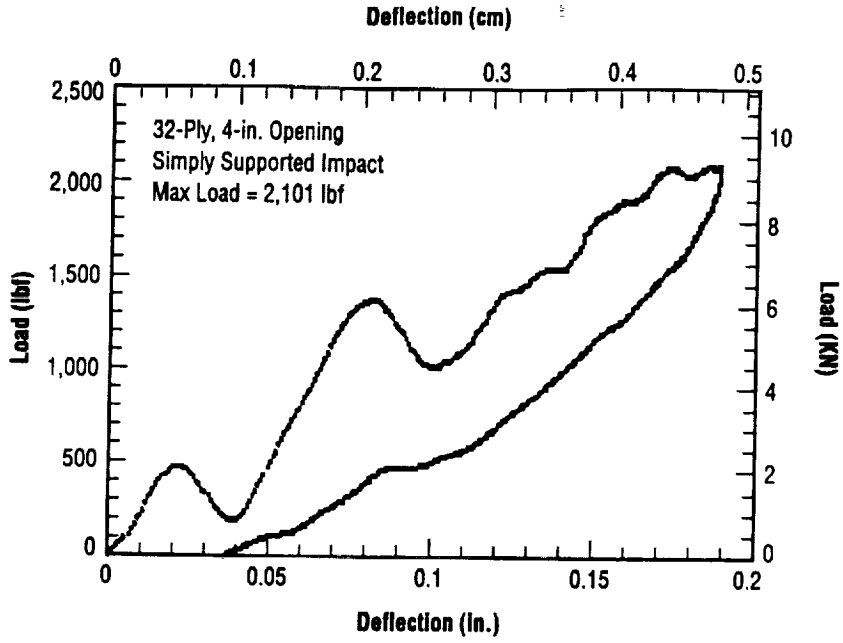

Figure 56. Load versus deflection specimen 727–19s.

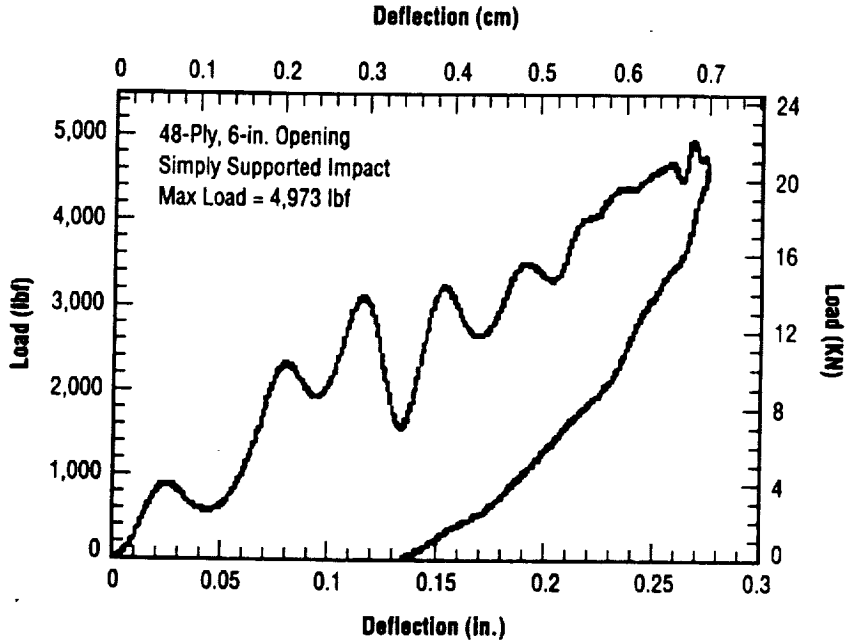

Figure 57. Load versus deflection specimen 727–02s.

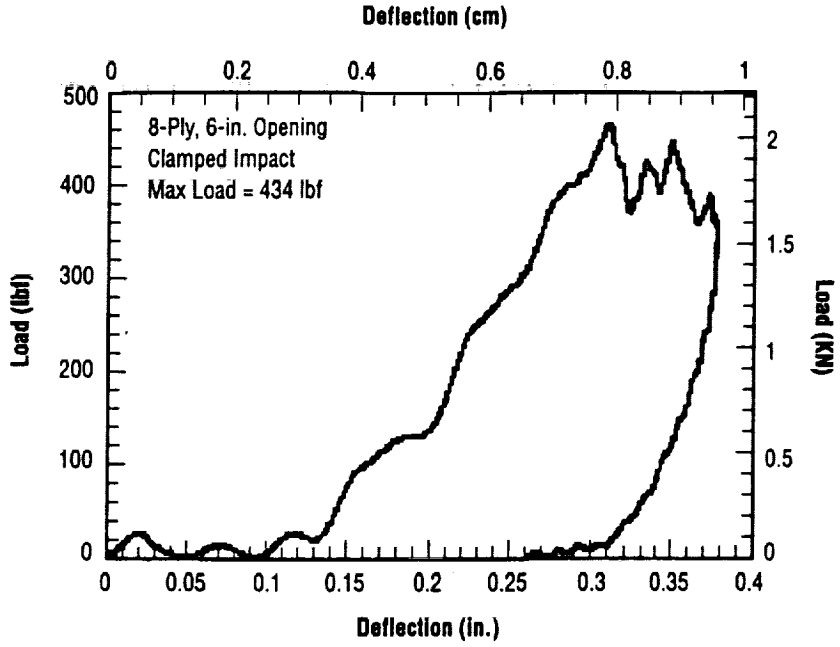

Figure 58. Load versus deflection specimen 616–15f.

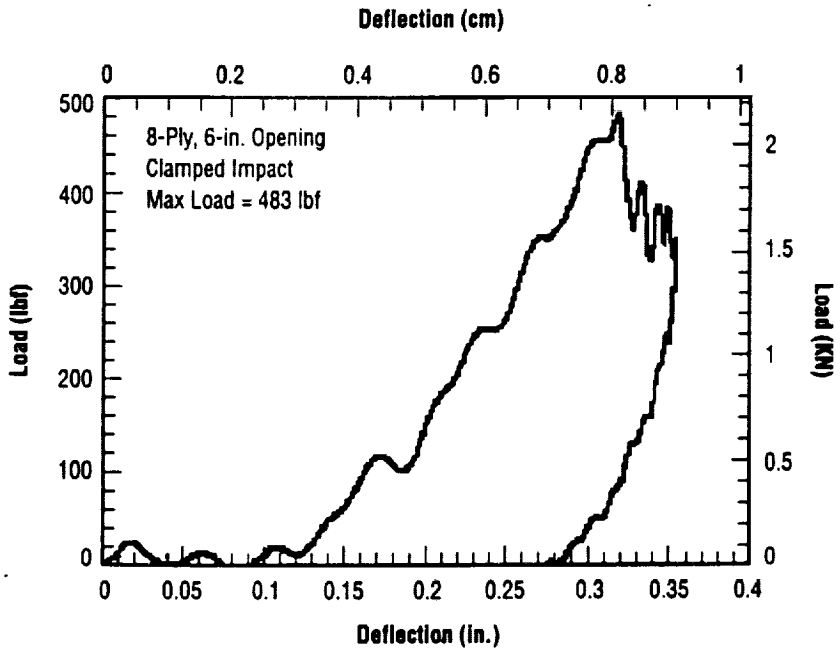

Figure 59. Load versus deflection specimen 616–16f.

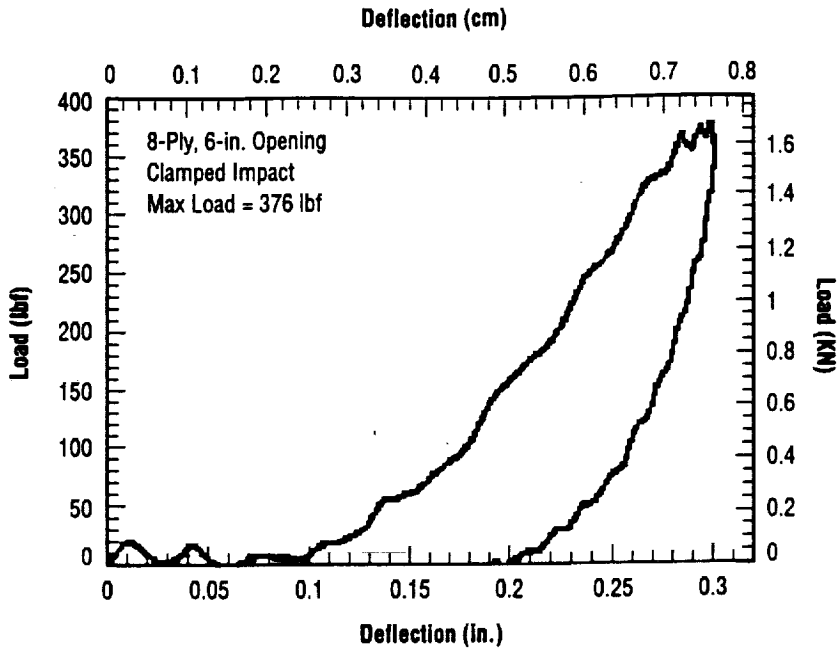

Figure 60. Load versus deflection specimen 616–17f.

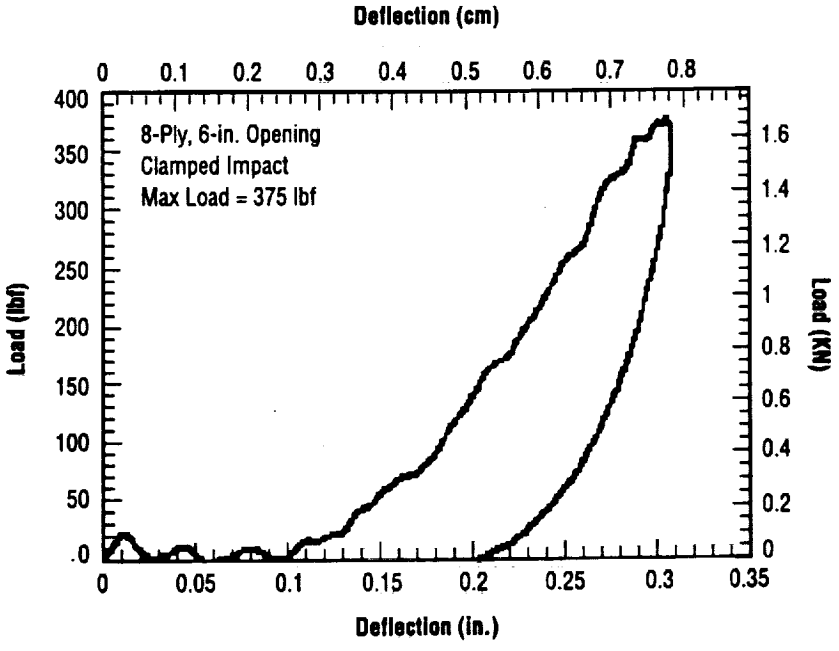

Figure 61. Load versus deflection specimen 616–18f.

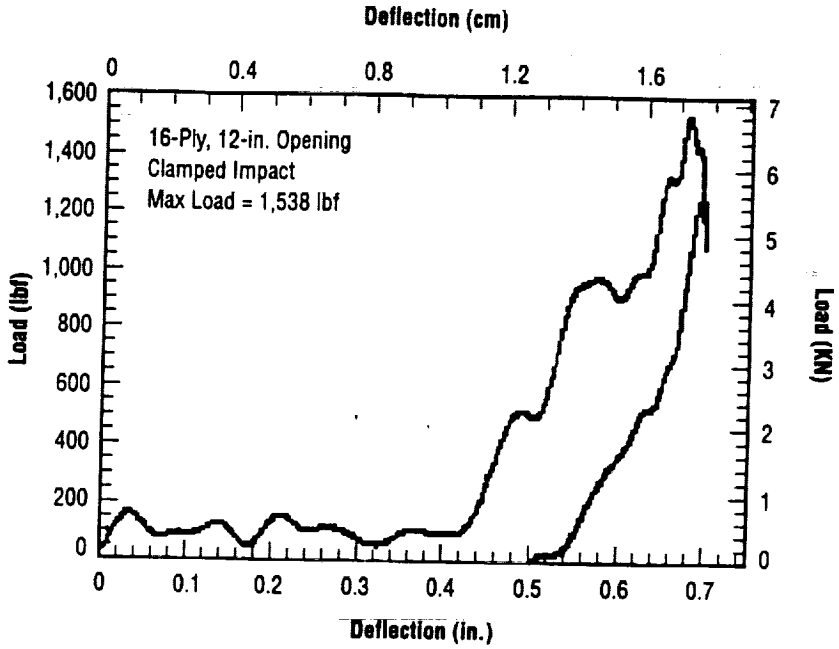

Figure 62. Load versus deflection specimen 616–01f.

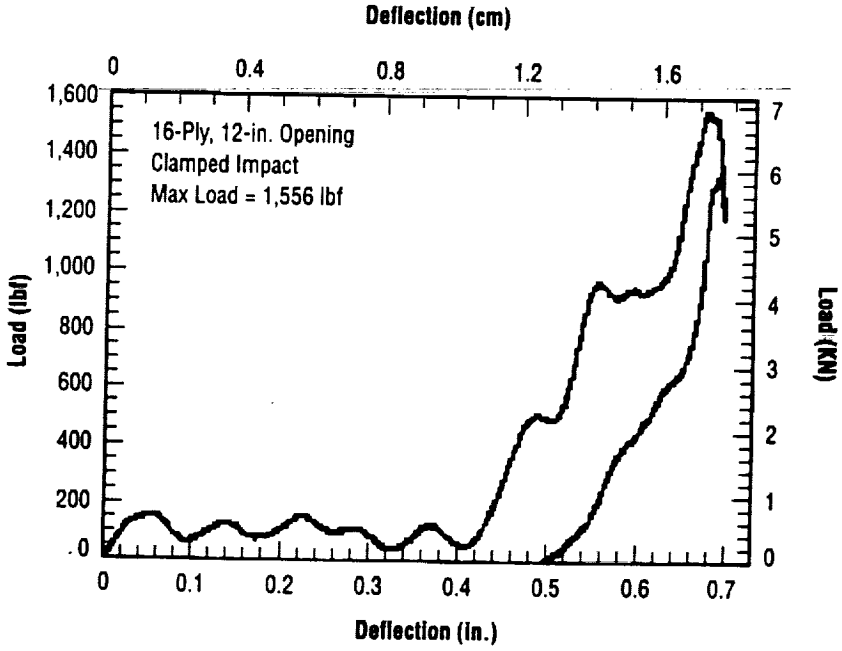

Figure 63. Load versus deflection specimen 616–02f.

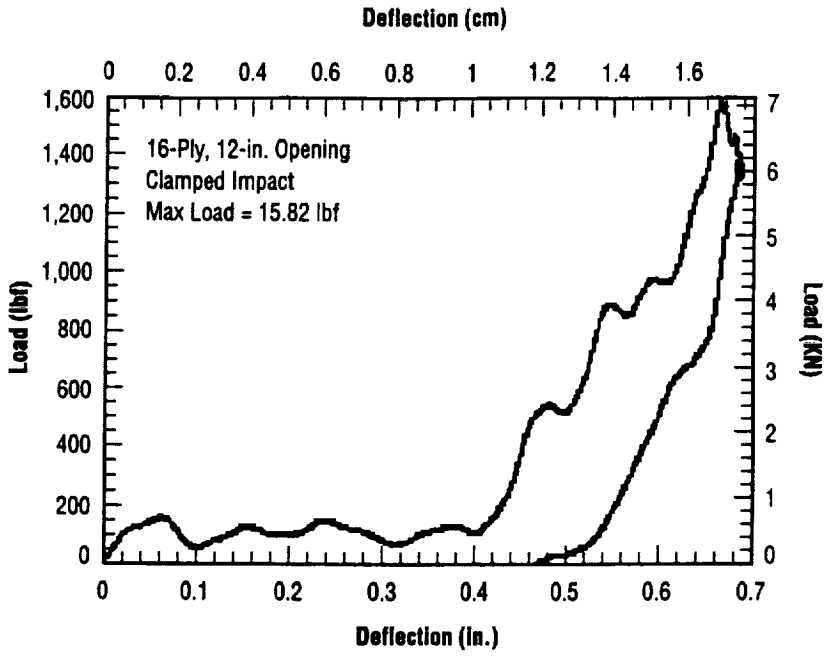

Figure 64. Load versus deflection specimen 616–03f.

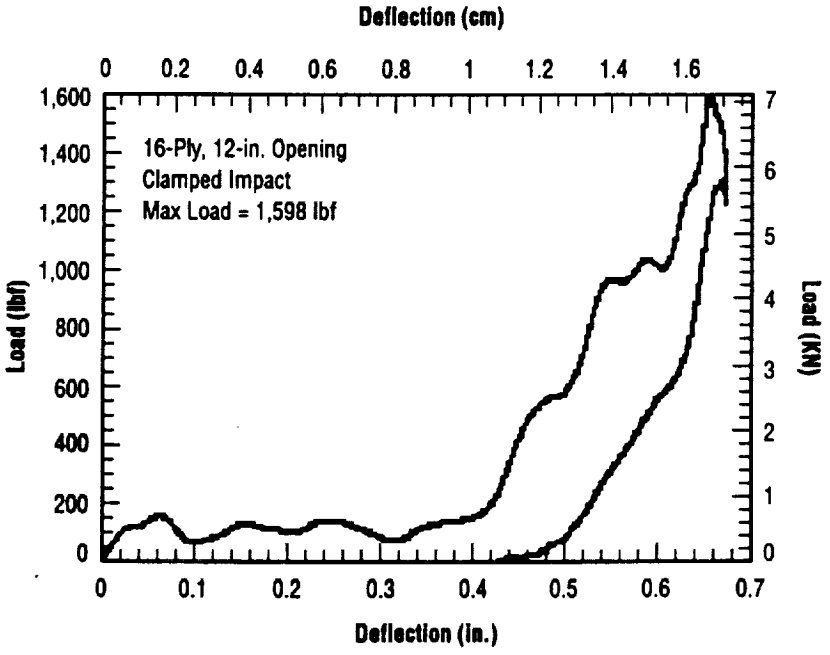

Figure 65. Load versus deflection specimen 616–04f.

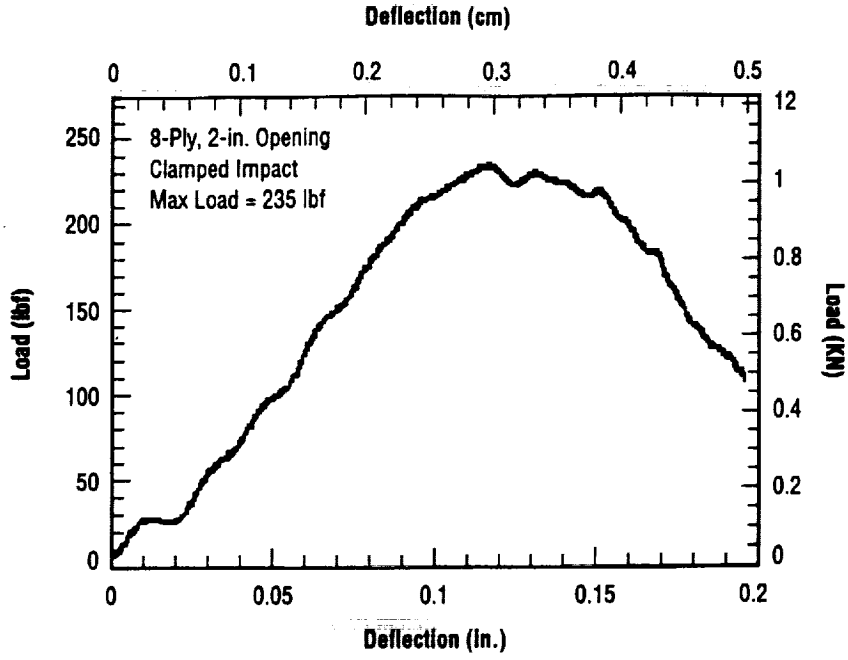

Figure 66. Load versus deflection specimen 616–37m.

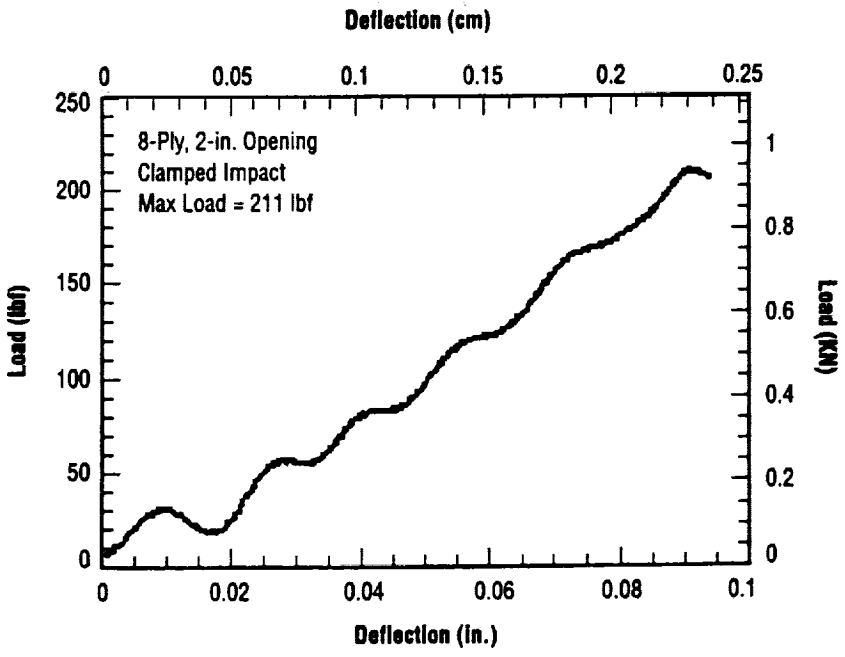

Figure 67. Load versus deflection specimen 616–38m.

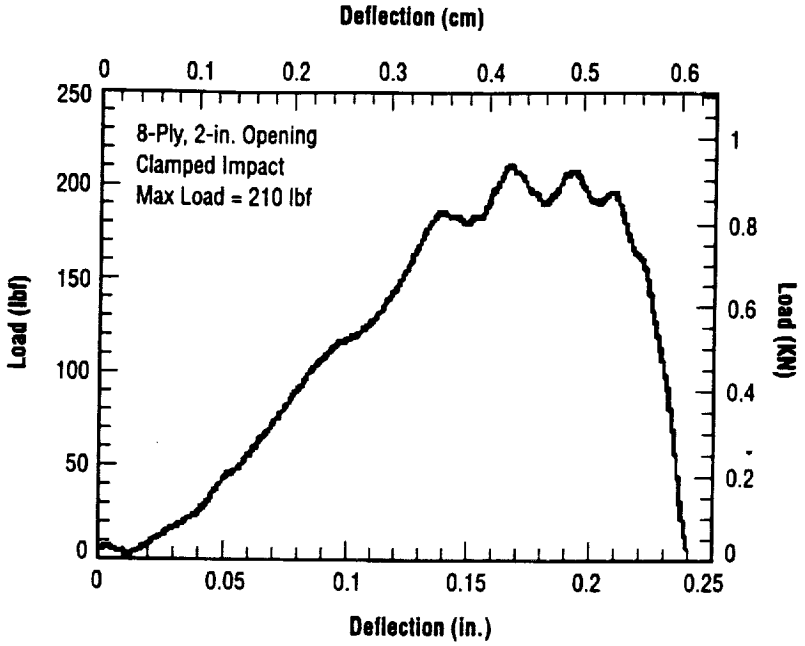

Figure 68. Load versus deflection specimen 728–09m.

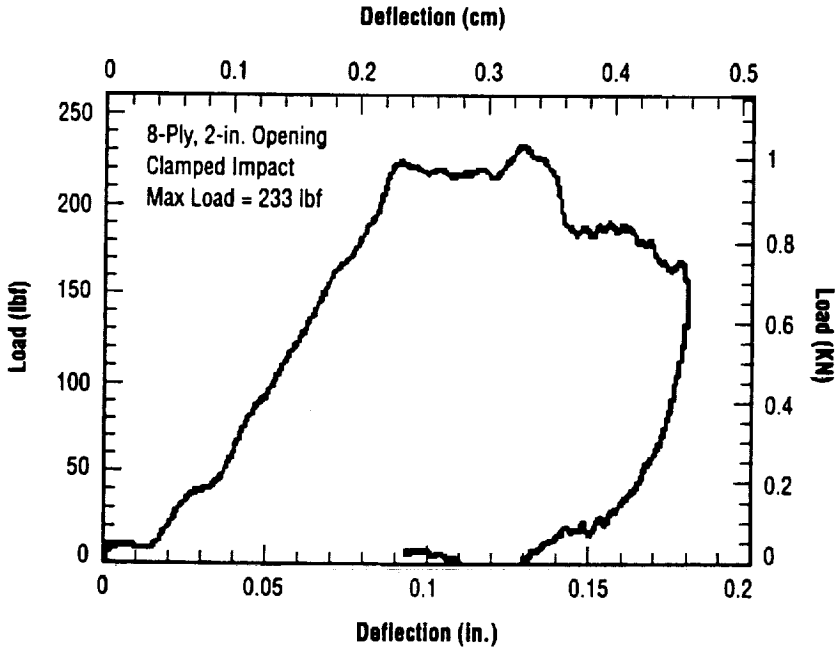

Figure 69. Load versus deflection specimen 728–11m.

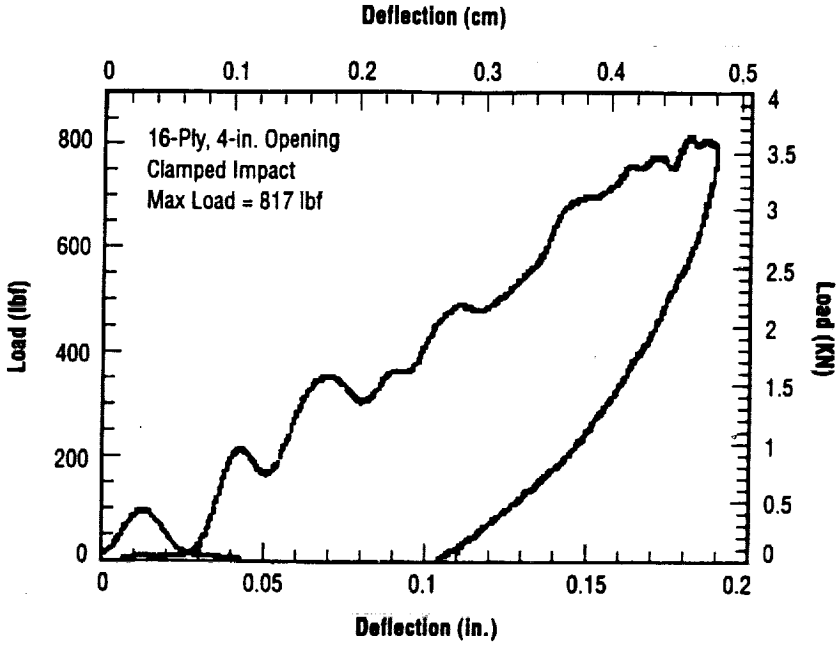

Figure 70. Load versus deflection specimen 616–25m.

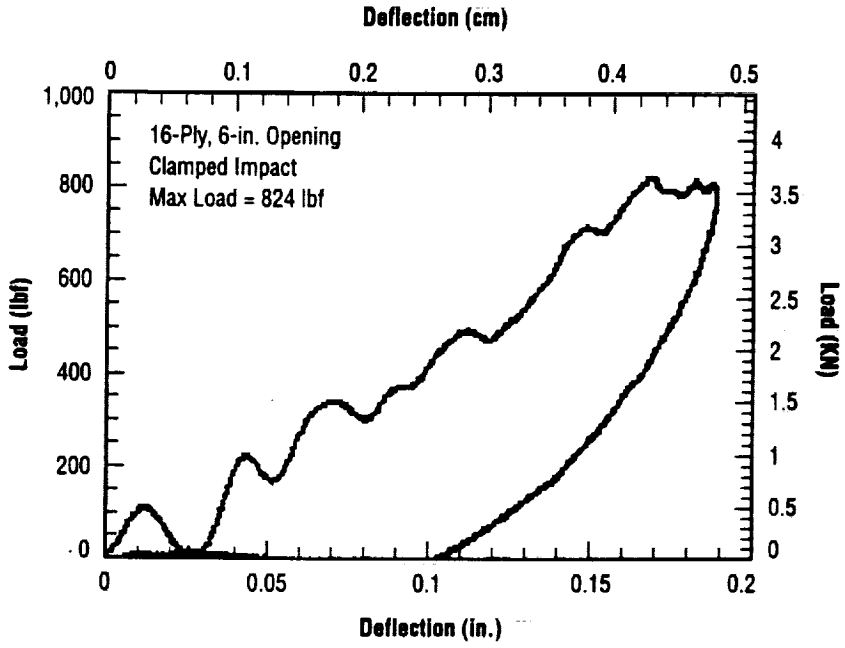

Figure 71. Load versus deflection specimen 616–26m.

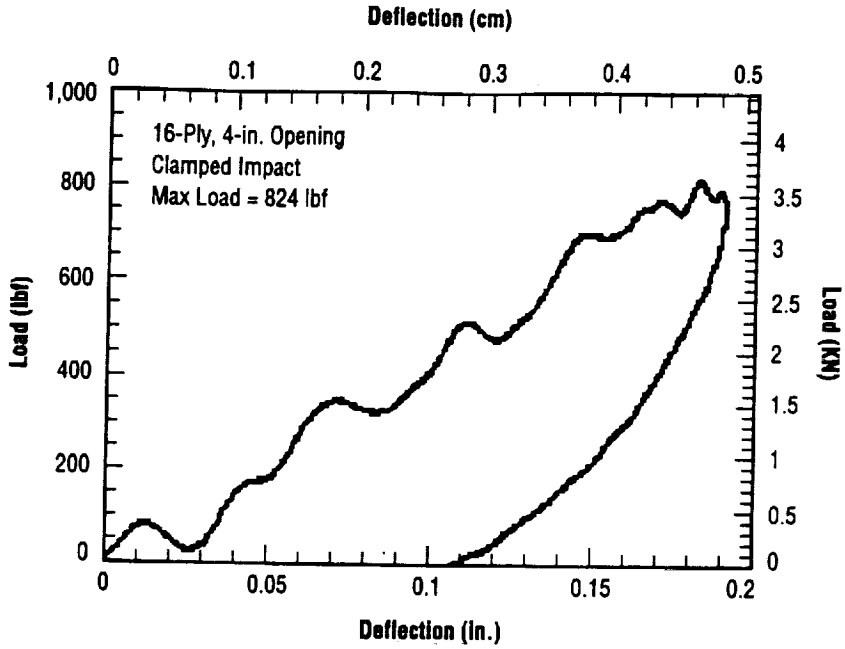

Figure 72. Load versus deflection specimen 616–27m.

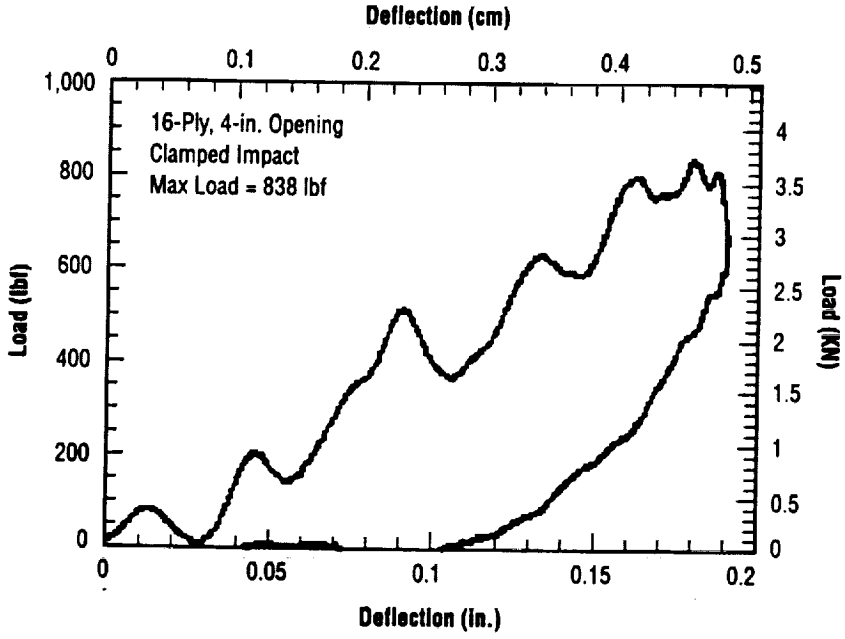

Figure 73. Load versus deflection specimen 616–28m.

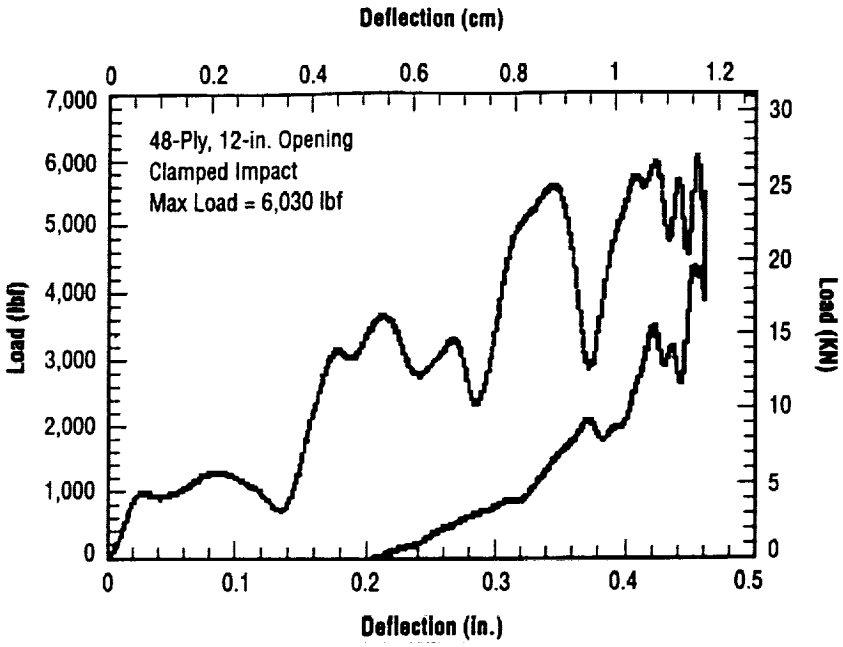

Figure 74. Load versus deflection specimen 61599–04m.

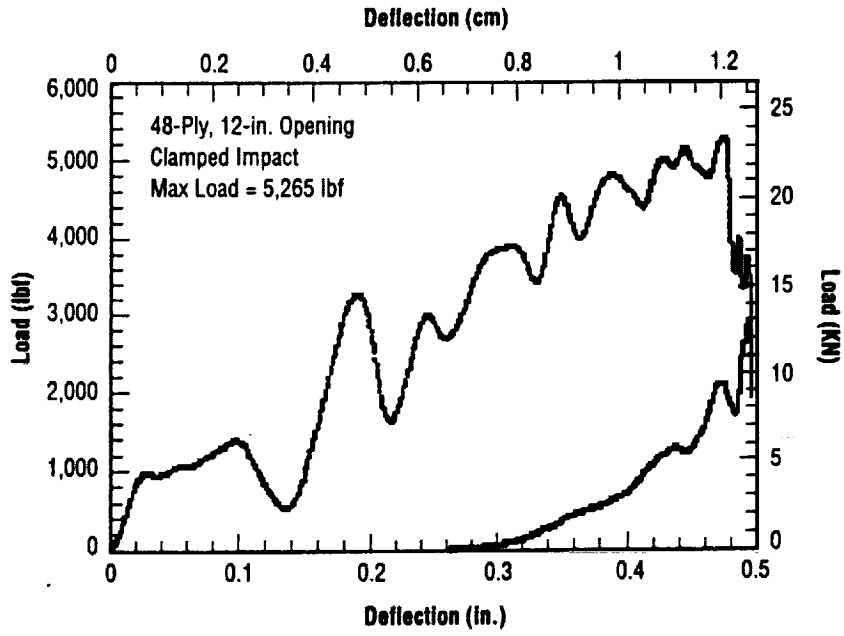

Figure 75. Load versus deflection specimen 61599–05m.

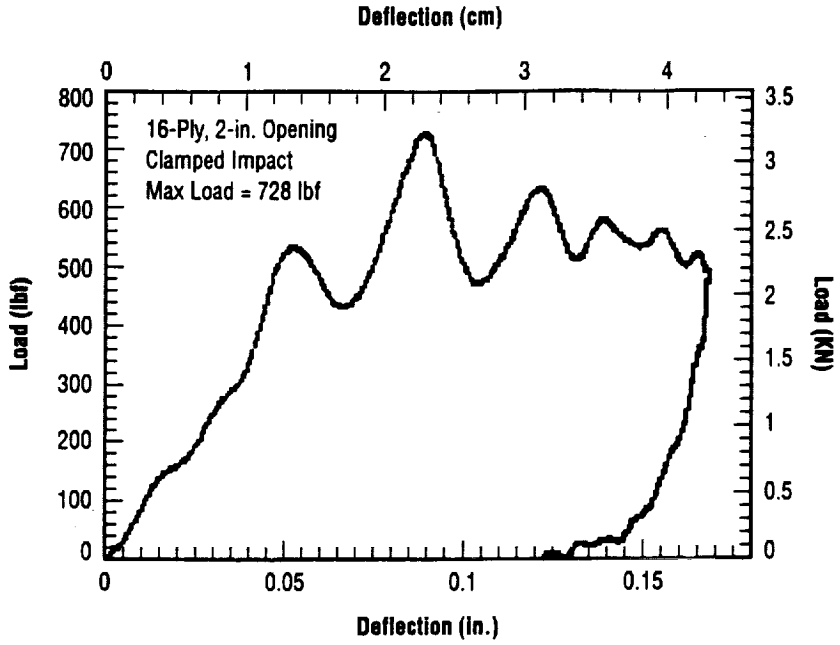

Figure 76. Load versus deflection specimen 616–29s.

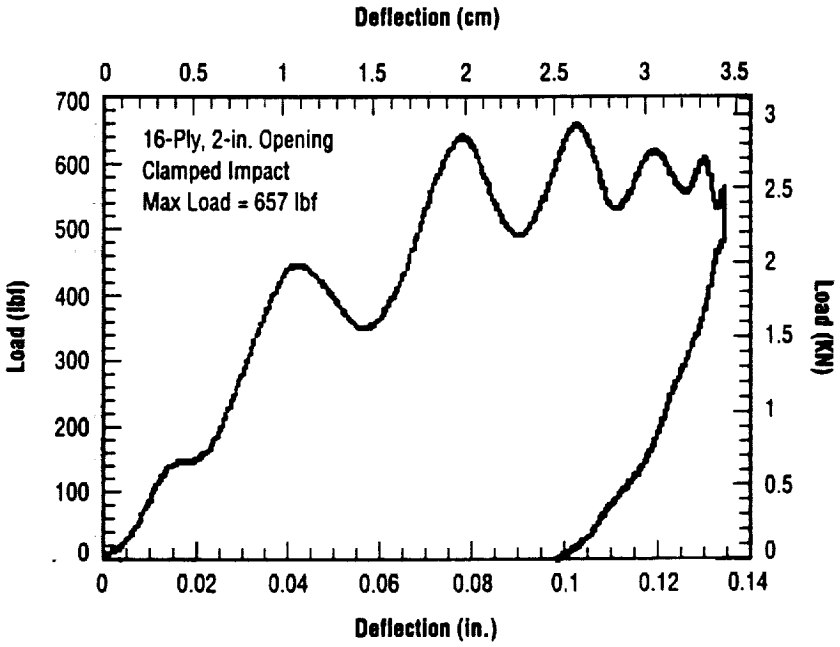

Figure 77. Load versus deflection specimen 616–30s.

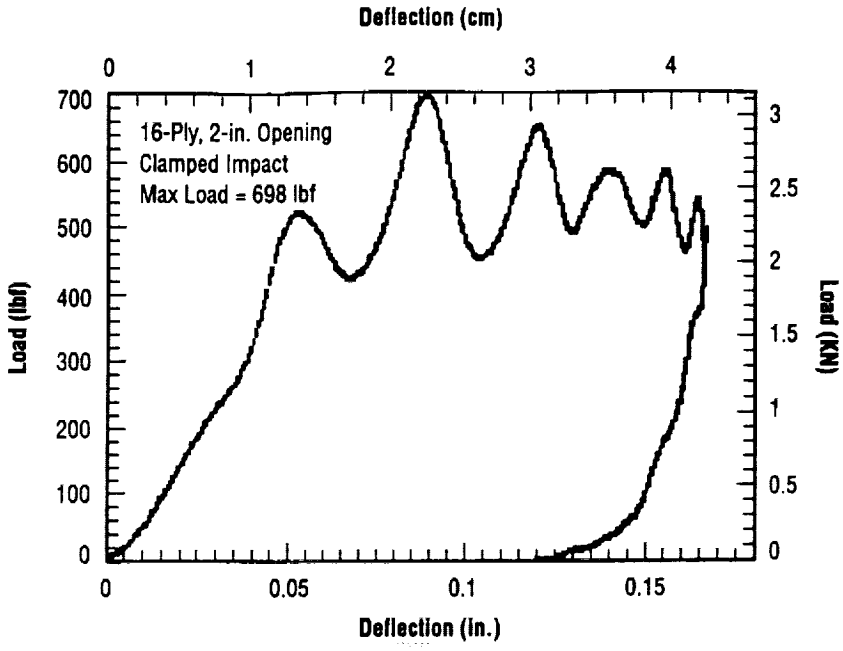

Figure 78. Load versus deflection specimen 616–31s.

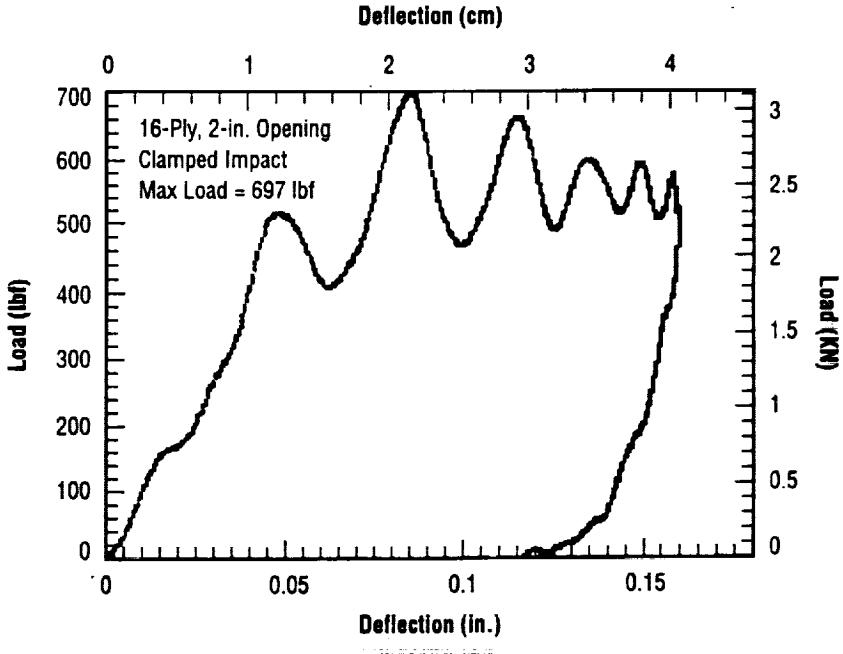

Figure 79. Load versus deflection specimen 616–32s.

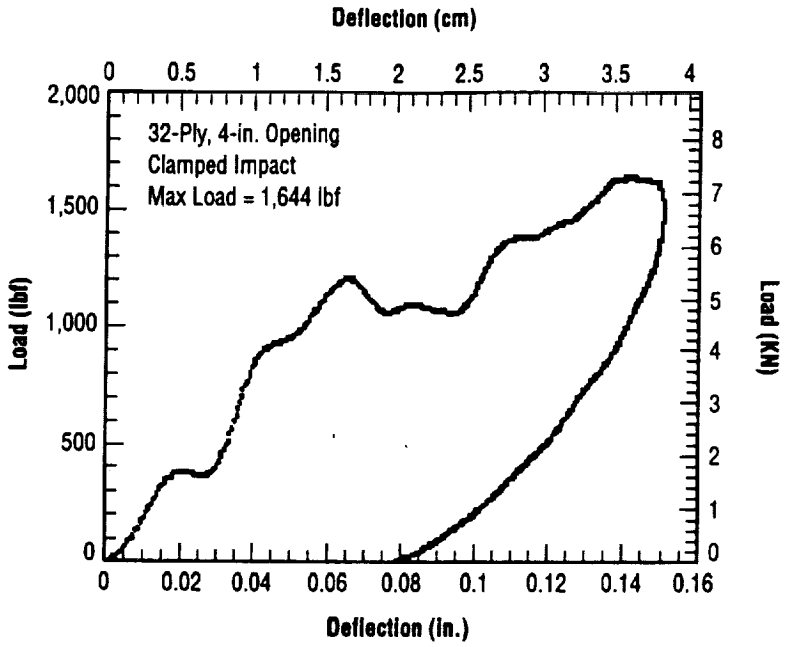

Figure 80. Load versus deflection specimen 616–20s.

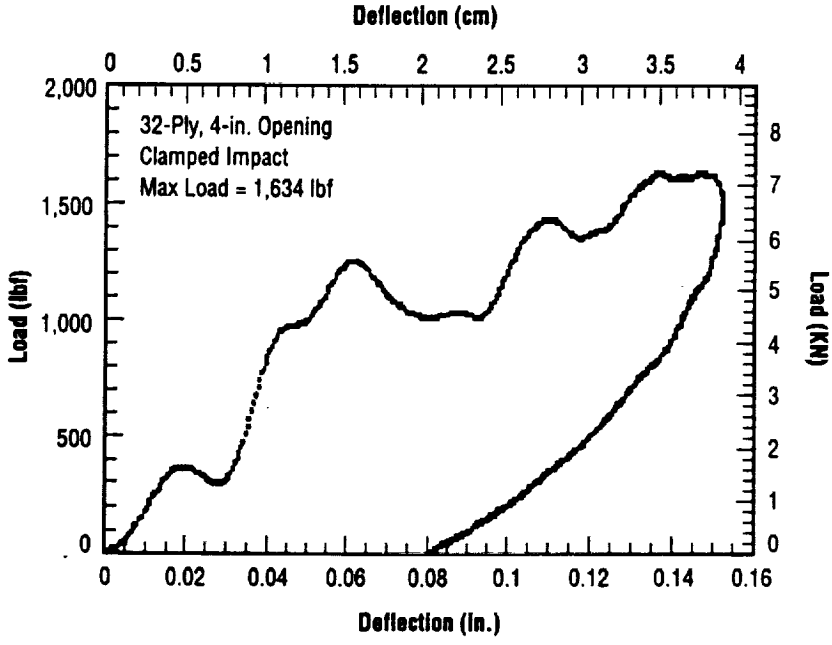

Figure 81. Load versus deflection specimen 616–21s.

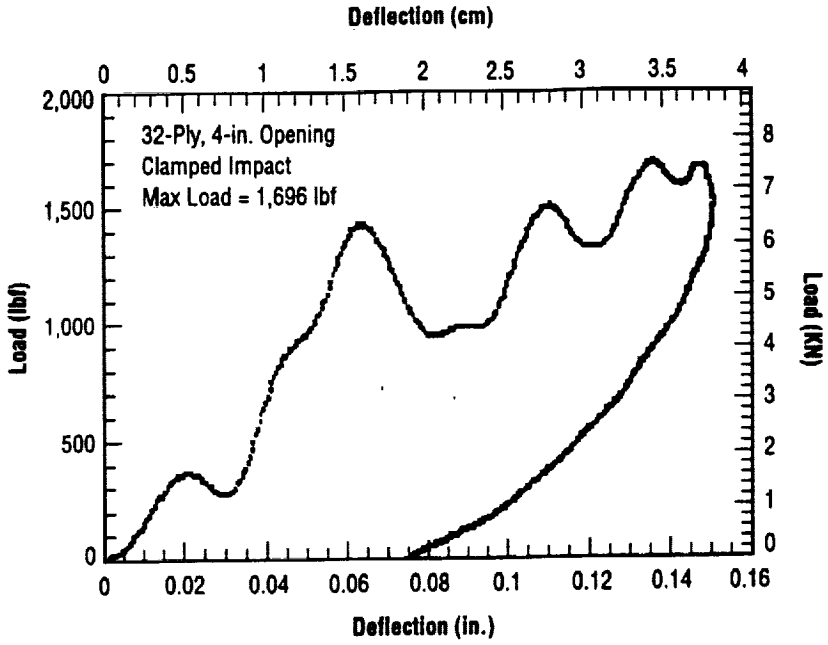

Figure 82. Load versus deflection specimen 616–22s.

APPENDIX C—LOAD VERSUS DEFLECTION PLOTS FOR QUASI-STATIC INDENTATION TESTS

Figures 83–97 show load versus deflection plots for quasi-static indentation tests.

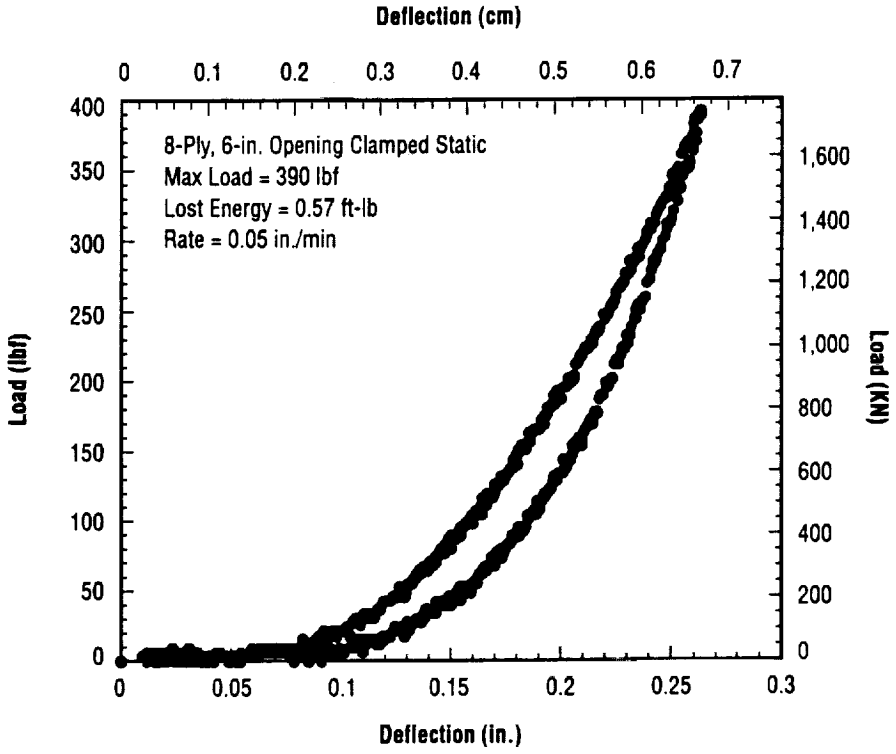

Figure 83. Load versus deflection specimen 708–10f.

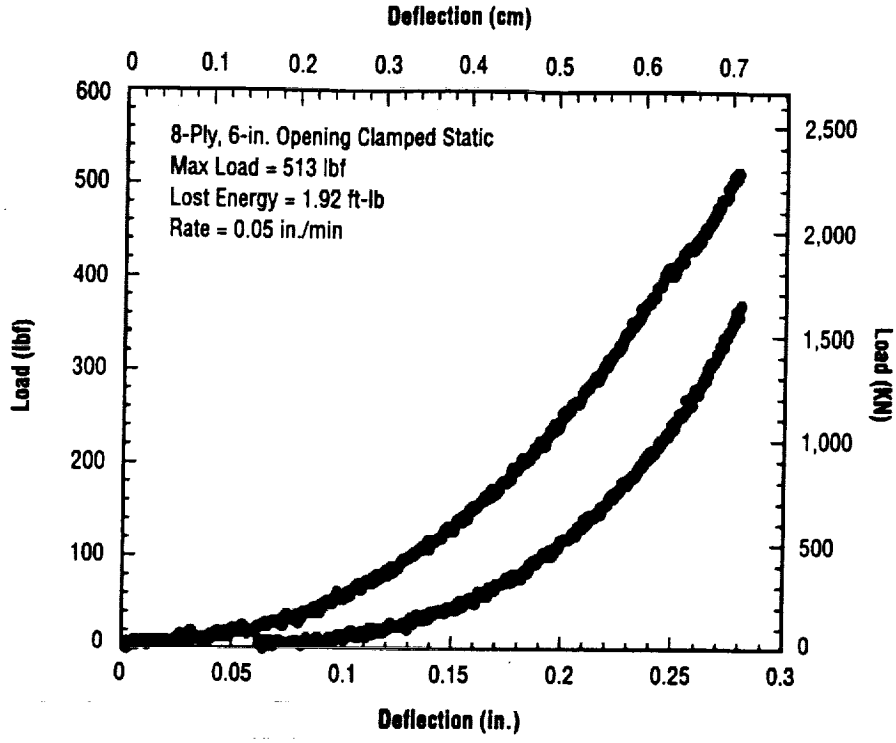

Figure 84. Load versus deflection specimen 708–11f.

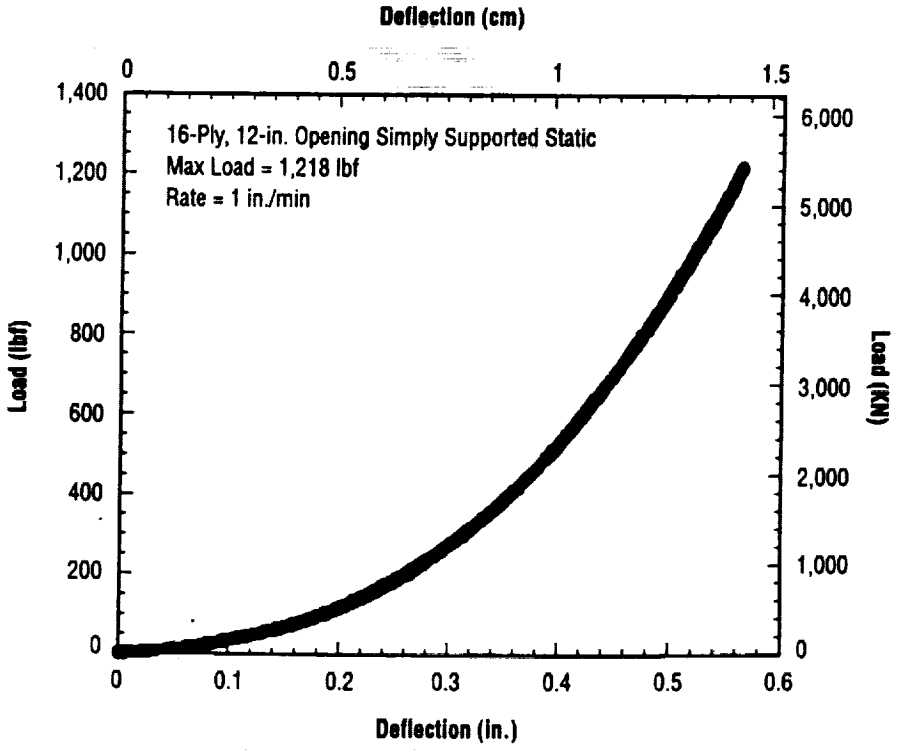

Figure 85. Load versus deflection specimen 1018–02f.

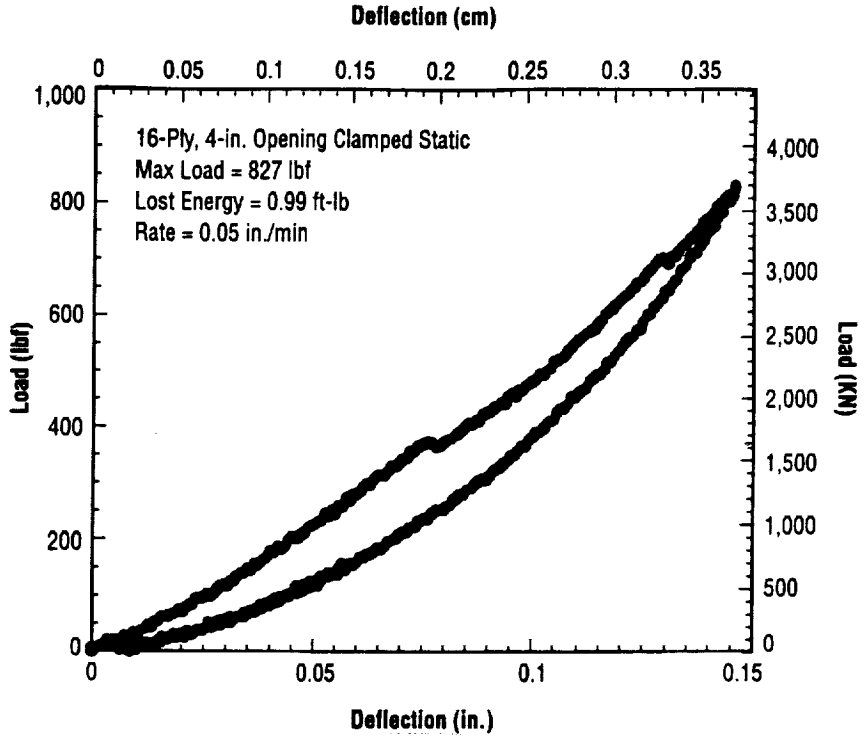

Figure 86. Load versus deflection specimen 708–03m.

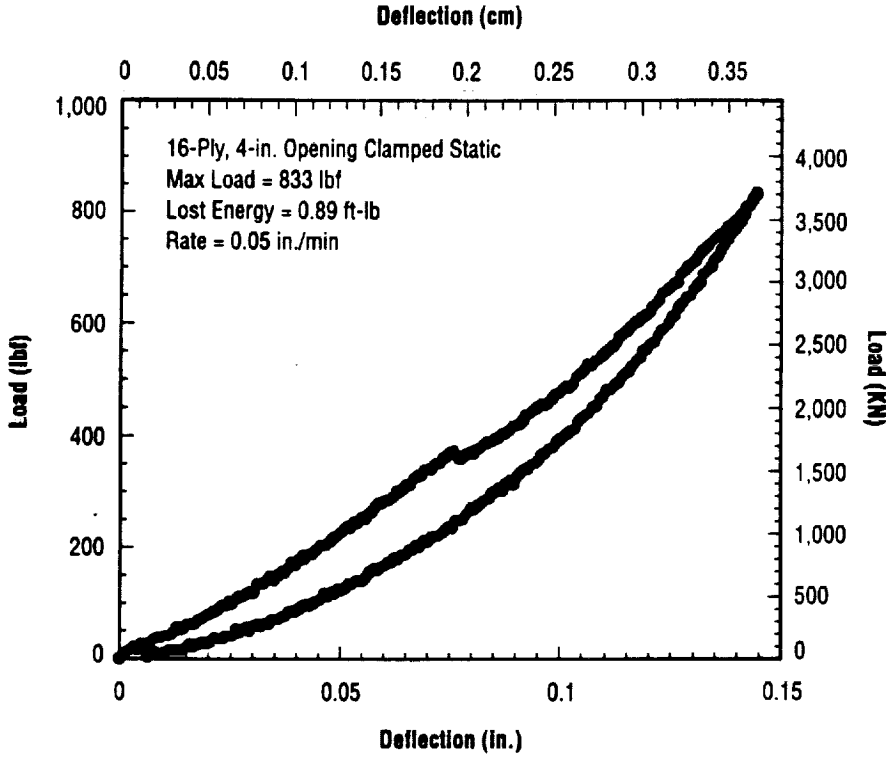

Figure 87. Load versus deflection specimen 708–02m.

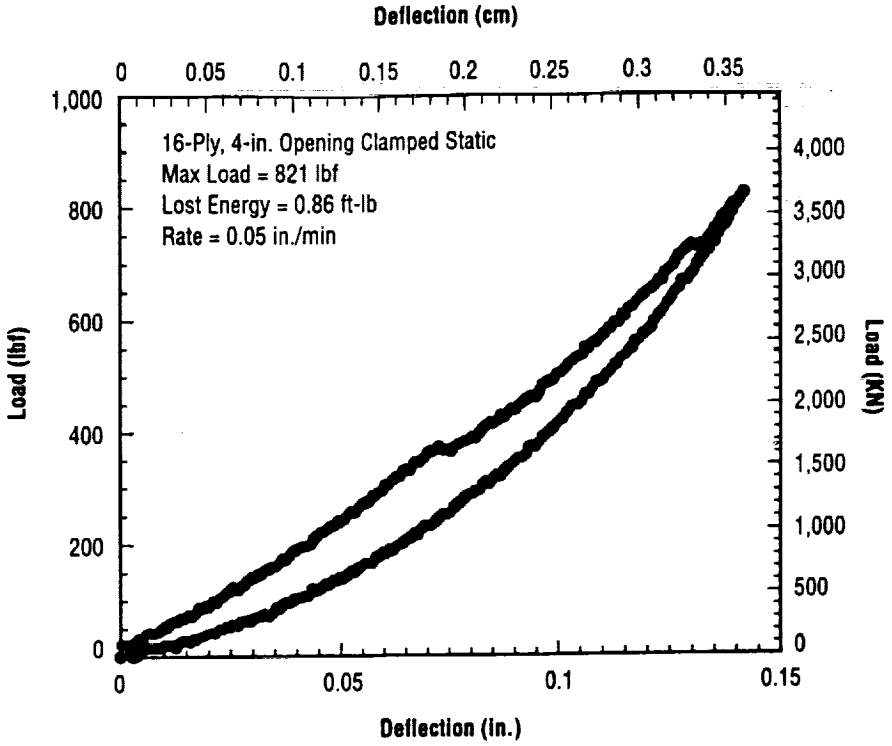

Figure 88. Load versus deflection specimen 708–04m.

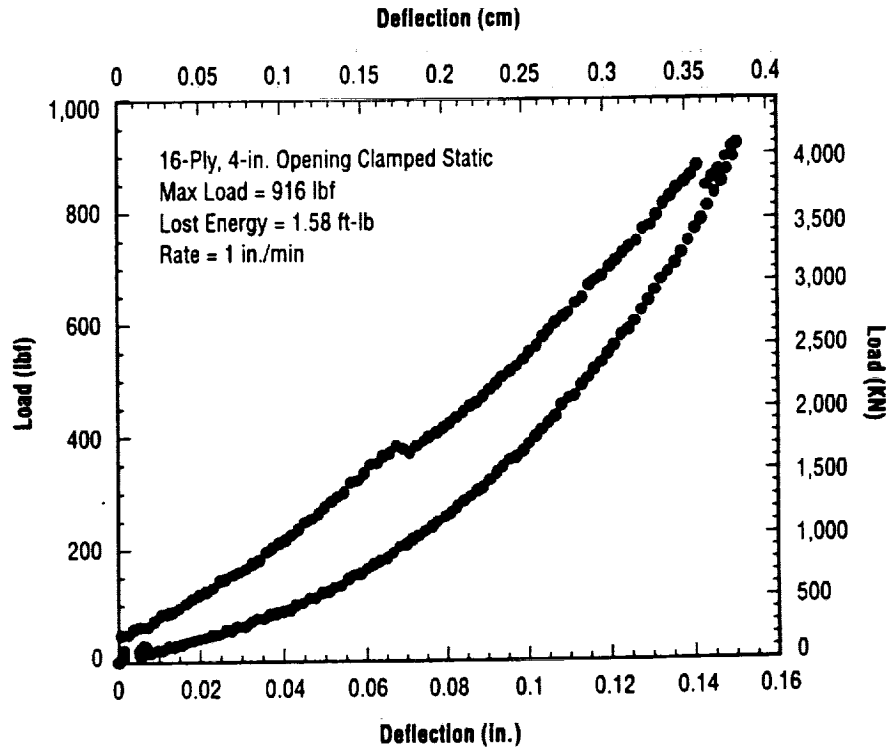

Figure 89. Load versus deflection specimen 708–05m.

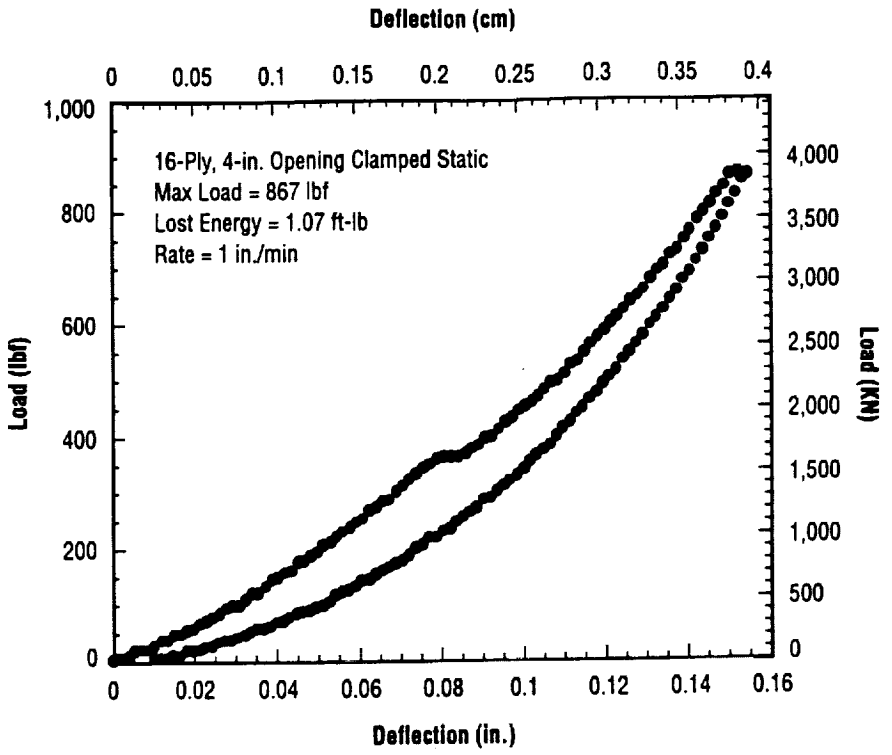

Figure 90. Load versus deflection specimen 708–06m.

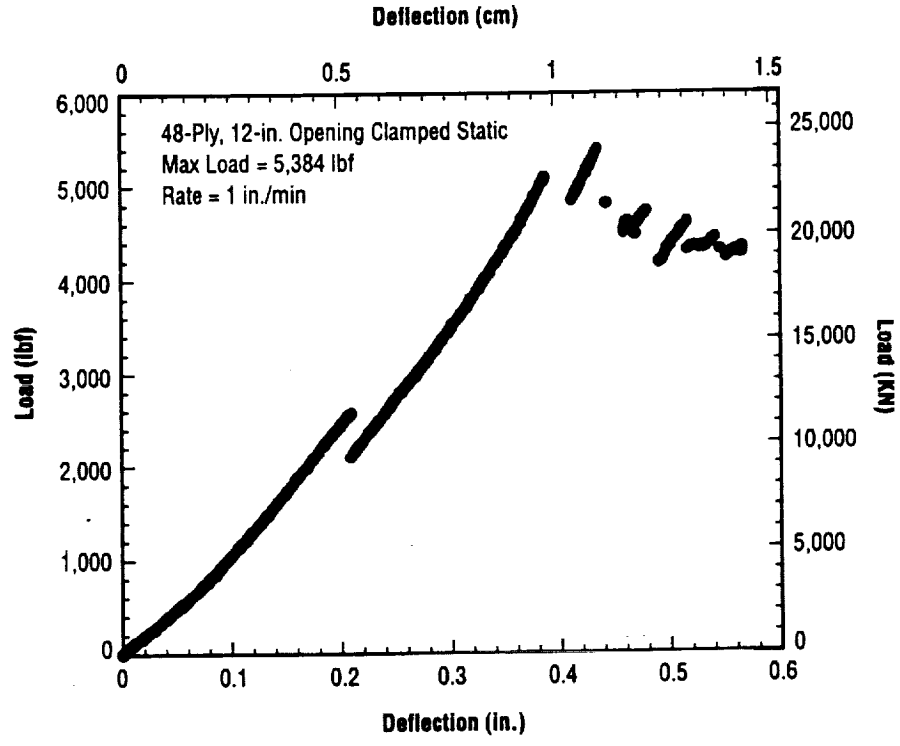

Figure 91. Load versus deflection specimen 1015–01m.

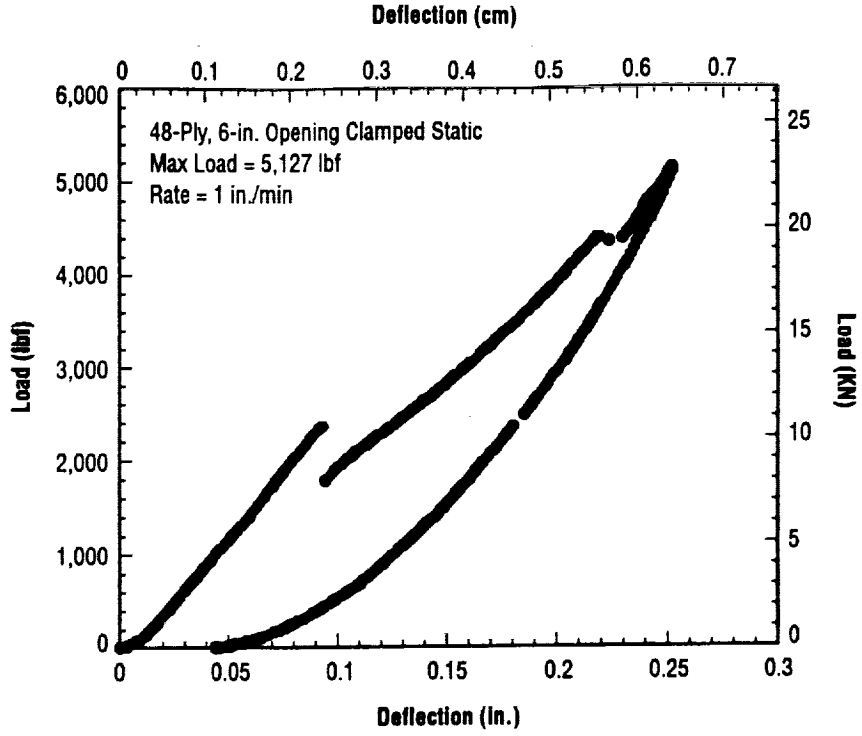

Figure 92. Load versus deflection specimen 1015–02s.

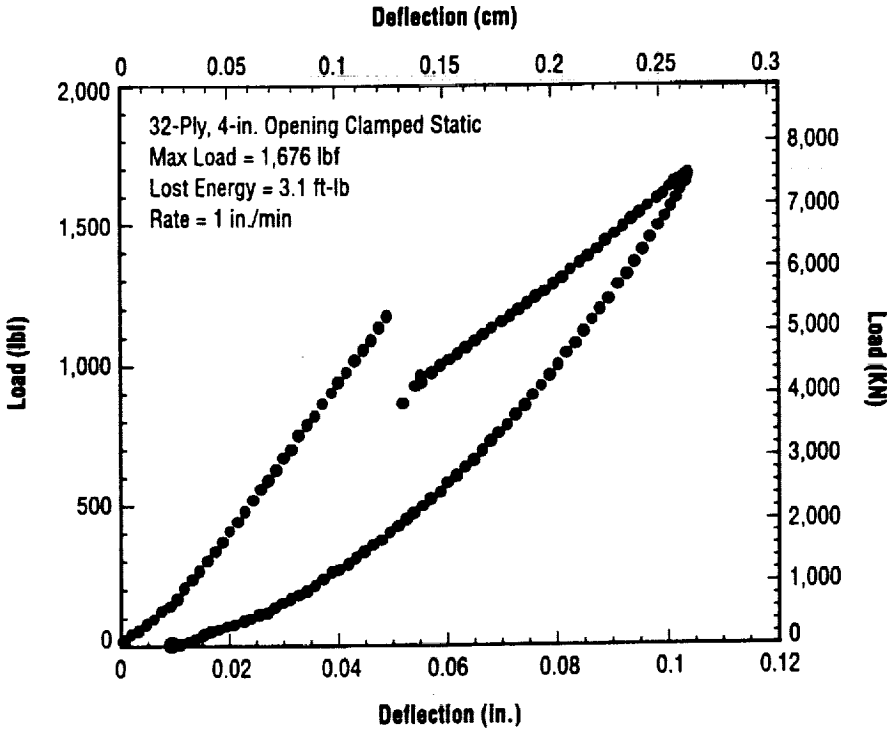

Figure 93. Load versus deflection specimen 708–07s.

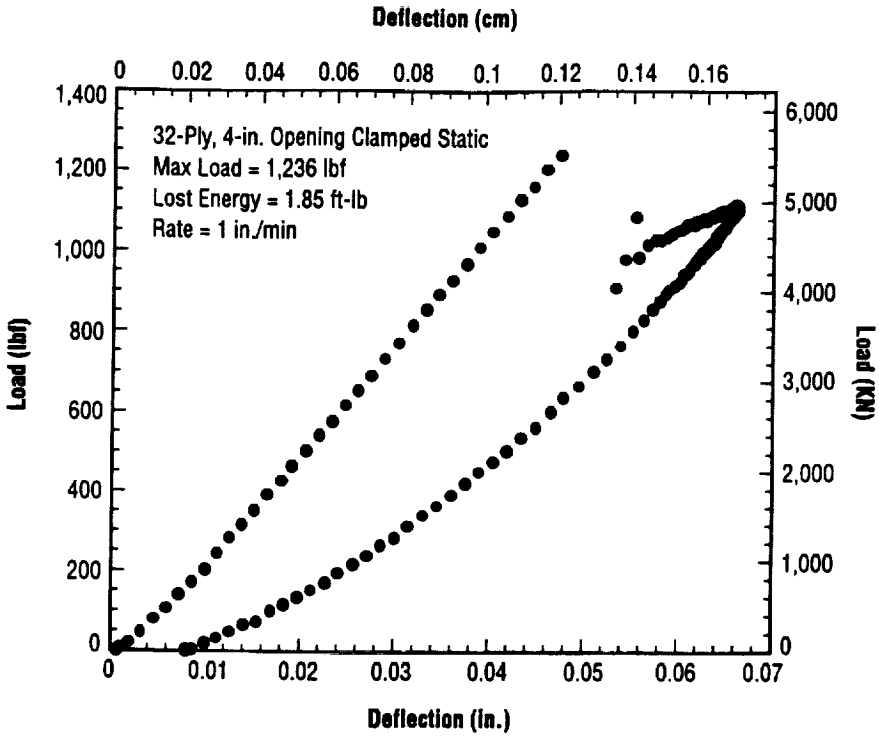

Figure 94. Load versus deflection specimen 708–08s.

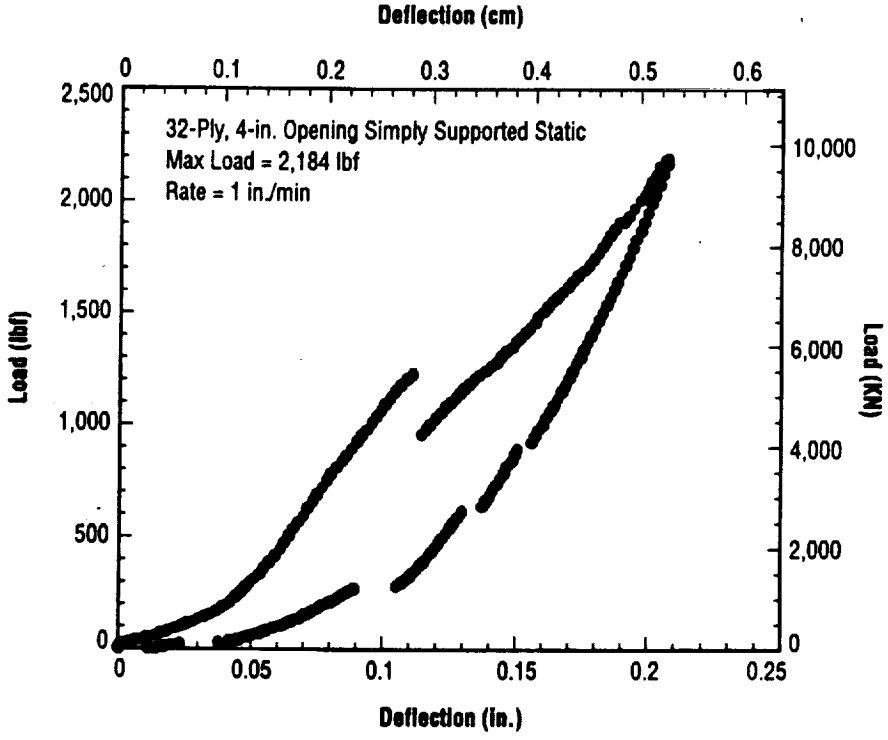

Figure 95. Load versus deflection specimen 1015–03s.

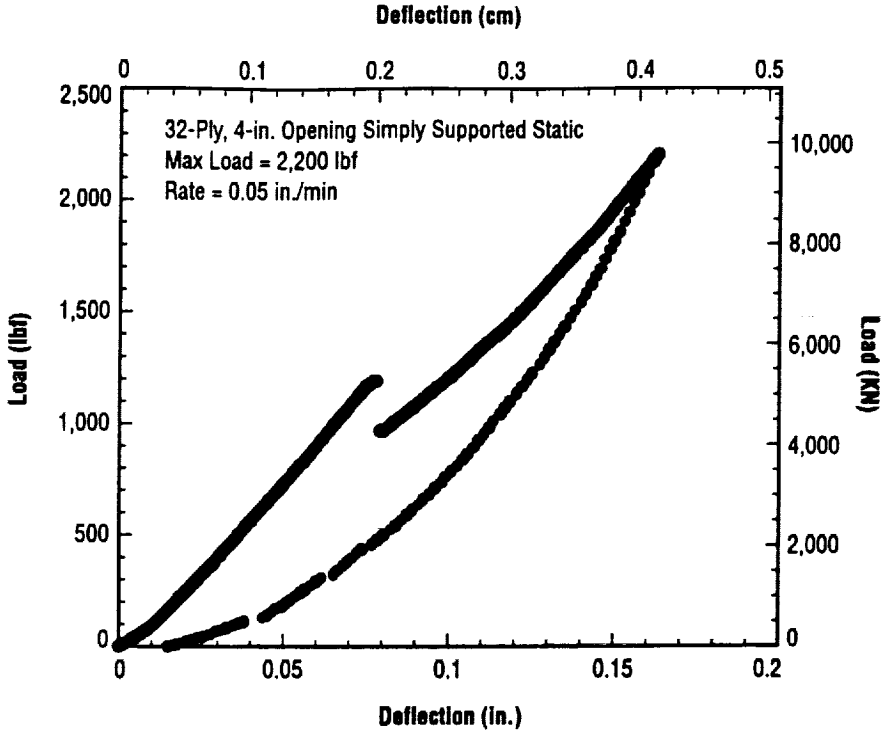

Figure 96. Load versus deflection specimen 1018–03s.

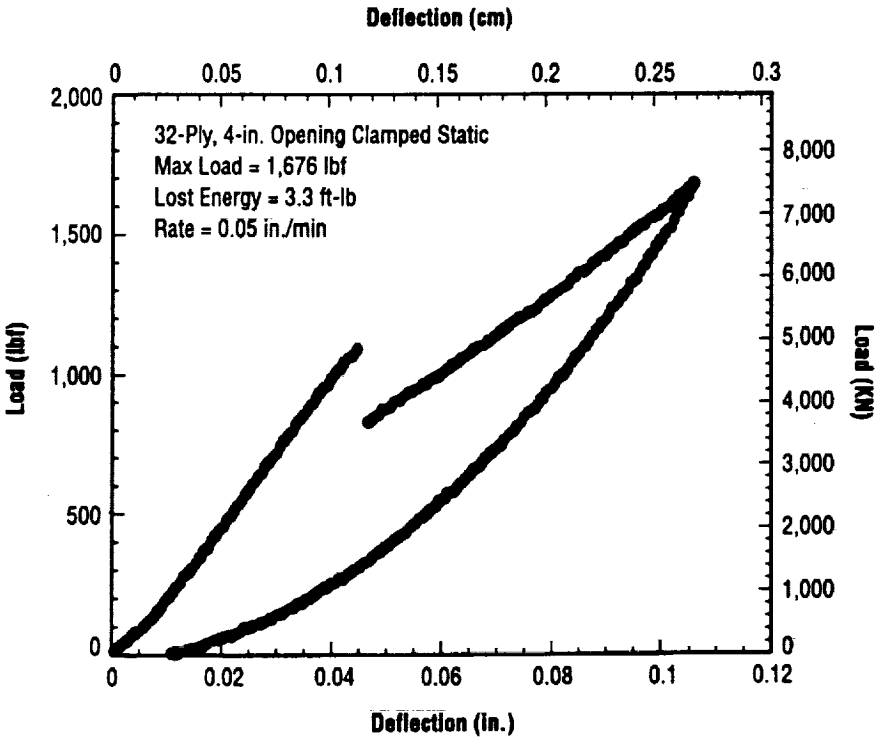

Figure 97. Load versus deflection specimen 706–01s.

APPENDIX D—NONDESTRUCTIVE EVALUATION ANALYSIS DATA

Tables 15–20 display simply supported and clamped flex data for nondestructive evaluation analysis.

Table 15. Simply supported flex.

8 Ply on 6-in. Platen				
Impact				
Specimen ID No.	**Max Load N (lbf)**	**Dent Depth mm (in.)**	**Crack Length mm (in.)**	**Delamination Area mm^2 ($in.^2$)**
727–06F	1,850 (416)	0.102 (0.004)	16.00 (0.63)	170 (0.28)
727–07F	1,766 (397)	0.075 (0.003)	47.75 (1.88)	216 (0.33)
727–08F	1,850 (416)	0.075 (0.003)	22.35 (0.88)	157 (0.24)
727–09F	1,873 (421)	0.075 (0.003)	25.4 (1.00)	223 (0.34)
727–10F	1,873 (421)	Not measurable	31.75 (1.25)	190 (0.29)
Quasi-Static				
817–10F	1,819 (409)	0.102 (0.004)	0.075 (0.003)	177 (0.27)
817–11F	1,859 (418)	0.102 (0.004)	Not measurable	111 (0.17)
817–04F	1,859 (418)	0.075 (0.003)	19.05 (0.75)	190 (0.29)
817–05F	1,850 (416)	0.075 (0.003)	22.35 (0.88)	190 (0.29)

16 Ply on 12-in. Platen				
Impact				
Specimen ID No.	**Max Load N (lbf)**	**Dent Depth mm (in.)**	**Crack Length mm (in.)**	**Delamination Area mm^2 ($in.^2$)**
728–05F	4,862 (1,093)	0.102 (0.004)	Not measurable	426 (0.65)
728–06F	5,400 (1,214)	0.102 (0.004)	31.75 (1.25)	499 (0.76)
728–07F	5,373 (1,208)	0.051 (0.002)	35.05 (1.38)	590 (0.90)
Quasi-Static				
818–05F	5,360 (1,205)	0.152 (0.006)	6.35 (0.25)	505 (0.77)
818–06F	5,458 (1,227)	0.127 (0.005)	6.35 (0.25)	538 (0.82)
818–03F	5,809 (1,306)	0.127 (0.005)	4.83 (0.19)	433 (0.66)
818–04F	5,667 (1,270)	0.127 (0.005)	9.65 (0.38)	472 (0.72)
1018–02F	5,420 (1,218)	No data	No data	416 (0.64)

Table 16. Simply supported medium.

8 Ply on 6-in. Platen				
Impact				
Specimen ID No.	**Max Load N (lbf)**	**Dent Depth mm (in.)**	**Crack Length mm (in.)**	**Delamination Area mm^2 ($in.^2$)**
728–02M	1,023 (230)	0.076 (0.003)	16.00 (0.63)	85 (0.13)
728–03M	974 (219)	0.076 (0.003)	16.00 (0.63)	79 (0.12)
728–04M	907 (204)	0.051 (0.002)	9.65 (0.38)	52 (0.08)
Quasi-Static				
819–01M	734 (165)	0.025 (0.001)	6.35 (0.25)	39 (0.06)
819–02M	907 (204)	0.076 (0.003)	4.83 (0.19)	46 (0.07)
819–07M	1,059 (238)	0.152 (0.006)	16.00 (0.63)	79 (0.12)
819–08M	1,059 (238)	0.127 (0.005)	19.05 (0.75)	105 (0.16)

16 Ply on 4-in. Platen				
Impact				
Specimen ID No.	**Max Load N (lbf)**	**Dent Depth mm (in.)**	**Crack Length mm (in.)**	**Delamination Area mm^2 ($in.^2$)**
727–11M	3,723 (837)	Penetrated	No data	No data
727–12M	3,701 (832)	0.279 (0.011)	28.70 (1.13)	492 (0.75)
727–13M	3,670 (825)	0.102 (0.004)	25.40 (1.00)	321 (0.49)
727–14M	2,998 (674)	0.051 (0.002)	6.35 (0.25)	171 (0.26)
727–15M	2,963 (666)	0.076 (0.003)	19.05 (0.75)	262 (0.40)
Quasi-Static				
819–16M	3,677 (827)	No data	No data	400 (0.61)
819–17M	3,670 (825)	0.102 (0.004)	9.65 (0.38)	308 (0.47)
819–09M	4,003 (900)	0.152 (0.006)	31.75 (1.25)	315 (0.48)
819–10M	3,777 (849)	0.203 (0.008)	31.75 (1.25)	328 (0.50)

48 Ply on 12-in. Platen				
Impact				
Specimen ID No.	**Max Load N (lbf)**	**Dent Depth mm (in.)**	**Crack Length mm (in.)**	**Delamination Area mm^2 ($in.^2$)**
61599–02M	23,557 (5,296)	0.614 (0.024)	112.13 (4.38)	3,214 (4.90)
61599–03M	29,496 (6,631)	0.205 (0.008)	118.53 (4.63)	3,011 (4.59)
Quasi-Static				
818–07M	23,878 (5,368)	0.635 (0.25)	Numerous cracks	25.80 (4.00)
818–01M	28,304 (6,363)	No data	No data	26.38 (4.09)

Table 17. Simply supported stiff.

16 Ply on 2-in. Platen				
Impact				
Specimen ID No.	**Max Load N (lbf)**	**Dent Depth mm (in.)**	**Crack Length mm (in.)**	**Delamination Area mm^2 ($in.^2$)**
727–20S	2,922 (657)	0.127 (0.005)	31.75 (1.25)	288 (0.44)
727–21S	2,771 (623)	0.178 (0.007)	35.05 (1.38)	334 (0.51)
727–22S	3,350 (753)	0.102 (0.004)	16.00 (0.63)	269 (0.41)
728–01S	3,051 (686)	0.152 (0.006)	26.92 (1.06)	295 (0.45)
Quasi-Static				
819–03S	2,904 (653)	Not measurable	1.27 (0.50)	269 (0.41)
819–04S	2,918 (656)	0.178 (0.007)	16.00 (0.63)	328 (0.50)
819–05S	2,758 (620)	0.356 (0.014)	38.10 (1.50)	348 (0.53)
819–06S	2,931 (659)	0.279 (0.011)	30.22 (1.19)	308 (0.47)

32 Ply on 4-in. Platen				
Impact				
Specimen ID No.	**Max Load N (lbf)**	**Dent Depth mm (in.)**	**Crack Length mm (in.)**	**Delamination Area mm^2 ($in.^2$)**
727–16S	8,696 (1,955)	0.152 (0.006)	38.10 (1.50)	984 (1.53)
727–17S	9,106 (2,047)	0.152 (0.006)	Not measurable	1,154 (1.76)
727–18S	9,853 (2,215)	0.178 (0.007)	Not measurable	1,141 (1.74)
727–19S	9,346 (2,101)	0.152 (0.006)	47.75 (1.88)	1,207 (1.84)
Quasi-Static				
819–14S	9,866 (2,218)	0.330 (0.013)	47.75 (1.88)	1,220 (1.86)
819–15S	9,844 (2,213)	0.330 (0.013)	47.75 (1.88)	1,233 (1.88)
819–12S	10,898 (2,450)	0.254 (0.010)	41.40 (1.63)	1,586 (2.42)
819–13S	10,925 (2,456)	0.279 (0.011)	28.70 (1.13)	1,614 (2.46)
1015–03S	9,718 (2,184)	No data	No data	1,232 (1.91)
1018–03	9,790 (2,200)	No data	No data	1,297 (2.01)

48 Ply on 6-in. Platen				
Impact				
Specimen ID No.	**Max Load N (lbf)**	**Dent Depth mm (in.)**	**Crack Length mm (in.)**	**Delamination Area mm^2 ($in.^2$)**
727–02S	22,121 (4,973)	0.279 (0.011)	1.27 (0.50)	3,339 (5.09)
727–03S	22,810 (5,128)	0.686 (0.027)	63.50 (2.50)	4,284 (6.53)
Quasi-Static				
817–08S	22,726 (5,109)	0.457 (0.018)	Numerous cracks	4,146 (6.32)
817–09S	22,383 (5,032)	1.067 (0.042)	55.63 (2.19)	4,146 (6.32)
817–06S	21,476 (4,828)	1.497 (0.059)	Numerous cracks	4,211 (6.42)
817–07S	20,987 (4,718)	1.016 (0.040)	31.75 (1.25)	3,765 (5.74)

Table 18. Clamped flex.

8 Ply on 6-in. Platen				
Impact				
Specimen ID No.	**Max Load N (lbf)**	**Dent Depth mm (in.)**	**Crack Length mm (in.)**	**Delamination Area mm^2 ($in.^2$)**
616–15F	1,930 (434)	0.203 (0.008)	85.85 (3.38)	676 (1.03)
616–16F	2,148 (483)	0.381 (0.015)	74.68 (2.94)	479 (0.73)
616–17F	1,673 (376)	0.051 (0.002)	19.05 (0.75)	112 (0.17)
616–18F	1,668 (375)	0.076 (0.003)	22.35 (0.88)	112 (0.17)
Quasi-Static				
708–10F	1,735 (390)	No data	No data	No data
708–11F	2,277 (512)	0.635 (0.025)	44.45 (1.75)	348 (0.53)
720–07F	1,415 (318)	0.152 (0.006)	12.70 (0.50)	92 (0.14)
720–08F	1,899 (427)	0.127 (0.005)	9.53 (0.38)	85 (0.13)

16 Ply on 12-in. Platen				
Impact				
Specimen ID No.	**Max Load N (lbf)**	**Dent Depth mm (in.)**	**Crack Length mm (in.)**	**Delamination Area mm^2 ($in.^2$)**
616–01F	6,841 (1,538)	0.152 (0.006)	41.28 (1.63)	774 (1.18)
616–02F	6,921 (1,556)	0.127 (0.005)	57.15 (2.25)	741 (1.13)
616–03F	7,037 (1,582)	0.127 (0.005)	38.10 (1.50)	833 (1.27)
616–04F	7,108 (1,598)	0.127 (0.005)	42.07 (1.66)	781 (1.19)
Quasi-Static				
720–03F	6,935 (1,559)	0.178 (0.007)	44.45 (1.75)	643 (0.98)
720–04F	6,993 (1,572)	0.203 (0.008)	44.45 (1.75)	708 (1.08)
720–05F	7,357 (1,654)	0.152 (0.006)	25.4 (1.00)	715 (1.09)
720–06F	7,517 (1,690)	0.178 (0.007)	35.05 (1.38)	840 (1.28)

Table 19. Clamped medium.

8 Ply on 2-in. Platen				
Impact				
Specimen ID No.	**Max Load N (lbf)**	**Dent Depth mm (in.)**	**Crack Length mm (in.)**	**Delamination Area mm^2 ($in.^2$)**
616–37M	1,045 (235)	Extensive damage		No data
616–38M	939 (211)	0.229 (0.009)	Numerous cracks	190 (0.29)
728–09M	936 (210)	0.102 (0.004)	22.35 (0.88)	92 (0.14)
728–11M	1,036 (233)	Extensive damage		131 (0.20)
Quasi-Static				
722–03M	1,183 (266)	0.076 (0.003)	16.00 (0.63)	66 (0.10)
722–04M	1,045 (235)	0.102 (0.004)	9.65 (0.38)	59 (0.09)
722–05M	939 (211)	0.127 (0.005)	6.35 (0.25)	52 (0.08)
722–06M	894 (201)	Not measurable	Not visible	46 (0.07)

16 Ply on 4-in. Platen				
Impact				
Specimen ID No.	**Max Load N (lbf)**	**Dent Depth mm (in.)**	**Crack Length mm (in.)**	**Delamination Area mm^2 ($in.^2$)**
616–25M	3,634 (817)	0.076 (0.003)	22.23 (0.88)	276 (0.42)
616–26M	3,629 (816)	0.076 (0.003)	34.93 (1.38)	348 (0.53)
616–27M	3,665 (824)	0.076 (0.003)	38.10 (1.50)	230 (0.35)
616–28M	3,728 (838)	0.127 (0.005)	44.45 (1.75)	335 (0.51)
Quasi-Static				
708–02M	3,705 (833)	0.152 (0.006)	Not measurable	348 (0.53)
708–03M	3,679 (827)	0.152 (0.006)	25.4 (1.00)	374 (0.57)
708–04M	3,652 (821)	0.152 (0.006)	22.35 (0.88)	308 (0.47)
708–05M	4,075 (916)	0.152 (0.006)	16.00 (0.63)	420 (0.64)
708–06M	3,857 (867)	0.127 (0.005)	Not measurable	420 (0.64)

48 Ply on 12-in. Platen				
Impact				
Specimen ID No.	**Max Load N (lbf)**	**Dent Depth mm (in.)**	**Crack Length mm (in.)**	**Delamination Area mm^2 ($in.^2$)**
61599–04M	26,823 (6,030)	0.794 (0.031)	80.00 (3.16)	3,640 (5.55)
61599–05M	23,420 (5,265)	1.434 (0.059)	70.40 (2.75)	3,378 (5.15)
Quasi-Static				
817–01M	26,293 (5,911)	0.333 (0.013)	99.20 (3.88)	4,159 (6.34)
817–02M	28,290 (6,360)	0.435 (0.017)	107.20 (4.19)	3,241 (4.94)

Table 20. Clamped stiff.

16 Ply on 2-in. Platen				
Impact				
Specimen ID No.	**Max Load N (lbf)**	**Dent Depth mm (in.)**	**Crack Length mm (in.)**	**Delamination Area mm^2 ($in.^2$)**
616–29S	3,239 (728)	0.457 (0.018)	50.80 (2.00)	382 (0.592)
616–30S	2,922 (657)	0.203 (0.008)	55.56 (2.19)	512 (0.794)
616–31S	3,105 (698)		66.68 (2.63)	624 (0.967)
616–32S	3,100 (697)	0.356 (0.014)	68.26 (2.69)	676 (1.048)
Quasi-Static				
722–01S	3,272 (736)	0.203 (0.008)	9.65 (0.38)	432 (0.670)
722–02S	3,109 (699)	0.178 (0.007)	19.05 (0.75)	560 (0.868)
722–07S	2,989 (672)	0.178 (0.007)	9.65 (0.38)	528 (0.818)
722–08S	3,003 (675)	0.305 (0.012)	22.35 (0.88)	536 (0.831)

32 Ply on 4-in. Platen				
Impact				
Specimen ID No.	**Max Load N (lbf)**	**Dent Depth mm (in.)**	**Crack Length mm (in.)**	**Delamination Area mm^2 ($in.^2$)**
616–20S	7,313 (1,644)	0.127 (0.005)	22.53 (0.88)	1,006 (1.56)
616–21S	7,268 (1,634)	0.152 (0.006)	19.20 (0.75)	1,012 (1.57)
616–22S	7,544 (1,696)	0.178 (0.007)	19.20 (0.75)	1,012 (1.57)
616–24S	7,322 (1,646)	0.152 (0.006)	28.93 (1.14)	987 (1.53)
Quasi-Static				
706–01S	7,455 (1,676)	0.203 (0.008)	Not measurable	1,256 (1.947)
708–07S	7,455 (1,676)	0.203 (0.008)	19.05 (0.75)	904 (1.401)
708–08S	5,498 (1,236)	0.203 (0.008)	Not measurable	

48 Ply on 6-in. Platen				
Impact				
Specimen ID No.	**Max Load N (lbf)**	**Dent Depth mm (in.)**	**Crack Length mm (in.)**	**Delamination Area mm^2 ($in.^2$)**
727–04S	22,788 (5,123)	0.381 (0.015)	73.03 (2.88)	5,412 (8.39)
727–05S	23,100 (5,193)	0.483 (0.019)	77.78 (3.06)	4,128 (6.40)
Quasi-Static				
720–01S	23,429 (5,267)	1.321 (0.052)	28.70 (1.18)	5,648 (8.754)
720–02S	22,196 (4,990)	1.19 (0.047)	22.35 (0.88)	5,244 (8.128)
817–02S	23,389 (5,258)	0.838 (0.033)	16.00 (0.63)	3,186 (4.94)
817–03S	23,389 (5,258)	1.19 (0.047)	31.75 (1.25)	4,880 (7.564)

REFERENCES

1. ASTM Standard D6264–8, *1999 ASTM Book of Standards*, Vol. 15.03.

2. Cantwell, W.J.; and Morton, J.: "Comparison of the Low- and High-Velocity Impact Response of CFRP," *Composites*, Vol. 20, No. 6, pp. 545–551, November 1989.

3. Wu, E.; and Chang, L.: "Loading Rate Effect on Woven Glass Laminated Plates by Penetration Force," *Journal of Composite Materials*, Vol. 32, No. 8, pp. 702–721, 1998.

4. Jackson, W.C.; and Poe, C.C.: "The Use of Impact Force as a Scale Parameter for the Impact Response of Composite Laminates," *NASA Technical Memorandum 104189*, January 1992.

5. Bucinell, R.B.; Nuismer, R.J.; and Koury, J.L.: "Response of Composite Plates to Quasi-Static Impact Events," Composite Materials: Fatigue and Fracture (Third Volume), ASTM STP 1110, pp. 528–549, 1998.

6. Swanson, S.R.: "Limits of Quasi-Static Solutions in Impact of Composite Structures," *Composites Engineering*, Vol. 2, No. 4, pp. 261–267, 1992.

7. Kwon, Y.S.; and Sankar, B.V.: "Indentation-Flexure and Low-Velocity Impact Damage in Graphite Epoxy Laminates," *Journal of Composites Technology and Research*, Vol. 15, No. 2, pp. 101–111, Summer 1993.

8. Lagace, P.A.; Williamson, J.E.; Wilson Tsang, P.H.; Wolf, E.; and Thomas, S.: "A Preliminary Proposition for a Test Method to Measure (Impact) Damage Resistance," *Journal of Reinforced Plastics and Composites*, Vol. 12, pp. 584–601, May 1993.

9. Kaczmarek, H.; and Maison, S.: "Comparative Ultrasonic Analysis of Damage in CFRP Under Static Indentation and Low-Velocity Impact," *Composites Science and Technology*, Vol. 51, pp. 11–26, 1994.

10. Wardle, B.L.; and Lagace, P.A.: "On the Use of Dent Depth as an Impact Damage Metric for Thin Composite Structures," *Journal of Reinforced Plastics and Composites*, Vol. 16, No. 12, pp. 1093–1110, 1997.

11. Nettles, A.T.; Douglas, M.J.; and Estes, E.E.: "Scaling Effects in Carbon/Epoxy Laminates Under Transverse Quasi-Static Loading," *NASA Technical Memorandum 209103*, March 1999.

12. Cheresh, M.C.; and McMichael, S.: "Instrumented Impact Test Data Interpretation," Instrumented Impact Testing of Plastics and Composite Materials, *ASTM STP 936*, pp. 9–23, 1987.

13. Found, M.S.; Howard, I.C.; and Paran, A.P.: "Interpretation of Signals from Drop-Weight Impact Tests," *Composite Structures*, Vol. 42, pp. 353–363, 1998.

14. Lee, S.M.; and Zahuta, P.: "Instrumented Impact and Static Indentation of Composites," *Journal of Composite Materials*, Vol. 25, pp. 204–222, February 1991.

15. Sjoblom, P.O.; Hartness, T.J.; and Cordell, T.M.: "On Low-Velocity Impact Testing of Composite Materials," *Journal of Composite Materials*, Vol. 22, pp. 30–52, January 1988.

16. Iber, W.: "Failure Mechanics in Low-Velocity Impacts on Thin Composite Plates," *NASA Technical Paper 2152*, 1983.

17. Highsmith, A.L.: "A Study of the Use of Contact Loading to Simulate Low-Velocity Impact," *NASA Contractor Report 97–206121*, January 1997.

The Affects of Shot and Laser Peening on Crack Growth and Fatigue Life in 2024 Aluminum Alloy and 4340 Steel

R.A. Everett, Jr. and W.T. Matthews
U.S. Army Research Laboratory
Vehicle Technology Directorate
Langley Research Center, Hampton, Virginia

R. Prabhakaran
Old Dominion University, Norfolk, Virginia

J.C. Newman, Jr.
Langley Research Center, Hampton, Virginia

M.J. Dubberly
M.J. Dubberly, Inc.,

Presented at the USAF Structural Integrity Program Conference
December 5-7, 2000
San Antonio, Texas

The Effects of Shot and Laser Peening on Crack Growth and Fatigue Life in 2024 Aluminum Alloy and 4340 Steel

[1]R.A. Everett, Jr., [1]W.T. Matthews, [2]R. Prabhakaran, [3]J.C. Newman, Jr., and [4]M.J. Dubberly

ABSTRACT

Fatigue and crack growth tests have been conducted on 4340 steel and 2024-T3 aluminum alloy, respectively, to assess the effects of shot peening on fatigue life and the effects of shot and laser peening on crack growth. This work is of current interest to the U.S. Air Force as well as the rotorcraft community. Two current programs in the aerospace community involving fixed and rotary-wing aircraft will not be using shot peened structures. The reason for not shot peening these aircraft comes from arguments based on the premise that the shot peening compressive residual stress depth is less than the 0.05-inch initial damage tolerance crack size. Therefore, shot peening should have no beneficial effects toward retarding crack growth. In this study cracks were initiated from an electronic-discharged machining flaw which was cycled to produce a fatigue crack of approximately 0.05-inches in length and then the specimens were peened. Test results showed that after peening the crack growth rates were noticeably slower when the cracks were fairly short for both the shot and laser peened specimens resulting in a crack growth life that was a factor of 2 to 4 times greater than the results of the average unpeened test. Once the cracks reached a length of approximately 0.1-inches the growth rates were about the same for the peened and unpeened specimens. Fatigue tests on 4340 steel showed that the endurance limit of a test specimen with a 0.002-inch-deep machining-like scratch was reduced by approximately 40 percent. However, if the "scratched" specimen was shot peened after inserting the scratch, the fatigue life returned to almost 100 percent of the unflawed specimens original fatigue life.

INTRODUCTION

It has been recognized for a long time (Ref. 1) that the introduction of residual compressive stresses in metallic components leads to enhanced fatigue strength. Many engineering components have been surface-treated with the fatigue strength enhancement as the primary objective or as a by-product of a surface hardening treatment. Examples of the former type of treatment are shot-peening, laser shock peening (LSP), and cold working; examples of the latter type of treatment are nitriding and physical vapor deposition.

In shot peening, a high velocity stream of hard particles is directed at a materials surface often resulting in compressive residual stresses being produced at and below the surface of the material with a peak value being reached at some depth below the surface (Ref. 2,3,4). This peak value can reach a value as high as 60 % of the materials ultimate strength. Because of the direct impact of the particles on the metallic surface, significant surface roughness can result with a thin layer at the surface being work hardened. The net result of shot peening is often a noticeable improvement in fatigue properties (Ref. 5). Shot peening under a prestress can produce an even higher level of compressive stresses (Ref. 3).

Laser-shock peening (LSP) was first used by Battelle Columbus Laboratories in 1974 (Ref. 6). In this process, the surface of the material is covered with a thin layer of opaque material (such as black paint) and over this layer a thick layer of transparent material (such as water) is placed. The laser beam passes through the transparent material and causes a thin layer of the opaque material to vaporize. The rapidly expanding gas is confined by the transparent overlay and creates very high pressures. The surface pressure propagates into the metallic substrate as a shock wave, causing plastic deformation and subsurface residual compressive stresses. LSP is reported not to cause surface roughness. While the residual stress across the treated laser beam spot is mostly uniform and compressive, it changes to tension towards the periphery of the spot and beyond. But, when large areas are treated by overlapping laser beam spots, there is no indication of tensile residual stresses in the overlap regions; the distribution of residual stress is said to be relatively uniform on the surface, while the distribution below the surface is similar to that of shot-peening.

1) Senior Aerospace Engineer and Aerospace Engineer, Army Vehicle Technology Directorate, ARL; 2) Professor, Old Dominion University; 3) Senior Scientist, NASA Langley Research Center; 4) Consultant.

Most of the publications dealing with shot-peening or LSP cite increases in fatigue strength as shown by higher values of the materials endurance limit. A few publications (Ref. 7,8) show crack-length-versus-fatigue-load-cycle curves which show enhanced crack initiation lives for peened specimens; the crack propagation rates appear to be the same for the peened and unpeened specimens. In a paper by Lincoln and Yeh (Ref. 5), they showed an increase in the crack-growth life of a factor of ten for peened compared to unpeened. This was for an analytical study. In the open literature, there appear to be few papers that show da/dN versus ΔK results for shot peened and unpeened specimens. This paper has two objectives. One objective was to investigate the effect of shot and laser peening on crack growth in the 2024 aluminum alloy. The second objective was to show the effect of shot peening on the fatigue life of 4340 steel with and without a machine-like flaw.

TEST PROGRAM

To assess the affect of peening on crack growth and fatigue life, constant amplitude fatigue tests were conducted on small laboratory test specimens fabricated from 2024-T3 aluminum alloy and 4340 steel, respectively. The 2024 aluminum alloy is typical of the material found in the wing structure of fixed-wing aircraft and 4340 steel is typical of the material found in the landing gear of fixed-wing aircraft and in the dynamic components of rotary-wing aircraft. This section describes the material, test specimen configuration, constant-amplitude tests, shot and laser peening, and the machine-like flaws machined on the surface of the 4340 steel fatigue test specimens.

Material and Test Specimen Configuration

The material used for the fatigue life study was 4340 steel heat treated to an ultimate strength of 210 ksi. The fatigue endurance limit for this heat of material was determined to be about 68 ksi at a stress ratio, R=-1. This agreed with the value given in the Military Handbook 5B (Ref. 9.) Specimens were machined to have a surface finish of 32 rms which is a similar finish used on helicopter dynamic components. The nominal thickness of the test specimens was 0.35 inches. Specimens were machined to an hour glass shape (see Fig. 1(a) and 1(b)) producing an elastic stress concentration factor, K_T, of 1.03 as determined by the boundary force method (Ref. 10.) The test specimen was 7 inches in length and 1.5 inches in width at the mid-length.

The material used for the crack growth portion of this study was 2024-T3 aluminum alloy machined to a test specimen thickness of 0.25 inches. Specimens were machined with two semi-circular holes on both edges of the specimen as shown in Figure 1c. This resulted in an elastic stress concentration factor, K_T, based on gross stress of 3.20. To initiate fatigue cracks , there was a 45-degree crack starter slot at the root of each semi-circular hole, with slots at opposite corners of the cross section of the specimen as shown in Figure 1c. Before the specimens were peened, a fatigue crack was initiated by fatigue cycling the test specimen at the same constant amplitude loads as used in the crack growth tests until a length of approximately 0.05 inches was achieved. It should be noted that the U.S. Air Force damage tolerance rogue flaw length is 0.05 inches.

Constant Amplitude Tests

For the crack growth and fatigue studies, constant amplitude tests were conducted in servohydraulic, electronically controlled test stands at a cyclic frequency of 3 to10 hertz with loads controlled to within 1 percent. For the crack growth tests the stress ratio, R, was 0.1 and for the fatigue tests R was minus one. All fatigue test lives reported herein on the 4340 steel were to specimen failure.

Shot Peening and Scratch Dimensions

For the crack-growth tests, after precracking to approximately 0.05 inches, six specimens were shot peened and four specimens were laser peened. The shot peened specimens were shot peened over all surfaces, including the notch radius, except for the grip regions. The shot peening intensity was .010 to .012 Almen A, with 100% coverage.

The laser peened specimens were shocked using a laser input of 100 J/cm^2. In the laser peening process a pulse of laser light is absorbed and rapidly forms a high pressure plasma of approximately 10^5 psi. A tamping layer confines the plasma and drives the pressure pulse into the material being peened. This pressure pulse induces the compressive residual stresses into the metallic material.

To show the effect of shot peening on the fatigue life of 4340 steel with and without a machine-like flaw, fatigue tests were conducted on test specimens with and without a machine-like flaw (see Figures 1(a) and 1(b).) The flaw for this study was a simulated machining scratch. Tests were also conducted on specimens that were shot peened after being scratched. The machine-like scratch was machined into the specimen surface using an end mill. The scratch was machined across the entire width of the specimen, but only on one side of the specimen (see Fig. 1(b).) Each specimen scratch was measured to insure uniformity in geometry of the scratches for the test specimens tested in this study. Measurements of the scratch depth of the test specimens showed a range in scratch depth of 0.0014 to 0.0029 inches with a mean value of 0.0020 inches and a standard deviation of 0.00036 inches. The width of the scratches was approximately twice the depth. The shot peening process on these specimens was done by a major U.S. helicopter manufacturer. X-ray diffraction measurements of the compressive residual stresses produced by the shot peening ranged from 60 to 90 ksi. The compressive residual stresses reached a zero stress level at about 0.006 inches below the specimen surface.

Fatigue Tests Specimen Types

Four different specimen types were used in the 4340 steel test program. For the baseline data, specimens were machined as pristinely as possible to provide fatigue life test data of specimens with no machining flaws. A second set of specimens were machined to the proper specimen geometry, then a machine-like scratch was machined on the specimen surface with the dimensions and procedures stated previously. A third set of specimens were shot peened after being machined. Finally, a fourth set was machined to the hour-glass geometry, then the machine-like scratch was machined on the specimen surface followed by shot peening.

TEST RESULTS

Corner cracks were formed in all 2024-T3 aluminum alloy specimens at the starter slots by fatigue cycling until a fatigue crack of approximately 0.05 inches was reached under constant amplitude loading with a maximum loading of either 10 or 13.3 ksi, gross stress, with an R-value of 0.1. The minimum load was then increased to obtain an R-value of 0.7 or 0.8 and the crack advanced approximately 0.005 inches in order to mark the shape of the corner crack for examination after failure.

Crack growth life

The effect of shot peening on crack growth lives is shown in Figures 2 and 3. Crack growth life being the number of load cycles it takes for the crack to grow from the initial crack size, approximately 0.05 inches, to failure. In general shot peening had a noticeable affect on crack growth life by increasing the time to failure between a factor of 2 to 4 for the lower applied stress level tests, Figure 2 at 10 ksi, or from 1.2 to 2.7 for the higher stress level, Figure 3 at 13.3 ksi. Because of the limited number of test specimens used in this study, it was not possible to determine what caused this scatter in the crack growth lives.

The primary influence of shot peening appears to occur during the very early extension of the crack even though the entire specimen was shot peened. These results suggest that the impact of the shot peening process at the precrack position is critical in affecting the crack growth lives.

The effect of laser peening on crack growth lives is shown in Figures 4 and 5. The crack growth lives for the laser peening tests showed less scatter than the shot peened tests. At the lower stress level of 10 ksi, Figure 4, the crack growth life was increased by approximately 1.8, while at the higher stress level of 13.3 ksi, Figure 5, the increase was between 2.1 and 2.6.

Crack Growth Rate

To assess the effect of shot and laser peening on crack growth, baseline tests were conducted on specimens that were not peened to compare with the peened test results. The test results from the unpeened specimens are shown in Figure 6. The solid curve is the ΔK versus rate curve for R = 0.1. The current results show good agreement with previous results on 2024-T3 aluminum alloy (solid line.) The dashed curve is the ΔK_{eff} versus rate curve for the thin-sheet aluminum alloy and the α -values denote a constraint-loss regime (plane-strain to plane-stress behavior.) Below a rate of 4×10^{-6} inches/cycle, the crack is under high constraint (α=2) and above 1×10^{-4} inches/cycle, the

crack is under plane-stress (α=1) conditions. The departure from the da/dN versus ΔK at R=0.1 as shown in Figure 6 at the higher ΔK values may be due to the effects of width on fracture. The current tests were conducted on specimens of 1.5 inches in width whereas the solid curve was on specimens that were 12 inches in width. Smaller width specimens have lower stress-intensity factors at failure than larger width specimens. The procedure to calculate the stress intensity for this specimen configuration with a corner and through crack is given in Appendix I.

As shown in Figures 7 and 8 , the test results from the shot and laser peening tests show that in general when the cracks are small (ΔK less than 10 ksi-in$^{1/2}$) peening does noticeably reduce the crack growth rates. This probably accounts for the longer crack growth lives shown in figures 2 through 5. Figure 7, which shows the shot peening test results, shows that the crack growth rate behavior at the higher ΔK values exhibited the same width effect as shown for the nonpeened test data.

The laser peening crack growth comparisons shown in Figure 8 show a tendency for higher crack growth rates when ΔK is approximately between 10 and 20 ksi-in$^{1/2}$ This is probably because the laser peening done on these test specimens seemed to be very severe thus possibly producing significant tensile stresses which are needed to equilibrate the residual compressive stresses that result near the surface because of the peening. The specimen surface on the laser peened specimens had a noticeable crater-like appearance. Comments in the literature indicate that laser peening should not cause a noticeable change in surface appearance (i.e., surface roughness).

Fatigue life

To assess the effect of shot peening on the fatigue life of 4340 steel with and without a machine-like flaw, constant amplitude fatigue tests were conducted on unnotched specimens with and without a machine-like scratch with a series of tests also conducted on specimens that were shot peened after the scratch was machined onto the specimen surface. The scratch was machined onto one side of the specimen to a nominal depth of 0.002 inches.

Figure 9 shows the results of the fatigue tests on the pristine specimens as well as the specimens that had been shot peened with no surface scratch (symbols with arrows indicate a runout, test stopped before failure.) The results of these data showed a definite increase in the fatigue life of the baseline material as a result of shot peening. Based on the limited amount of tests, the endurance limit of the baseline material appears to be about 10 percent higher with a shot- peened surface. It is also noted that the baseline material endurance limit of about 68 ksi agrees very well with that found in Military Handbook 5B (Ref. 9.) A general increase in fatigue life at all the stress levels tested is noted from the data shown in Figure 9. The shape of the two S/N curves seems to be similar, but with the limited amount of tests run this similarity can only be assumed.

Figure 10 shows the results of the fatigue tests on the specimens with machine-like scratches compared to the pristine specimens. As seen in this figure the endurance limit was reduced from 68 ksi for the pristine specimen to about 40 ksi for the specimen with a 0.002 inch deep scratch. This is a decrease of about 40 percent. A scratch of this size could easily be missed by an optical inspection of an aircraft component. With this magnitude of reduction in the endurance limit resulting from a fairly small machine-like scratch, it can be seen that some fabrication procedure is needed to protect against this possible loss in fatigue strength.

As somewhat of a standard practice, most helicopter manufacturers shot peen their life limited dynamic components after machining. Figure 11 shows the effect on the fatigue life of specimens that have been shot peened after a scratch was machined onto the specimen surface. As shown by the test data, the fatigue life of the specimens containing a scratch with shot peening is almost the same as that of the pristine specimen. Hence, shot peening is potentially a successful method in keeping the fatigue strength of a material at its pristine value when a fabrication flaw may be present in of the structure.

Fatigue life analysis

Since about the mid-1980's, a trend has been developing to predict total fatigue life (from the first load cycle to failure) using only fatigue crack growth considerations (Ref. 11.) In order for this to be accomplished, a very small initial crack size (0.00004 to 0.002 inches) had to be assumed to exist in the material. Furthermore, as shown by numerous investigations (Ref. 12-14), these very small cracks have crack growth characteristics that are considerably different than large cracks (cracks longer than 0.08 inches). In fact, these small cracks are considered

to exhibit a "small-crack effect" which as described by linear-elastic fracture mechanics (LEFM), are small cracks that grow faster than long cracks at the same stress intensity factor range and grow at stress intensity factors below the long-crack threshold (ΔK_{th}). A review of the concepts involved in "small-crack" theory is given by Newman in reference (Ref. 15).

After conducting the fatigue life experimental portion of this study, it was decided to investigate the ability of the small-crack crack theory to predict the fatigue life of the test specimens that contained the machine-like scratch. Since several studies by Newman and his colleagues (Ref. 16-18) had shown a crack growth analysis using small-crack considerations could predict total fatigue life using only a crack growth analysis, it was logical to try to employ these concepts to predict the fatigue life of the test specimens with the machine-like scratches. In Newman's studies he used a crack-closure based model (Ref. 19) to predict total fatigue life (Ref. 11). While the work in reference 11 illustrates analysis only on aluminum alloys, this method has also been shown to work on high aircraft quality steels (Ref. 16).

As a first step in the analysis of the machine-like scratch, it was decided to use the small-crack analysis to predict the life of the as-manufactured test specimens in order to check the basic material data input into the crack-growth computer code. As stated previously, perhaps the most important input to this analysis is the initial crack size. The long and small crack characteristics of the 4340 steel used in this study were thoroughly investigated as part of an AGARD study done during the 1980's (Ref. 16). In the study, conducted by Swain et al, examination of 35 crack initiation sites described the distribution of initiation sites as shown in Figure 12. The dominate initiation site was a spherical (calcium-aluminate) particle as shown in Figure 13. The mean defect size was determined to be a radius of about 0.0005 inches. From Figure 12 it is seen that defects found in this study ranged from a radius of about 0.0002 to 0.0016 inches.

Most of the analysis done previously using FASTRAN has been done on specimen configurations that contained a hole with an elastic stress concentration, K_T, of about three (Ref. 16-18). As stated previously, the test specimen used in these tests had a nominal K_T of one. In a K_T = 1 stress distribution a much larger volume of material is available for the crack to initiate. In this larger volume of material, it is probable that a larger defect would exist that could initiate the crack. Newman, in his analysis of K_T =1 specimens made of the aluminum alloy 2024-T3, required a 0.00079 inch radius crack to fit the constant amplitude test data for stress ratios, R = 0 and -1. But in a K_T = 3 specimen, a 0.00024 inch radius crack was needed to predict total fatigue life (Ref. 11). For the analysis conducted on the K_T =1 geometry used in this study the mean defect size, 0.0005 inches, as shown in Figure 12 was used as the initial fatigue crack to predict the solid curves as shown in Figure 14. The FASTRAN analyses compared well with the test data, even predicting the endurance limit.

In order to predict the total fatigue life of the machine-like scratch test specimen, the geometry of the initial crack must be chosen in order to define the stress intensity factor to use in the crack growth analysis. For this study, it was decided to model the scratch as a single-edge crack under a tensile loading. As stated previously, measurements of the scratch depth of the test specimens showed a range in scratch depth of 0.0014 to 0.0029 inches with a mean value of 0.002 inches and a standard deviation of 0.00036 inches. Using the average scratch depth as the initial crack length, the crack geometry of a single-edge crack, and using the applied stress as the applied load divided by the cross-sectional area of the test specimen, the resulting predictions from FASTRAN are shown as the dashed curve in Figure 14. As shown, the agreement between the FASTRAN analysis and the test data is very good.

CONCLUDING REMARKS

The test results obtained in this study have shown similar effects of shot and laser peening on crack growth lives and fatigue life that have been previously reported in the literature. In general, both crack growth life and fatigue life are improved as a result of shot and laser peening. This study also indicates that when cracks are small, peening also has a noticeable affect on the crack growth rate producing a reduction in the crack growth rate. As previously postulated by others the peening depth being relative small would only affect the crack growth rates of fairly small cracks. There is some evidence that the compressive residual stresses from laser peening may approach a depth of 0.05 inches (Ref. 7).

The data from these tests as well as other data in the literature (Ref. 3) show the beneficial effects on fatigue life. Some data in the literature(Ref. 3) show an increase in fatigue life by as much as a factor of 10 at a given stress

level. The fatigue life improvement of the 4340 steel tests in this study did not show that much benefit. It did show, however, that the endurance level of a flawed part can almost be returned to that of a pristine part if the part is peened after the flaw is induced.

The effect of laser peening on crack-growth life was not as beneficial in this study as has been shown by Clauer (Ref. 22). Clauer's study showed an increase in crack growth life even greater than a factor of 10. He also showed similar benefits in fatigue life.

The following conclusions are drawn from the work described herein.

1. The shot and laser peening processes used in this study had a noticeable affect on the crack growth rate of the 2024-T3 aluminum alloy in reducing the rates when the cracks are fairly small with ΔK being approximately less than 10 ksi-in$^{1/2}$.

2. In general shot peening had a noticeable affect on crack growth life by increasing the time to failure from a factor of 2 to 4 for the lower applied stress level tests, 10 ksi, or from 1.2 to 2.7 for the higher stress level, 13.3 ksi.

3. For laser peening the crack growth life at the lower applied stress level of 10 ksi was increased by approximately 1.8, while at the higher stress level of 13.3 ksi, the increase was between 2.1 and 2.6.

4. Shot peening of high strength 4340 steel produced a higher endurance limit by about 10 percent.

5. A machine-like scratch in high strength 4340 steel reduced the endurance limit by about 40 percent.

6. Shot peening a material that contains a machine-like scratch restored the endurance limit of the material to within about 10 percent of its original value.

7. A crack-growth closure based analysis using small-crack theory predicted the total fatigue life of pristine test specimens and specimens with a machine-like crack with very good accuracy.

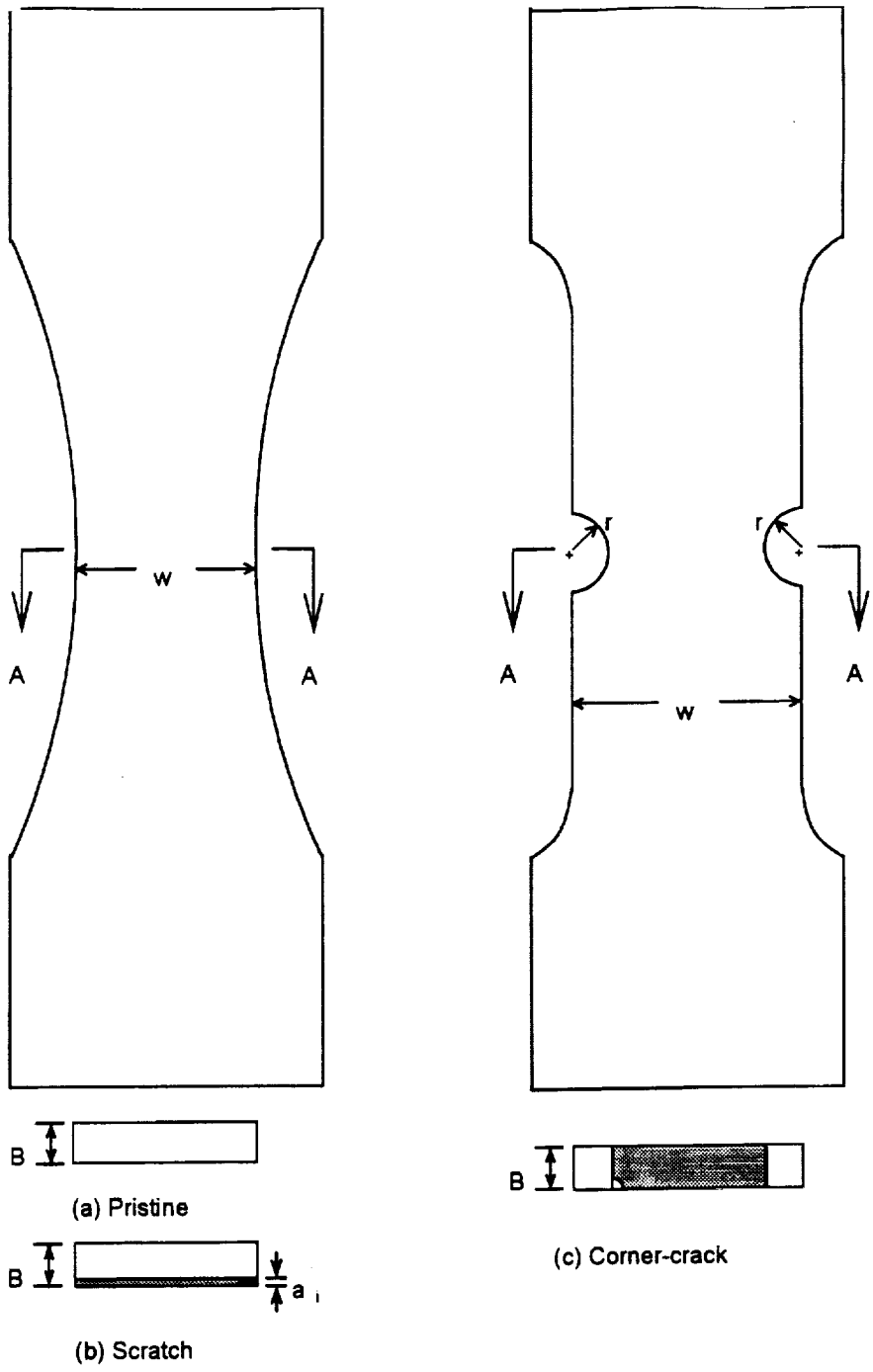

Figure 1. Fatigue (4340 steel) and crack-growth (2024-T3) specimens.

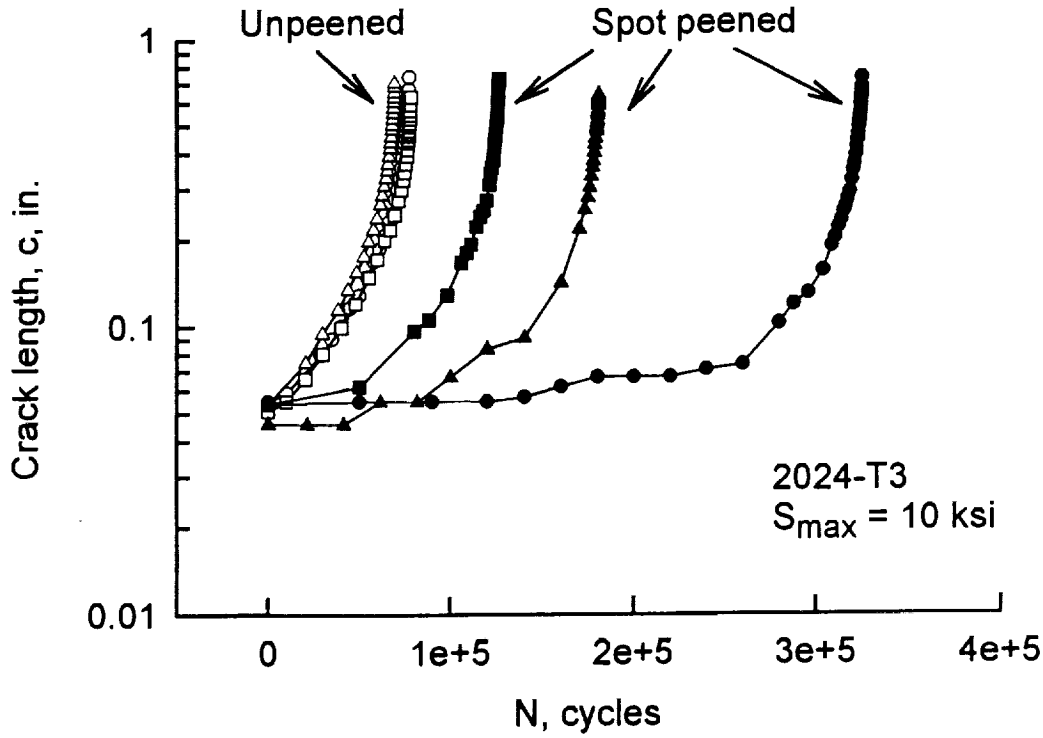

Figure 2. Crack length against cycles for unpeened and shot-peened specimens at an applied gross stess of 10 ksi.

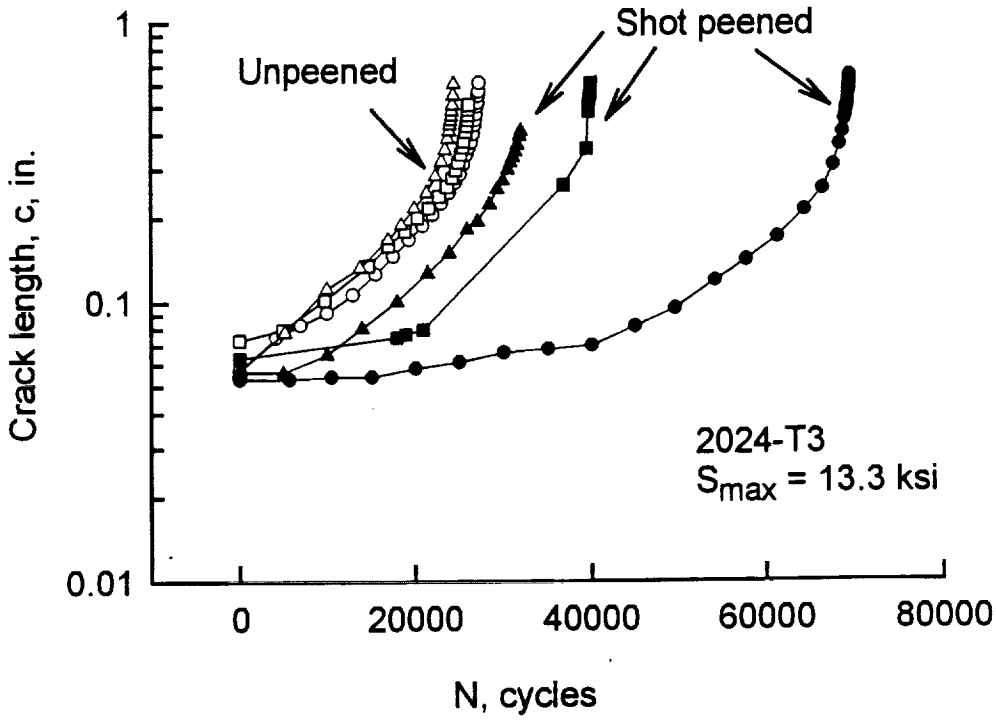

Figure 3. Crack length against load cycles for unpeened and shot-peened specimens at an applied gross stress of 13.3.ksi.

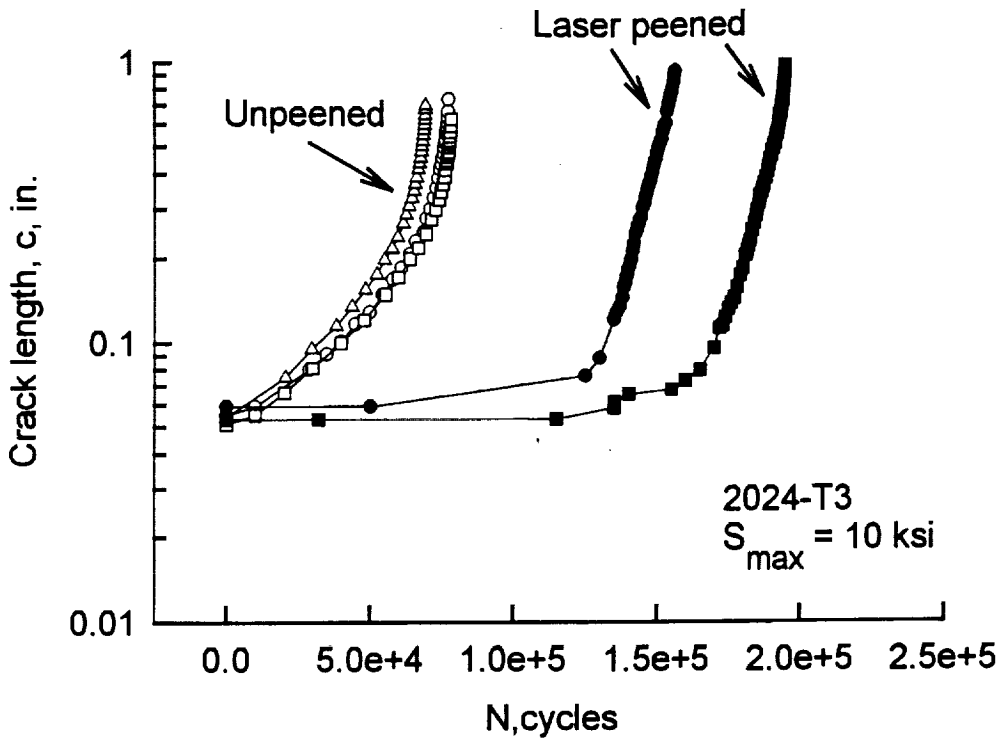

Figure 4. Crack length against load cycles for unpeened and laser-peened specimens at an applied gross stress of 10 ksi.

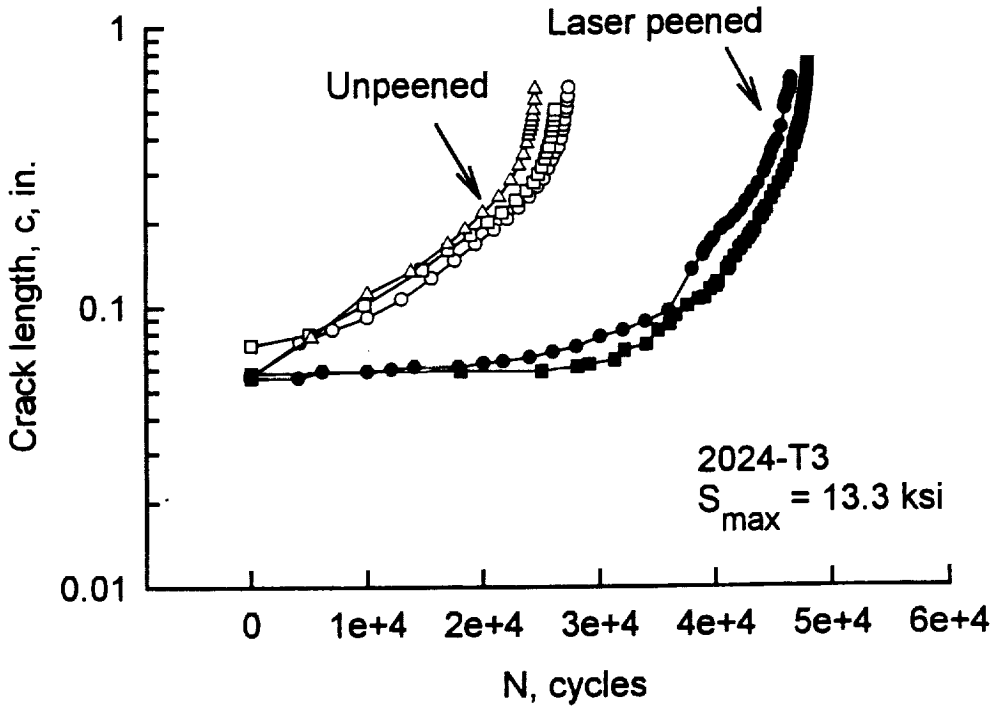

Figure 5. Crack length against load cycles for unpeened and laser-peened Specimens at an applied gross stress of 13.3 ksi.

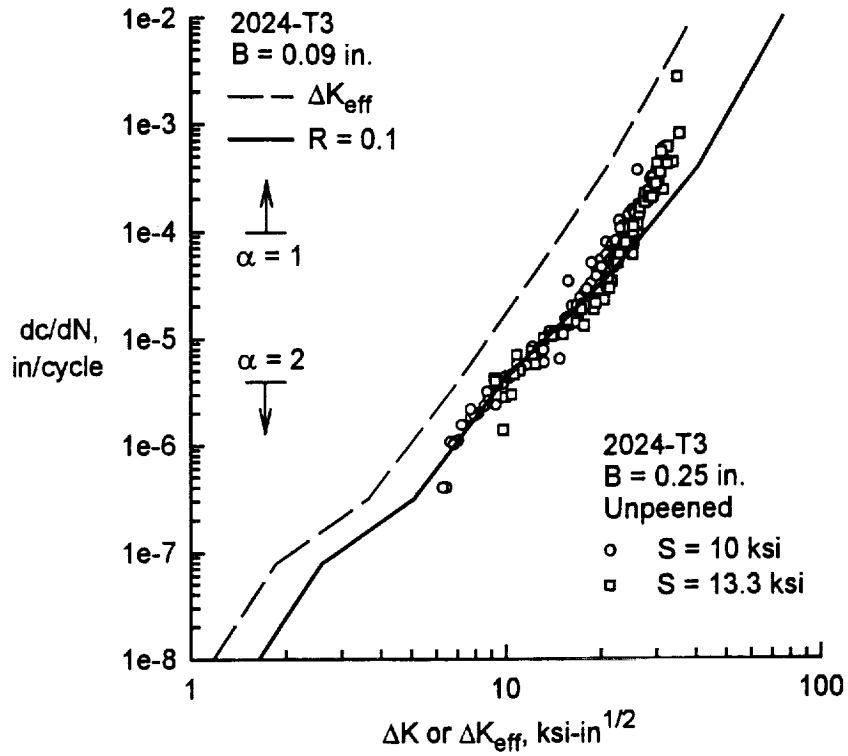

Figure 6. Comparison of crack growth rates for unpeened specimens with results from thin sheet 2024-T3.

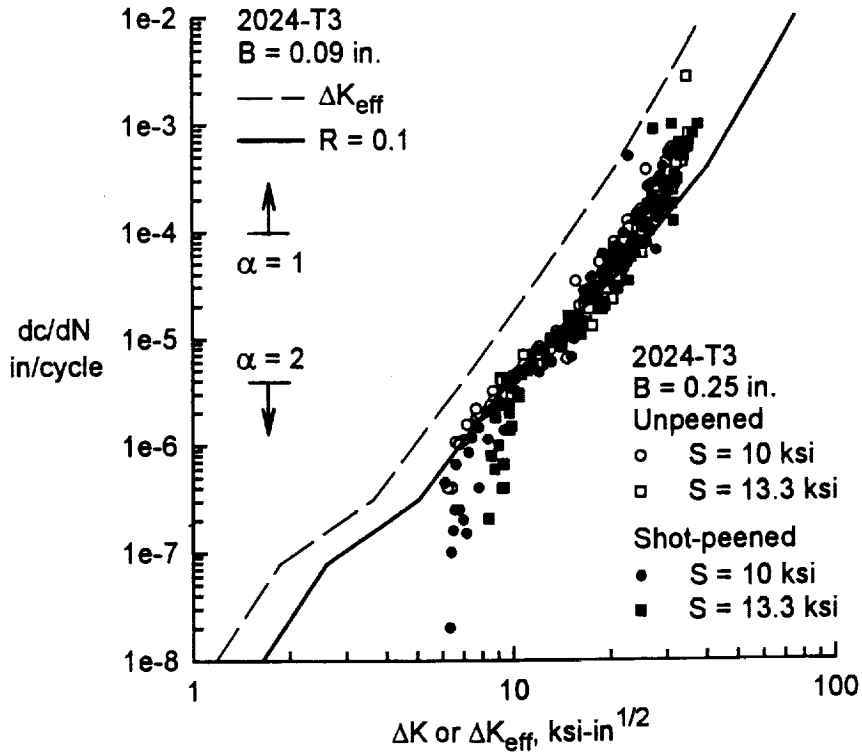

Figure 7. Crack growth rates for shot-peened specimens.

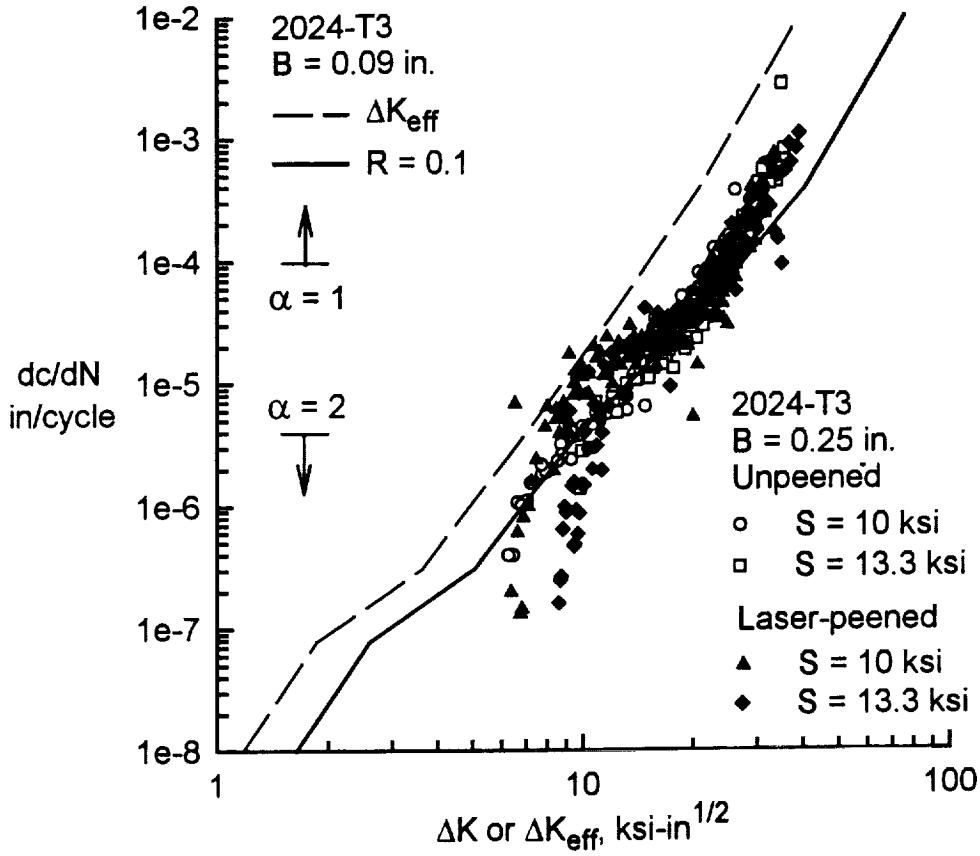

Figure 8. Crack growth rates for laser-peened specimens.

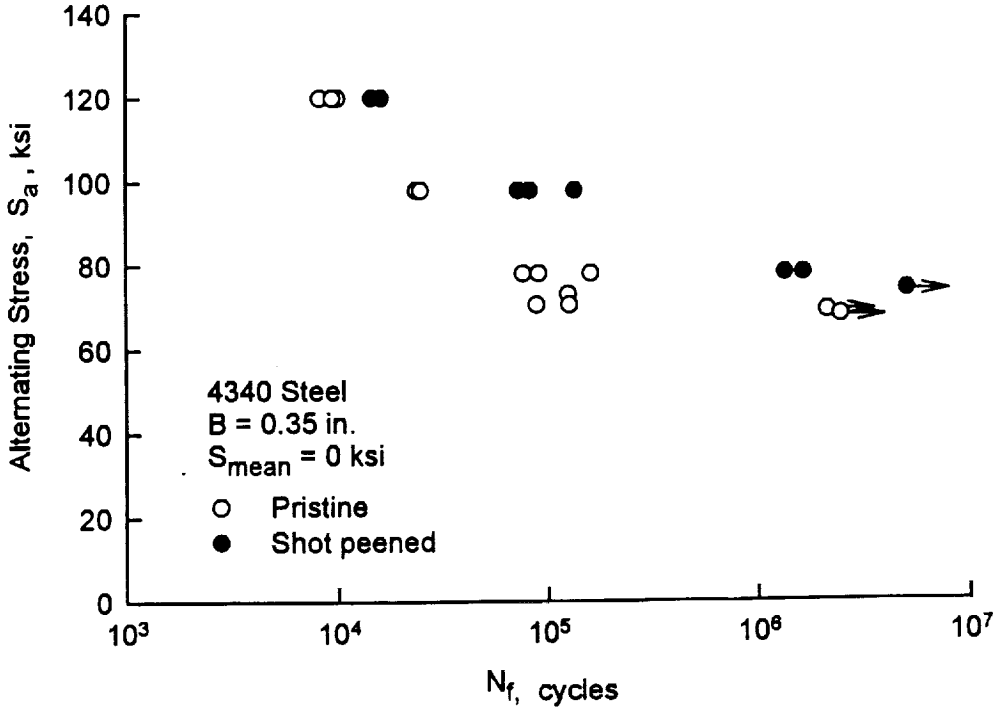

Figure 9. Fatigue life of pristine and shot-peened specimens for 4340 steel. (arrows indicate runout).

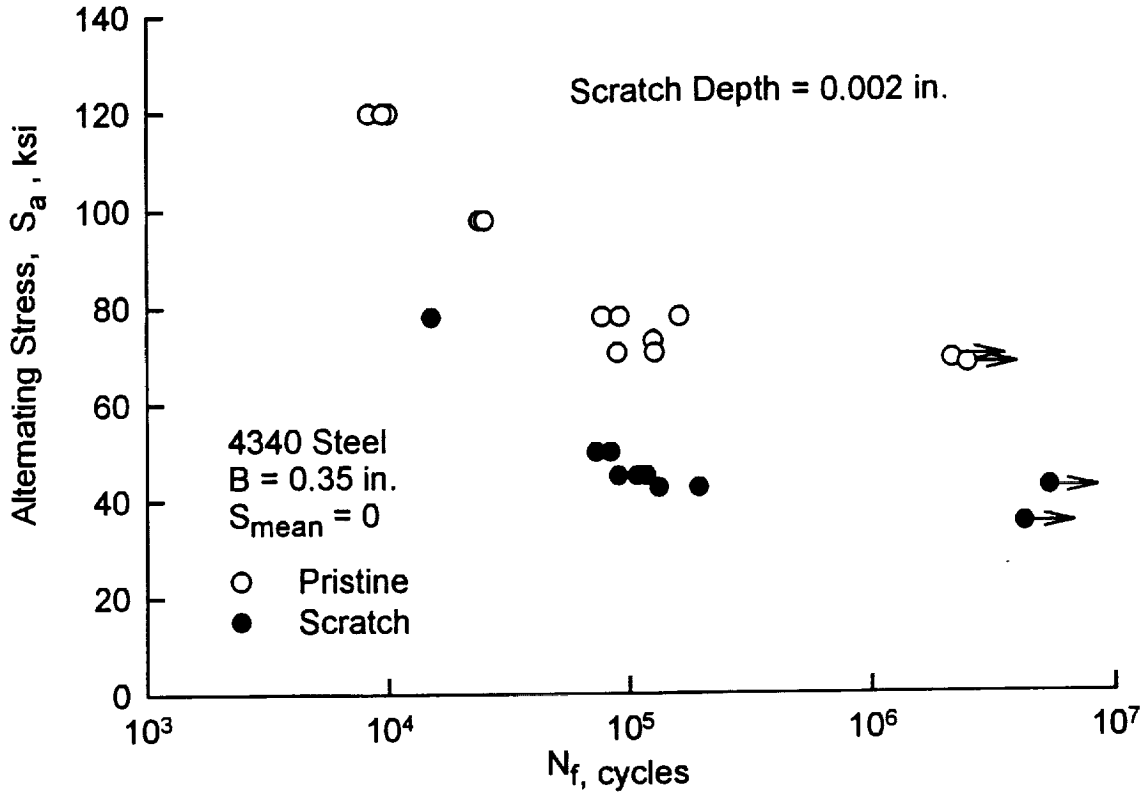

Figure 10. Fatigue life of pristine and scratch specimens (arrows indicate runout).

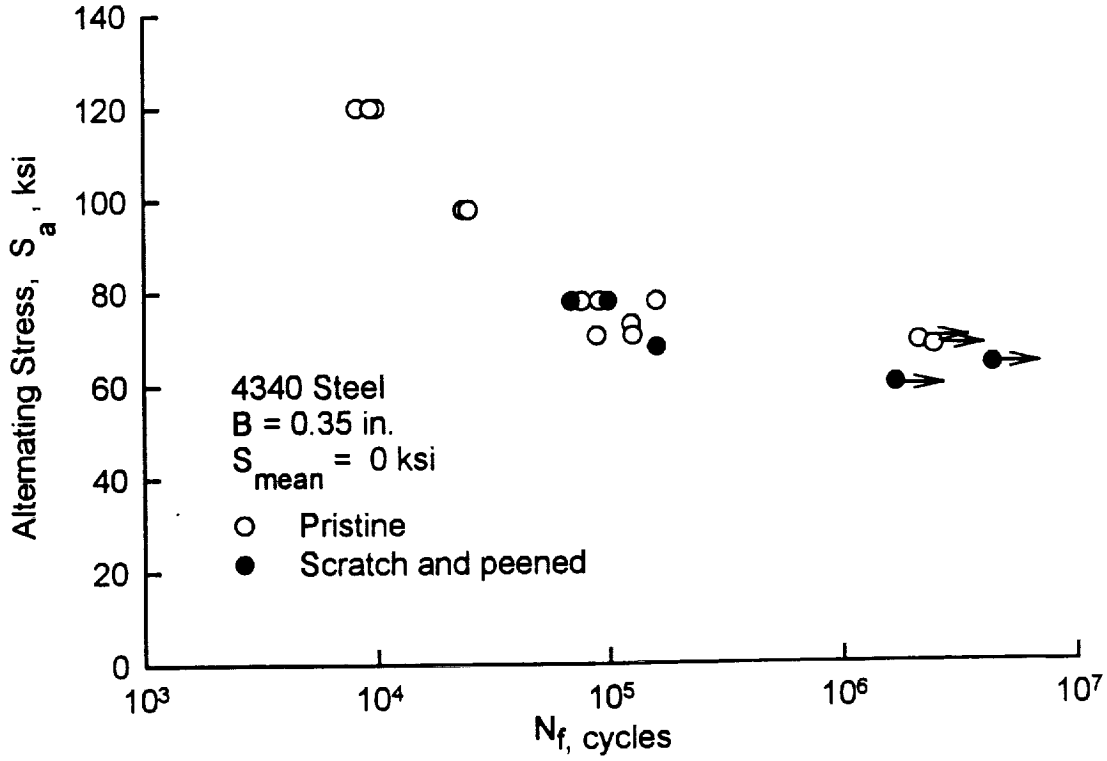

Figure 11. Fatigue and life of pristine and scratch-peened specimens (arrow indicates runout).

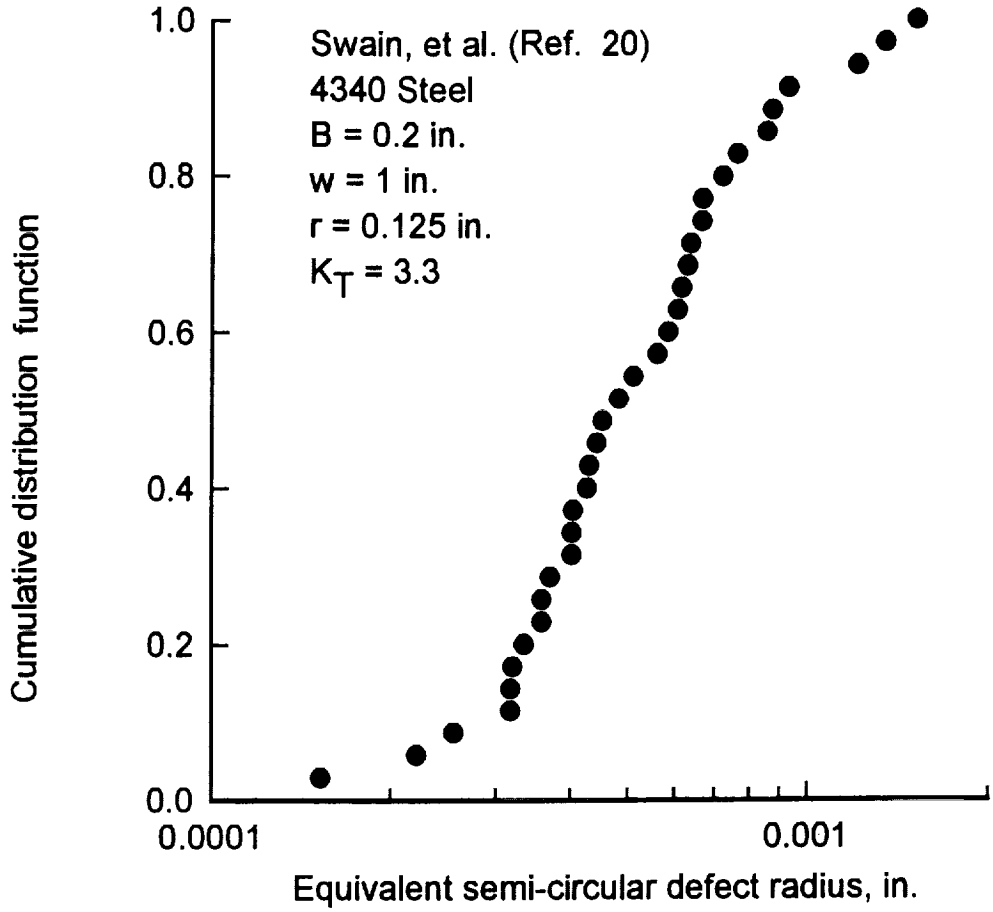

Figure 12. Cumulative distribution function for initiation sites in 4340 steel.

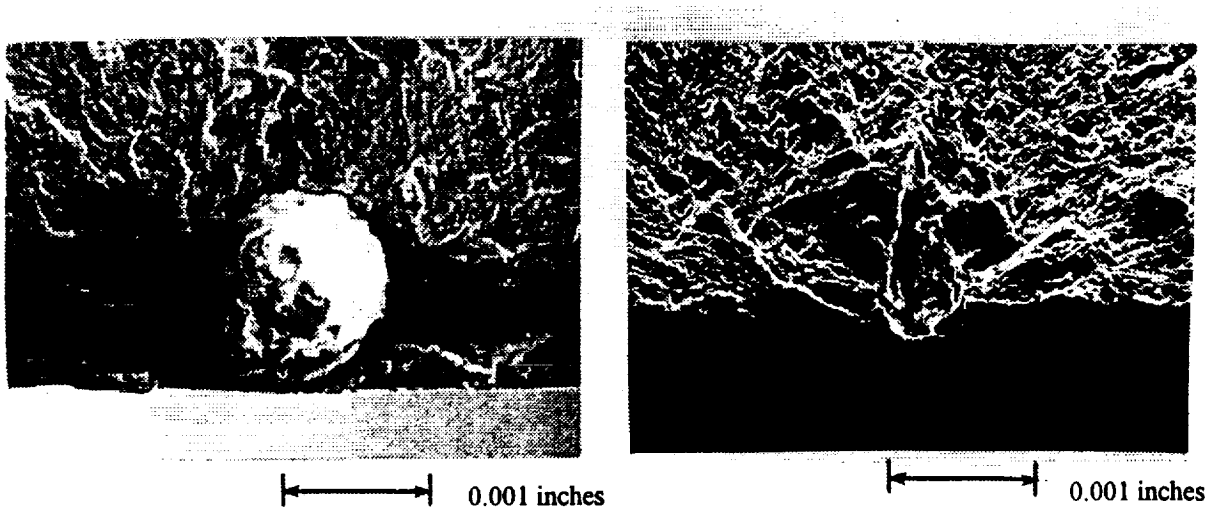

Figure 13. Crack initiation sites at spherical-inclusion particle and stringer in 4340 steel.

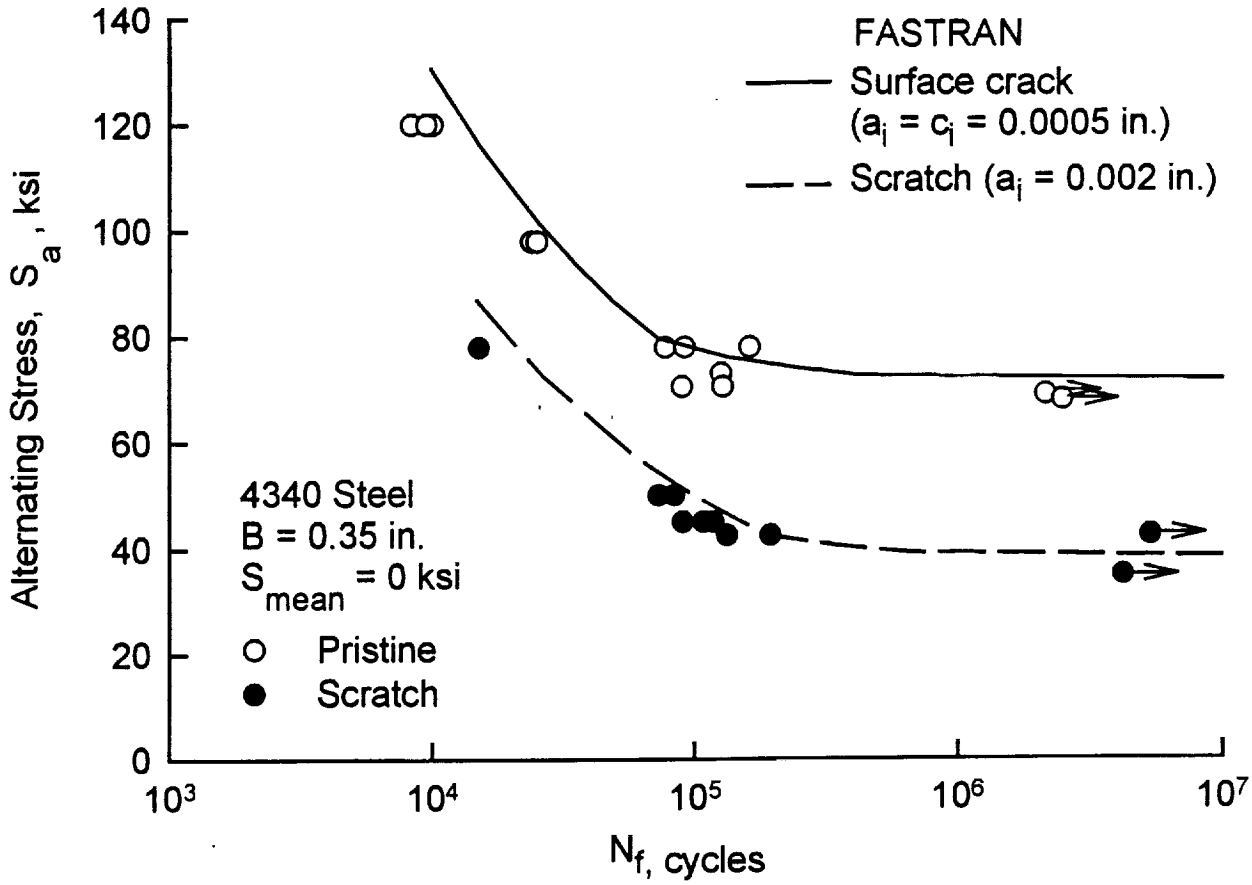

Figure 14. FASTRAN prediction of S-N behavior of pristine and scratch specimens (arrows indicate runout).

APPENDIX I

Stress-Intensity Factors

The stress-intensity factor (K) equations for a through crack and a corner crack emanating from a single notch in the double-edge-notch specimen, as shown in Figure A1, are developed herein. The FADD2D code (Ref. 23) was used to obtain the stress-intensity factors for a through crack and an engineering estimate (Ref. 24) was used to develop the stress-intensity factors for the corner crack. The FADD2D code is a boundary-element analysis. For the corner crack, the engineering estimate was based on previous finite-element analyses and equations for corner cracks at a hole in an infinite plate subjected to remote tensile stress (Ref. 25.)

Through crack at semi-circular edge notch:

The FADD2D code was used to analyze a single through crack emanating from one of the notches in the double-edge-notch specimen. The specimen was subjected to either remote uniform stress or uniform displacement. The normalized stress-intensity factor or boundary-correction factor (F) for these two cases are shown in Figure A2. Because the test specimens were loaded with hydraulic grips, a uniform displacement at the grip ends was suspected to be the most appropriate boundary conditions. An equation for the stress-intensity factor for a through crack was developed to fit the numerical calculations (circular symbols in Fig. A2). The equation is given by

$$K = S\,(\pi c)^{1/2}\,F \qquad (1)$$

where $F = f_1\, g_1\, f_w$ for $c/r \le 3.5$. The function f_1 and g_1 account for the notch behavior and f_w accounts for the finite-width effect. Equations for the f_1, g_1, and f_w functions are:

$$f_1 = 1 + 0.358\,\lambda + 1.425\,\lambda^2 - 1.578\,\lambda^3 + 2.156\,\lambda^4 \quad \text{where } \lambda = 1/(1 + c/r)$$

$$g_1 = K_T\,[0.36 - 0.032/(1 + c/r)^{1/2}] \quad \text{where } K_T = 3.05$$

$$f_w = 1 + 0.61\,\gamma + 3.46\,\gamma^2 - 7.55\,\gamma^3 + 5.82\,\gamma^4 \quad \text{where } \gamma = c/(w - 2r).$$

Equation (1) is shown as the solid curve in Figure A2 and is within about 1 percent of the numerical calculations from the FADD2D code.

Corner crack at semi-circular edge notch:

In lieu of conducting fully three-dimensional analyses for a corner crack emanating from the double-edge-notch specimen (Fig. A1(b)), an approximate method was used to estimate the K solutions. The approach was to take the ratio of the corner-crack (K_{cc}) solution to the through-crack (K_{tc}) solution for the same crack length, c, emanating from a hole in an infinite body subjected to remote applied stress. Then the stress-intensity factor for a corner crack at the edge notch can be estimated by multiplying the K_{cc}/K_{tc} ratio times the stress intensity factors for the through crack at the edge notch (Fig. A1(a)).

The stress-intensity factor for a corner crack at a hole was obtained from Newman and Raju (Ref. 25) and the through-crack solution from Newman (Ref. 26). Because the crack-growth analysis for the corner crack was treated as an average crack-growth process, the K values at the 10 and 80-degree locations were averaged to calculate Kcc. The K_{cc}/K_{tc} ratios for various corner-crack shapes (a/c ratios) are plotted in Figure A3 as symbols. An expression was chosen to fit these numerical values and the ratio is given by

$$K_{cc}/K_{tc} = 0.8 + 0.2\,a/B - 0.2\,(1 - a/B)\,(a/c) - 0.05\,(1 - a/B)^{15} \qquad (2)$$

Using equation (2), the K_{cc}/K_{tc} ratio approaches unity as the corner crack becomes a through crack (a/B = 1).

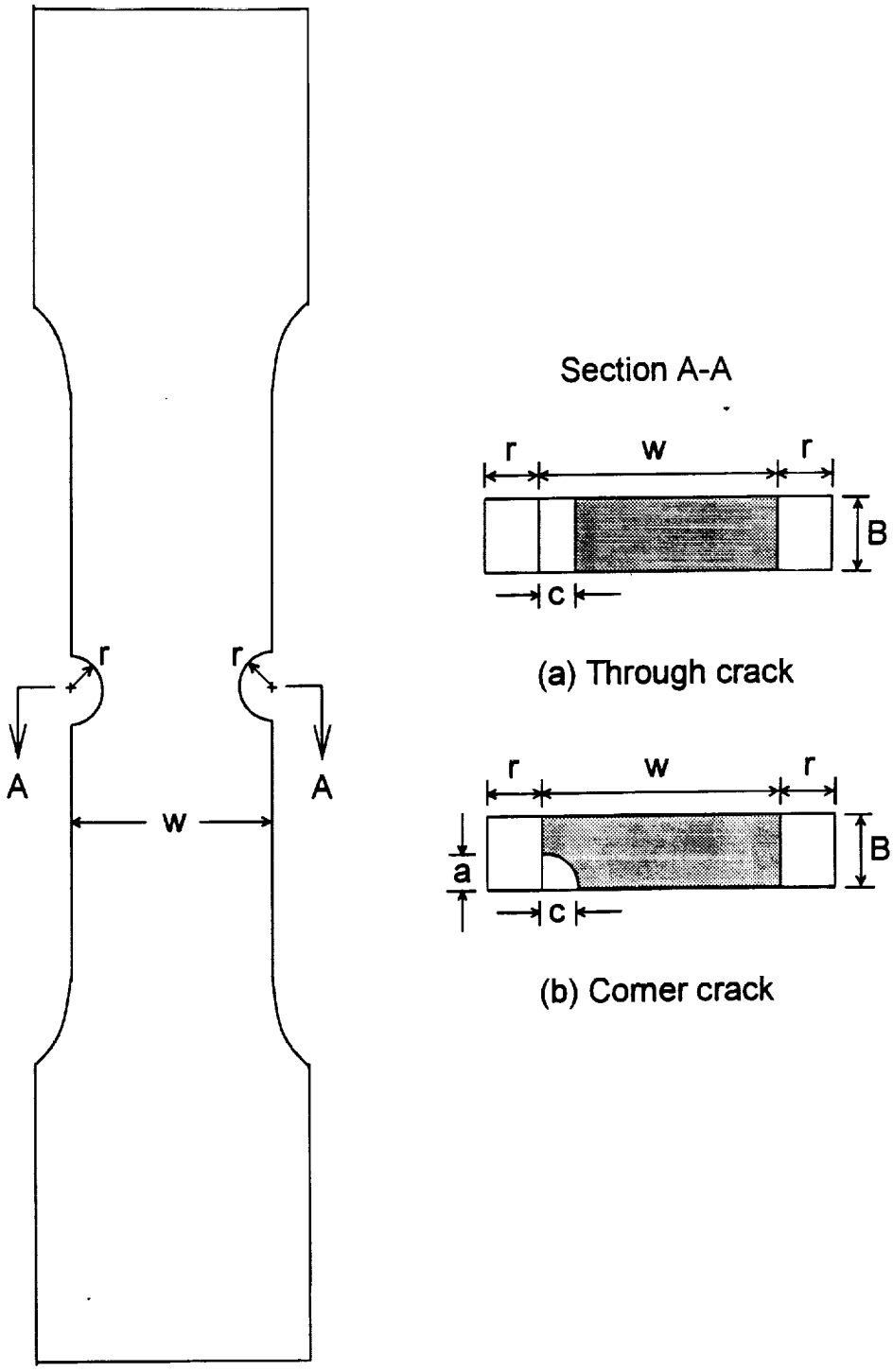

Figure A1. – Double-edge-notch tensile specimen.

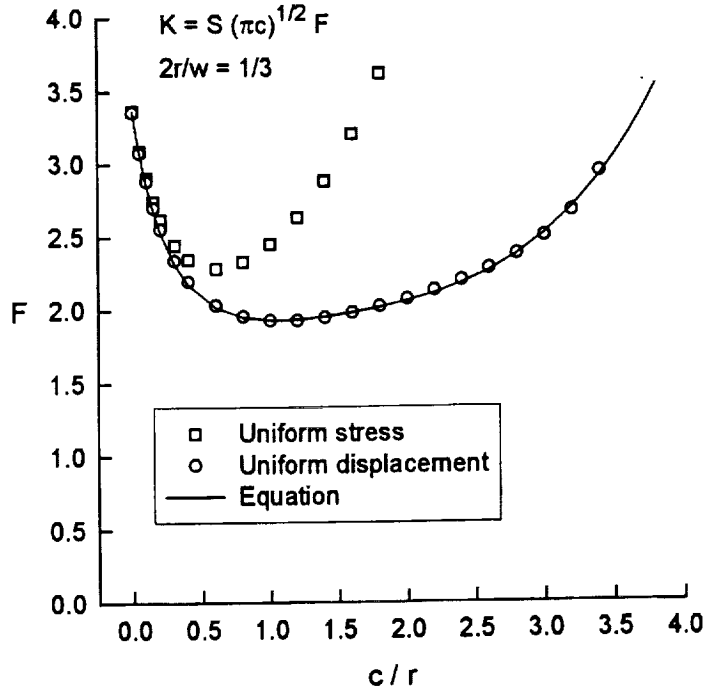

Figure A2. – Normalized stress-intensity factors for a through crack at an edge notch in the double-edge-notch tensile specimen.

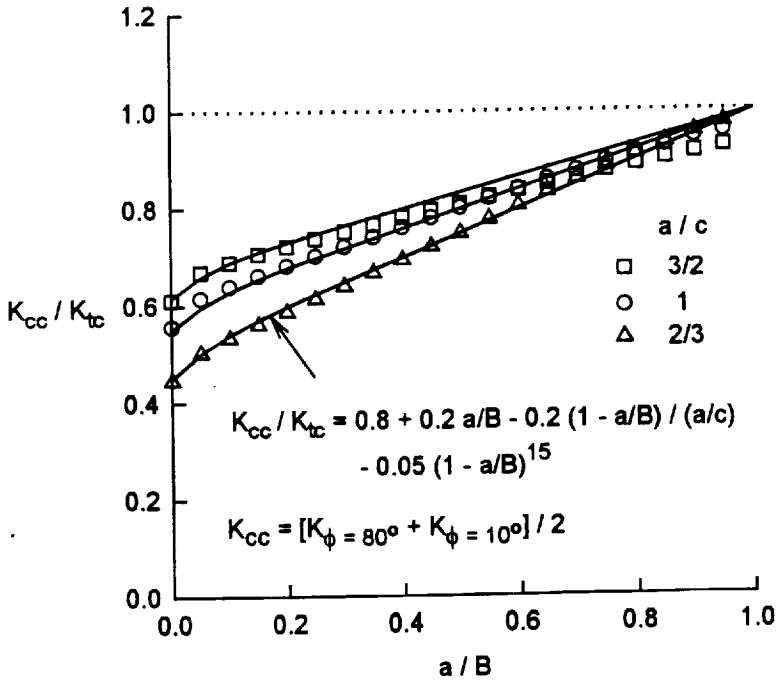

Figure A3. – Ratio of stress-intensity factors for corner crack and through crack at a hole in an infinite plate subjected to remote applied stress.

REFERENCES

1. Fuchs, H.O. and Stephens, R.I., *Metal Fatigue In Engineering*, John Wiley & Sons, 1980.
2. Chu, J.P., Rigsbee, J.M, Banas, G., and Elsayed-Ali, H.E., "Laser-Shock Processing Effects on Surface Microstructure and Mechanical Properties of Low Carbon Steel," Materials Science and Engineering A260, 260-268, 1999.
3. Berns, H. and Weber, L., "Influence of Residual Stresses on Crack Growth," Impact Surface Treatment, edited by S.A. Meguid, Elsevier, 33-44, 1984.
4. Ferreira, J.A.M., Boorrego, L.F.P., and Costa, J.D.M., "Effects of Surface Treatments on the Fatigue of Notched Bend Specimens," Fatigue, Fract. Engng. Mater., Struct., Vol. 19 No.1, 111-117,1996.
5. Lincoln, J.W. and Yeh, H.C., "Treatment of High-Cycle Vibratory Stress in Rotorcraft Damage Tolerance Design," in *Application of Damage Tolerance Principles for Improved Airworthiness of Rotorcraft*, RTO Meeting Procedures, RTO MP-24, Corfu, Greece, February 2000.
6. "Laser Shock Processing Increases the Fatigue Life of Metal Parts," Materials and Processing, Elsevier Science Publishing Co., 3-6, September 1991.
7. Clauer, A.H., Walters, C.T., and Ford, S.C., "The Effects of Laser Shock Processing on the Fatigue Properties of 2024-T3 Aluminum," Lasers in Materials Processing, ASM, Metals Park, Ohio, 1983.
8. Clauer,.A.H., Dulaney, R.C., Rice, R.C., and Koucky, J.R., "Laser Shock Processing for Treating Fastener Holes in Aging Aircraft," Durability of Metal Aircraft Structures, in proceedings of the International Workshop on Structural Integrity of Aging Aircraft, 350-361, 1992.
9. Military Standardization Handbook, MIL-HDBK-5B, August 1975.
10. Tan, P.W., Raju, I.S., and Newman, J.C., "Boundary Force Method for Analyzing Two-Dimensional Cracked Plates," ASTM STP 945, Feb 1988.
11. Newman,J.C., Jr., Swain, M.H. and Phillips, E.P.,"An assessment of the small-crack effect for 2024-3 aluminum alloy", Small Fatigue Cracks , The Metallurgical Society, Inc., Warrendale, PA, 427-452, 1986.
12. Pearson, S. "Initiation of fatigue cracks in commercial aluminum alloys and the subsequent propagation of very short cracks", Engng.Fract.Mechs., 7,235-247, 1975.
13. Zocher, H. (ed.) "Behavior of Short Cracks in Airframe Components" AGARD CP- 328, 1983.
14. Miller, K.J. and de los Rios, E.R. (eds.) The Behavior of Short Fatigue Cracks , European Group on Fracture, Publication No. 1, 1986.
15. Newman, J.C., Jr. "Fracture mechanics parameters for small fatigue cracks", Small Crack Test Methods , ASTM STP 1149, J. Allison and J. Larsen (eds.) 6-28, 1992.
16. Swain, M.H., Everett, R.A., Jr., Newman,J.C., Jr., and Phillips, E.P.,"The growth of short cracks in 4340 steel and aluminum-lithium 2090", AGARD R-767, P.R. Edwards and J.c. Newman, Jr. (eds.) 7.1-7.30, 1990.
17. Everett, R.A., Jr., "A comparison of fatigue life prediction methodologies for rotorcraft", 7*Journal of the American Helicopter Society*, Vol. 37, (2), April 1992.
18. Newman, J.C., Jr., "Fatigue-life prediction methodology using crack-closure model", *Journal of Engineering Materials and Technology*, 117, 433-439, 1995.
19. Newman, J.C., Jr., "FASTRAN-II - A fatigue crack growth structural analysis program", NASA TM 104159, 1992.
20. Arden, R.W., "Hypothetical fatigue life problems", American Helicopter Society, National Specialists' Meeting on Helicopter Fatigue Methodology, St. Louis, Mo., March 1980.
21. Everett, R.A., Jr., Bartlett, F.D., Jr., and Elber, W., "Probabilistic fatigue methodology for safe retirement lives," *Journal of the American Helicopter Society*, Vol. 37, (2), April 1992.
22. Clauer, A.H., "Laser Shock Peening for Fatigue Resistance," in *Surface Performance of Titanium*, J.K. Gregory, H.J. Rack, D. Eylon, Eds., TMS, Warrendale, PA, 217-230, 1996.
23. Chang, C. and Mear, M. E., "A Boundary Element Method for Two-Dimensional Linear Elastic Fracture Analysis," International Journal of Fracture, Vol. 74, 1996, pp. 219-251.
24. Newman, J. C., Jr., Harris, C. E., James, M. A. and Shivakumar, K. N., "Fatigue-Life Prediction of Riveted Lap-Splice Joints Using Small-Crack Theory," Fatigue in New and Ageing Aircraft, R. Cook and P. Poole, eds., Vol. I, EMAS Publishing, 1997, pp. 523-552.
25. Newman, J. C., Jr. and Raju, I. S., "Stress-Intensity Factor Equations for Cracks in Three-Dimensional Finite Bodies Subjected to Tension and Bending Loads," Computational Methods in Mechanics of Fracture, S.N. Atluri, ed., Elsevier Publishing, 1986, pp. 311-334.
26. Newman, J. C., Jr., "An Improved Method of Collocation for the Stress Analysis of Cracked Plates with Various Shaped Boundaries," NASA TN D-6376, August 1971.

R. Prabhakaran[1], M. Saha[2], M. Douglas[3], and A. Nettles[4]

Damage Resistance and Damage Tolerance of Pultruded Composite Sheet Materials

REFERENCE: Prabhakaran, R., Saha, M., Douglas, M., and Nettles, A., **"Damage Resistance and Damage Tolerance of Pultruded Composite Sheet Materials,"** *Composite Materials: Testing, Design, and Acceptance Criteria, ASTM STP 1416*, A. T. Nettles and A. Zureick, Eds., American Society for Testing and Materials, West Conshohocken, PA, 2002.

ABSTRACT: The damage resistance of pultruded composites to quasi-static transverse indentation is characterized and the damage tolerance of transversely indented composites under subsequent compression is assessed. Two specimen thicknesses are investigated. In each case four specimens are transversely indented to failure. Five load levels are selected and sets of five specimens are loaded up to each of these load levels and then unloaded. Extensive data are gathered: load-central displacement, back surface crack length, damage area obtained from x-radiography, optical photomicrographs obtained for specimens sectioned in different orientations, etc. This information is analyzed to develop the damage initiation and progression in pultruded composites. Open hole compression tests are performed on specimens of the two thicknesses, with seven hole sizes. The specimens damaged at five load levels, during transverse indentation, are tested in compression (simulating compression after impact). From the measured compressive strengths, the concept of an 'equivalent hole diameter' for damaged specimens is explored. The strain distributions are also compared.

KEYWORDS: pultruded composites, transverse indentation, damage resistance, damage tolerance, compression, equivalent hole diameter

Damage resistance of composites is usually studied under either low velocity impact loading or static (quasi-static) transverse indentation loading. The former is more difficult and expensive to perform. Damage tolerance of composites is usually assessed by testing composite specimens, with prior damage, in tension or compression. Compression after impact (CAI) is a common method of assessing damage tolerance. An overwhelming majority of damage resistance and damage tolerance studies have been conducted with aerospace composites, such as carbon-polymer (thermoset or thermoplastic) composites. The present investigation deals with damage resistance of

[1] Old Dominion University, Department of Mechanical Engineering, Norfolk, VA 23529.
[2] Tuskegee University, Department of Mechanical Engineering, Tuskegee, AL 36088
[3] International Construction Equipment, Matthews, NC 28104.
[4] Marshall Space Flight Center, AL 35812

pultruded composites under quasi-static indentation and subsequent damage tolerance under compression.

Instrumented impact and static indentation tests of graphite-epoxy composites, with comparisons based on damage width rather than damage area, have been reported [1] to show large scatter due to vibrations in the drop-weight crosshead absorbing significant energy. The influence of indentor size and laminate stacking sequence on the response of graphite-epoxy composites to contact loads and low velocity impact was investigated [2]. Some investigations [3-5] have shown that there is a correlation between quasi-static indentation and drop-weight impact testing, while some others [6, 7] have concluded that quasi-static indentation tests can not be used to simulate impact tests. More recently, it has been reported [8], on the basis of extensive experimentation with a carbon fiber reinforced epoxy composite, that static indentation can be used to represent a low-velocity impact event.

Considerable work has been done in the area of compressive strength of composite plates containing cutouts or prior impact damage. The use of hole strength data to predict impact damage strength has been questioned [9]. The compressive failure mechanisms of 45° ply dominated carbon epoxy laminates with circular holes or impact damage have been investigated [10]. Very limited information is available regarding impact damage, transverse indentation or compressive strength degradation due to cutouts/damage in pultruded composites. The low-velocity impact response of a complex geometry pultruded glass fiber reinforced polyester matrix composite box section has been studied [11].

Test Material

The material tested in this investigation was an E-glass fiber reinforced polyester pultruded composite. The composite consisted of layers of unidirectional roving fibers in the pultrusion direction sandwiched between layers of continuous strand mats (CSM). The pultruded composite is available in different thicknesses and in different shapes. In this investigation, pultruded sheets of 6.3 mm and 12.7 mm thicknesses were used to prepare all the specimens. The lay-up configuration and percentage of glass were slightly different for the two thicknesses. The 6.3 mm thick sheet had two roving fiber layers sandwiched between five CSM layers, while the 12.7 mm thick sheet had four roving layers sandwiched between nine CSM layers. Both sheets had approximately 60 percent by volume of glass; the 6.3 mm thick sheet had 58 percent of the glass in the form of CSM, while 64 percent of the glass in the 12.7 mm thick sheet was in the form of CSM. It may also be mentioned here that the outer layers of all the pultruded sheets were made of CSM.

Quasi-Static Transverse Indentation Test

This section describes the damage resistance part of the investigation. All the specimens were tested in the simply supported boundary condition in a test fixture that is commonly used for indentation tests [8].

Specimen Configuration

Plate specimens of 6.3 mm and 12.7 mm thicknesses were tested under transverse indentation. Specimens with a length of 152 mm and width of 102 mm were prepared from the 6.3 mm thick pultruded sheet and specimens with a length of 254 mm and width 178 mm were machined from the 12.7 mm thick pultruded sheet. A total of thirty specimens were prepared for each thickness.

Testing Procedure

The quasi-static indentation tests were performed on an 89 kN servo-hydraulic Tinius-Olsen testing machine. A square aluminum platen, 51 mm thick, with an outside dimension of 406 mm, was located on top of a 51 mm thick steel base plate. The composite specimens were placed on the aluminum platen, with a square cut-out, for the simply supported boundary condition on all four edges. The specimens with 6.3 mm thickness were loaded by a 19 mm diameter spherical steel indentor, on a supporting platen with a 51 mm square cut-out. The specimens with 12.7 mm thickness were loaded by a 38 mm diameter spherical steel indentor, on a supporting platen with a 102 mm square cut-out. Two direct current differential transformers (DCDTs) were used to measure the indentor movement and the central plate displacement directly under the indentor. The tests were conducted in a stroke control mode at a rate of 1.27 mm per minute. The load and the displacements were recorded using a data acquisition system.

Damage Evaluation

Four types of measurement were performed on each specimen after the quasi-static indentation test. These were: measurement of the permanent (or residual) dent depth, measurement of the back surface crack length, x-radiography photographs, and photomicrographs of sectioned surfaces. Dent depth measurements were made 24 hours after the indentation test, with a DCDT. The DCDT was traversed along the length and width directions across the dent and the data (maximum depth) were averaged. A digital caliper was used to measure the visible crack length on the back surface.

The x-radiography technique provides a through-thickness integrated view of delamination and matrix cracking. The specimens were soaked on both sides with a zinc iodide penetrant solution for 24 hours and were then x-rayed using a Faxitron™ x-ray machine. A piece of photographic film was placed directly under the specimen to capture the image of the internal damage in the form of a negative. Some specimens did not show any damage, especially at low force levels; in such cases, a small hole of 0.8 mm diameter was drilled near the damage area, the dye-penetrant was injected through a syringe into the hole and the specimen was x-rayed again. Prints from the negatives were viewed against a transparent grid with small squares and the damaged area was measured.

In the fourth damage evaluation method, quasi-statically loaded specimens were sectioned along the longitudinal and transverse directions and the sectioned specimens were examined under a stereo microscope with a camera attachment.

Repeatability Tests

As the study involved evaluation of damage in specimens transversely indented to different percentages of the failure load and the comparison of compressive behavior of specimens with different damage levels with specimens having circular holes, tests were conducted to establish the repeatability in pultruded composites. Four identical specimens of each thickness were tested under quasi-static indentation. Each specimen was loaded up to the maximum indentation force and was unloaded once the indentation force started dropping. The indentation force-central displacement curves for the 6.3 mm thick specimens and the 12.7 mm thick specimens are shown in Figs. 1 and 2, respectively.

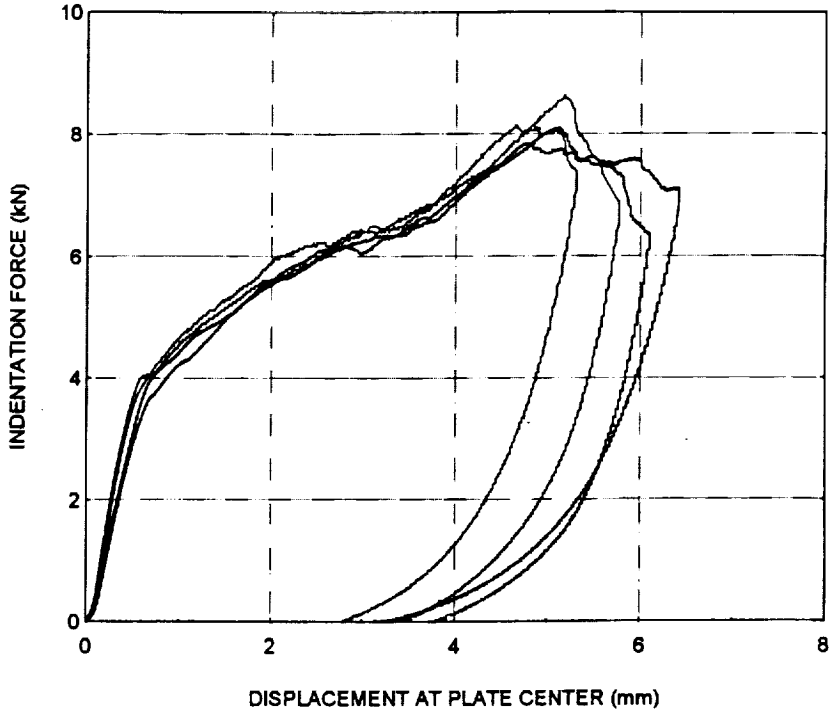

FIG. 1- *Indentation force as a function of the plate center displacement for the repeatability test (6.3 mm thick)*

These figures show that the indentation force-displacement curves are very close to each other for each thickness. The repeatability tests were also performed in terms of damage parameters, such as maximum deflection, back-surface crack length, energy absorption and damage area. These results are summarized in Table 1 for the 6.3 mm thick specimens and in Table 2 for the 12.7 mm thick specimens. These tables show that considering the inherent material variability in civil engineering infrastructure pultruded composites, the repeatability is good.

Tests for Damage Characterization and Tolerance

After the repeatability tests, damage resistance of the pultruded composite was investigated. Damage was introduced at various transverse indentation force levels, selected from the force-displacement curves up to failure. The selected load levels are

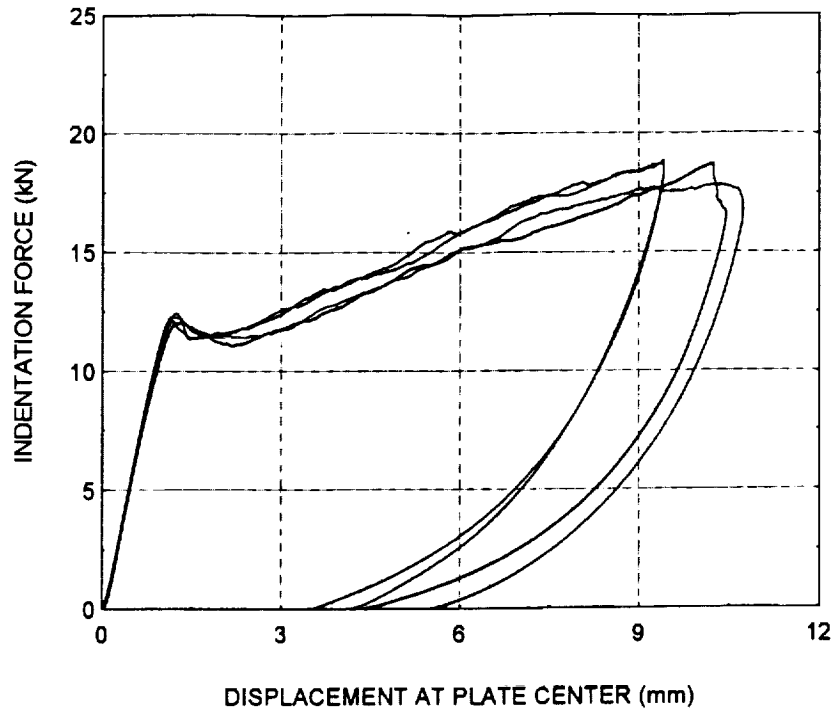

FIG. 2- *Indentation force as a function of the plate center displacement for the repeatability test (12.7 mm thick)*

TABLE 1 – *Summary of repeatability test results for the 6.3 mm thick specimens*

Specimen Number	Max. Deflection (mm)	Max. Indentation force (kN)	Damage area (cm^2)	Back surface crack length (mm)	Energy absorbed (N-m)
1	5.8	6.9	17.0	51.3	30.5
2	5.3	7.3	17.6	43.2	26.0
3	6.1	6.3	15.3	47.2	32.1
4	6.5	7.1	16.6	50.5	32.2

shown in Fig. 3 for the 6.3 mm thick composite and in Fig. 4 for the 12.7 mm thick composite. At each load level, five identical specimens were loaded and unloaded. The surface damage was measured for all the five specimens. Two specimens at each load level were sectioned along the longitudinal and transverse directions following the x-radiography examination. The rest of the specimens were reserved for the compression tests to characterize the damage tolerance.

TABLE 2 – *Summary of repeatability test results for the 12.7 mm thick specimens*

Specimen Number	Max. Deflection (mm)	Max. Indentation force (kN)	Damage area (cm^2)	Back surface crack length (mm)	Energy absorbed (N-m)
1	10.7	17.9	65.4	96.5	123.1
2	10.4	18.7	68.3	73.7	115.2
3	9.4	18.9	-	81.3	99.6
4	9.4	18.6	-	97.3	101.4

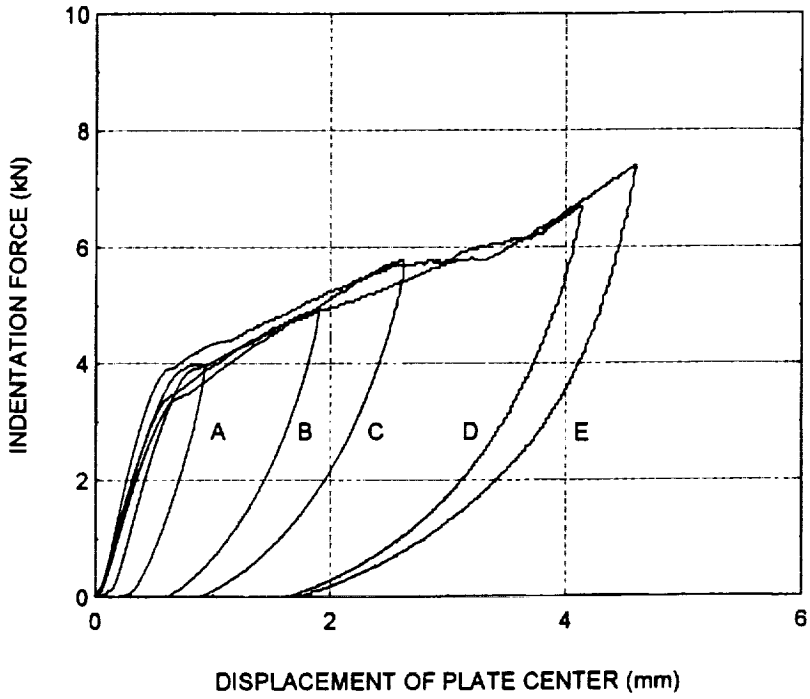

FIG. 3 – *Indentation force as a function of plate center displacement at various unloading stages for 6.3 mm thick specimen*

The back-surface crack was mostly in the form of an s-shaped crack, as shown in Fig. 5 for a 12.7 mm thick specimen. A typical x-radiograph showing the internal damage in a 12.7 mm thick specimen is shown in Fig. 6.

Compression Tests

This section describes the damage tolerance part of the investigation. Specimens with circular holes of different diameters were tested under compression in a compression fixture [12]. Specimens subjected to transverse indentation at different load levels were

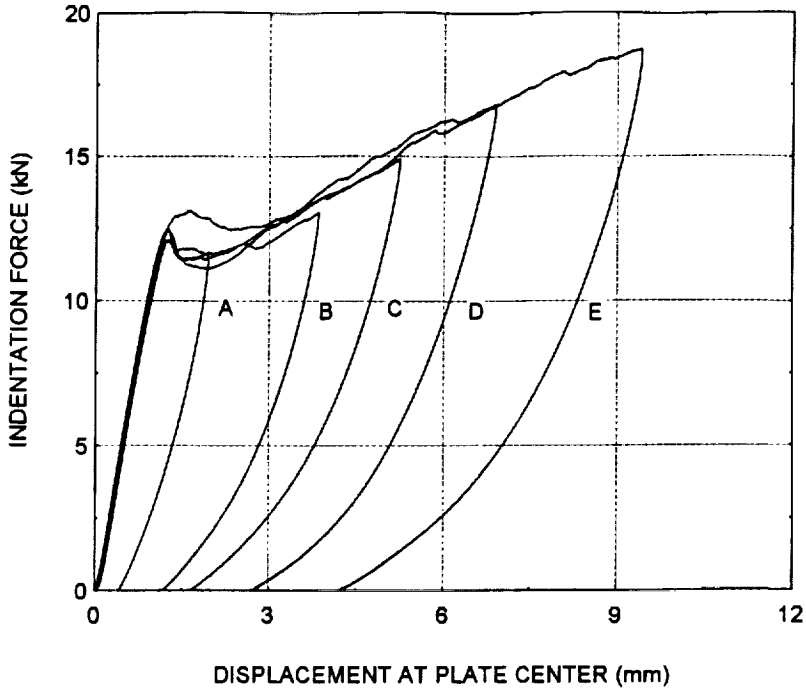

FIG. 4 – *Indentation force as a function of plate center displacement at various stages for 12.7 mm thick specimen*

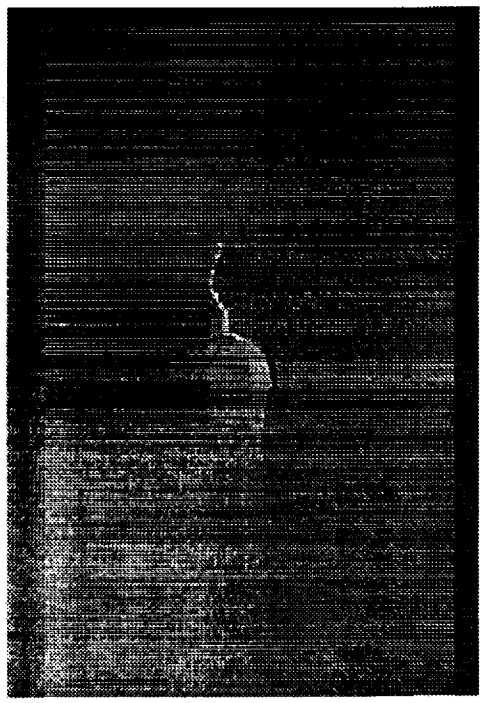

FIG. 5 – *Photograph showing back surface crack at static indentation load of 16.8 kN (12.7 mm thick)*

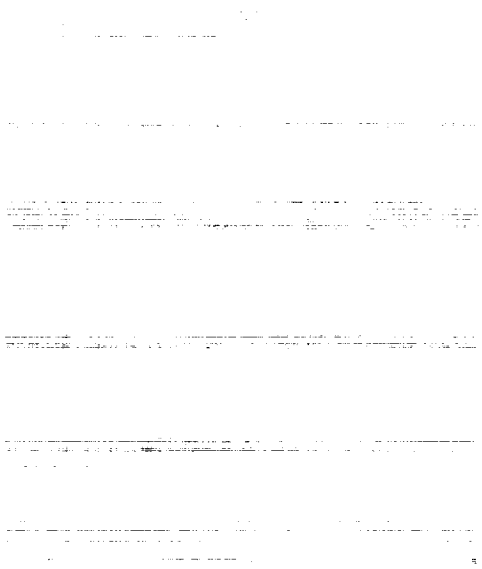

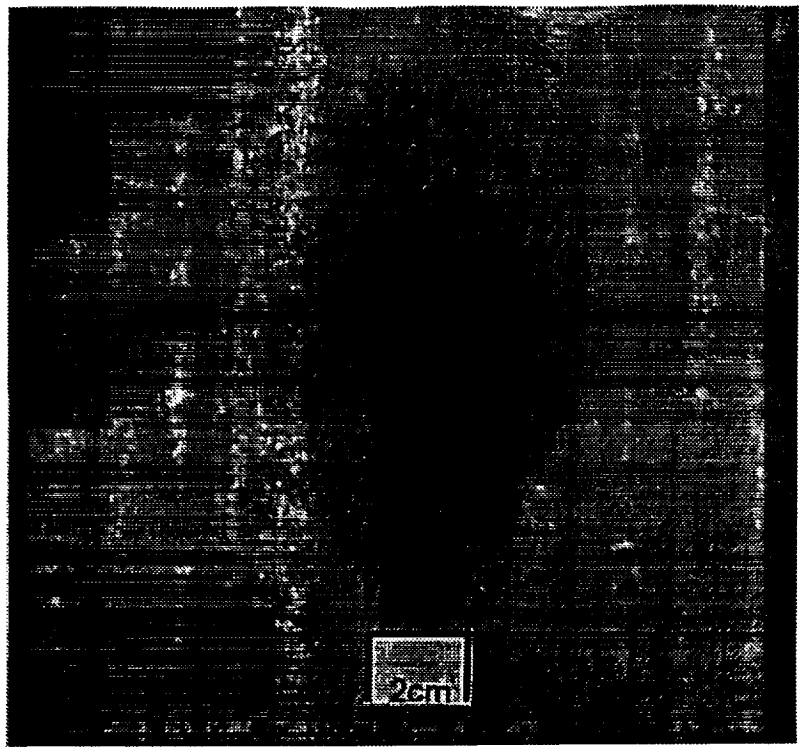

FIG. 6 - *Typical x-radiograph showing the internal damage due to quasi-static indentation loading up to failure (12.7 mm thick)*

also tested under compression. These results were compared to establish the concept of an 'equivalent hole diameter' for damaged specimens.

Specimen Configuration

The dimensions for the compression specimens, of both the thicknesses, were chosen so that a strength failure would more likely occur than a buckling mode failure. Specimens of 152 mm length and 102 mm width were prepared from the 6.3 mm thick pultruded composite sheet, while specimens of 254 mm length and 178 mm width were made from the 12.7 mm thick sheet. The length direction of all the specimens was oriented parallel to the pultrusion direction. A total of thirty specimens for each thickness were prepared. Circular holes of different diameters were machined in these specimens, to give a wide range of diameter to width ratios of 0.075 to 0.75. The holes were machined with special tools and by following careful procedures so as to minimize the influence of machining.

Some of the specimens were instrumented with strain gages. Back to back strain gages were used to minimize bending effects. Strain gages, away from the hole and along the specimen width, verified the uniformity of the compressive loading. In addition, strain gages on the inside surface of the holes captured strain concentrations, while strain gages along the width across the minimum cross section were used to record the strain gradients.

Testing Procedure

The end-gripped compression test fixture was used in this investigation. This fixture has two pairs of adjustable grips to accommodate specimens of different thicknesses. Two side fixtures with knife-edge restraints attached were placed along the specimen sides. Thus clamped boundary conditions were applied at the loaded ends, while simply supported boundary conditions on the sides prevented column buckling. All the compression specimens were loaded quasi-statistically using a Tinius Olsen 1.78 MN capacity hydraulic testing machine. During the tests, two DCDTs were used: one at the specimen center and oriented transverse to the specimen to measure the out-of-plane displacements (specimens with a hole had the DCDT offset) and one along the loading direction to measure the end shortening. The load, the DCDT signals and the strain gage data were all recorded using a data acquisition system. The specimens with prior indentation damage were also instrumented with strain gages and tested in compression following the same procedure.

Results

This section summarizes some of the important results from the damage resistance and damage tolerance tests.

Damage Resistance

As mentioned earlier, the damage parameters were assessed in terms of back surface crack length, damage area by x-radiography and photomicrographs after sectioning, at five load levels for each thickness. The average damage area as a function of the indentation force is shown in Fig. 7 for the 6.3 mm and 12.7 thick specimens. This figure shows a linear relationship between the damage area and the indentation force. The figure also shows that the thicker material withstands larger forces, with correspondingly larger damage areas. The back surface crack length is shown as a function of the indentation force in Fig. 8. It is clear that the back surface crack length and the damage area both increase as the indentation force increases.

Photomicrographs, taken at different load levels, of the longitudinal (along the pultrusion direction) and transverse sections through the center of the specimens showed the progressive failure mechanisms. At lower load levels (for instance 4 KN for the 6.3 mm thickness), there was no visible damage. At higher load levels, matrix cracks begin to form; then delamination between the roving and CSM layers on the tension side begins. Then extensive delamination spreads across the thickness, accompanied by fiber breakage in the roving layers. Extensive delamination and failure in the 6.3 mm thick specimen at the failure load are shown in Fig. 9.

Damage Tolerance

The damage tolerance of the pultruded composite was evaluated in terms of the compressive strength of specimens which were subjected to different levels of transverse indentation loading. The measured compressive strengths of these damaged specimens were compared with the compressive strength of similar specimens with a circular hole.

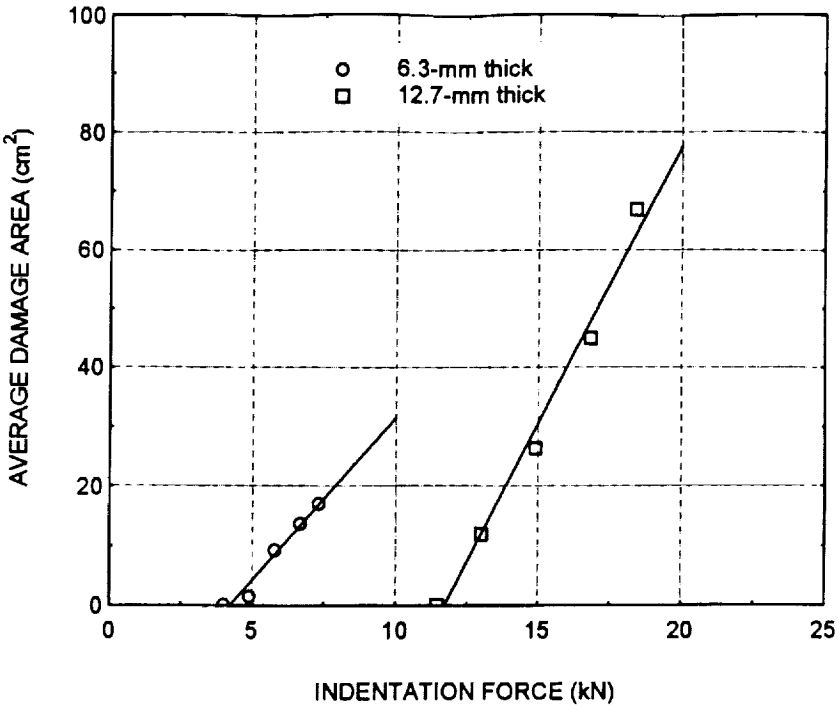

FIG. 7 – *Damage area as a function of indentation force*

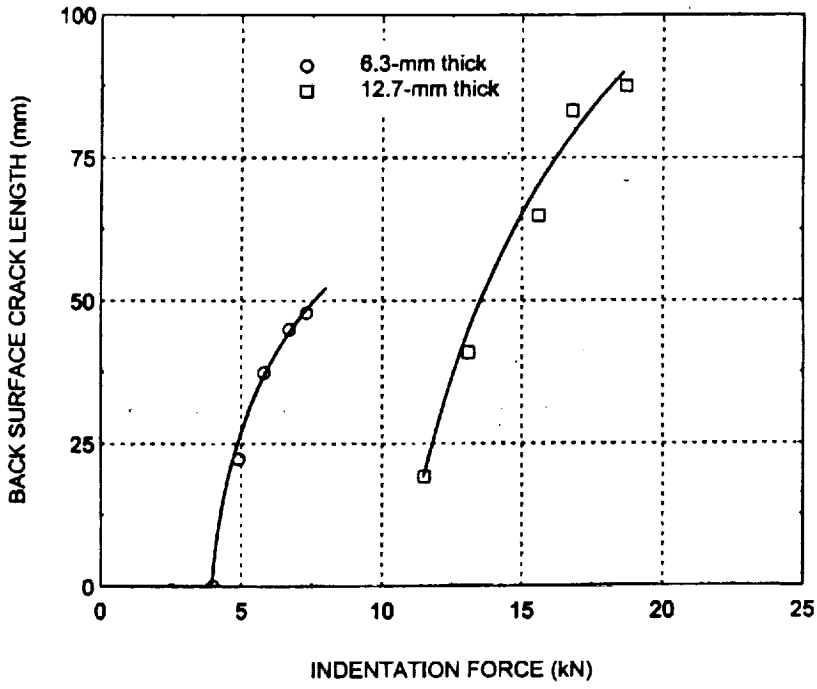

FIG. 8 – *Back surface crack length as a function of indentation force*

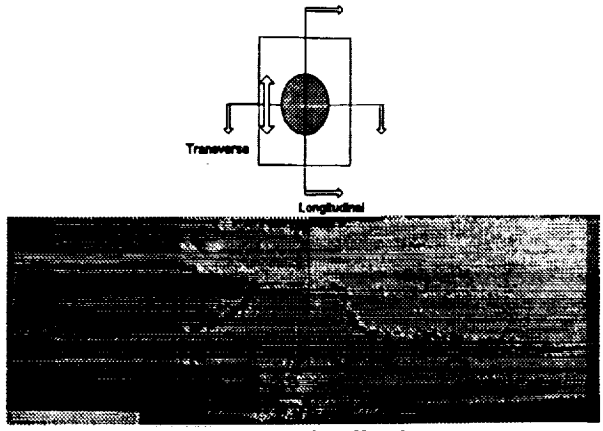

(a) Longitudinal

(b) Transverse

FIG. 9 - *Photomicrographs showing extensive delamination and fiber breakage at failure load of 7.3 kN (6.3 mm thick)*

Compression Strength of Specimens with Holes

The strength results for the compression specimens with holes of different diameters are summarized for the two thicknesses in Fig. 10. This figure shows the compression strength based on the net section; each point represents the average strength of at least three specimens. The 6.3 mm thick specimens exhibited higher compressive strengths compared to the 12.7 mm thick specimens, probably because of more internal flaws observable in the thicker material. As the ratio of hole diameter to specimen width increased, the differences between the two thicknesses became less significant. As explained later, this figure was used as a master curve to compare the damaged specimens with the specimens with circular holes to arrive at an 'equivalent hole diameter'.

As mentioned earlier, many of the compression specimens were instrumented with electrical resistance strain gages. The axial strain distribution in the vicinity of the hole for several hole sizes is shown in Fig. 11 for the 12.7 mm thick composite. Such plots provided information for determining the strain concentration factors as well as for comparison with the behavior of specimens with indentation damage.

Compression Strength of Specimens with Damage

Specimens of both thicknesses, damaged at different transverse indentation loads, were tested in subsequent compression. A number of these specimens were also instrumented with strain gages on both surfaces, to capture the strain gradients. The strain

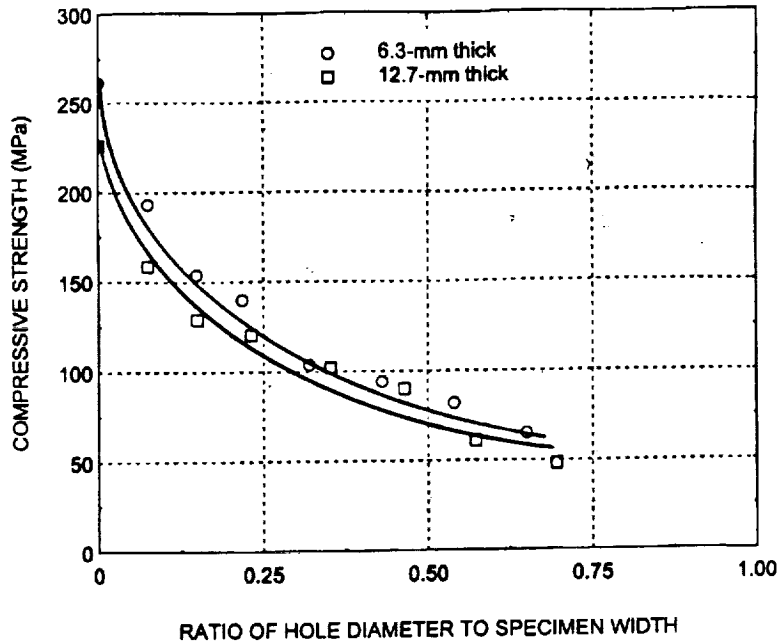

FIG. 10 – *Compressive strength as a function of the hole diameter to specimen width ratio for 6.3 mm and 12.7 mm thick plate specimens*

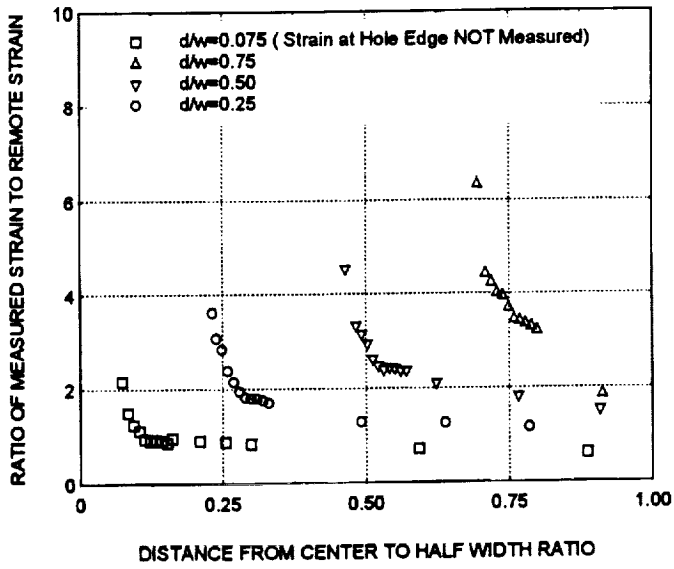

FIG. 11 – *Axial strain distribution in the vicinity of a hole for several hole diameters in 178 mm wide plate specimens of 12.7 mm thickness*

gages were located close to the damaged region. Typical strain variations for a 6.3 mm thick specimen at a prior indentation load of 7.3 kN are shown in Fig. 12. This figure

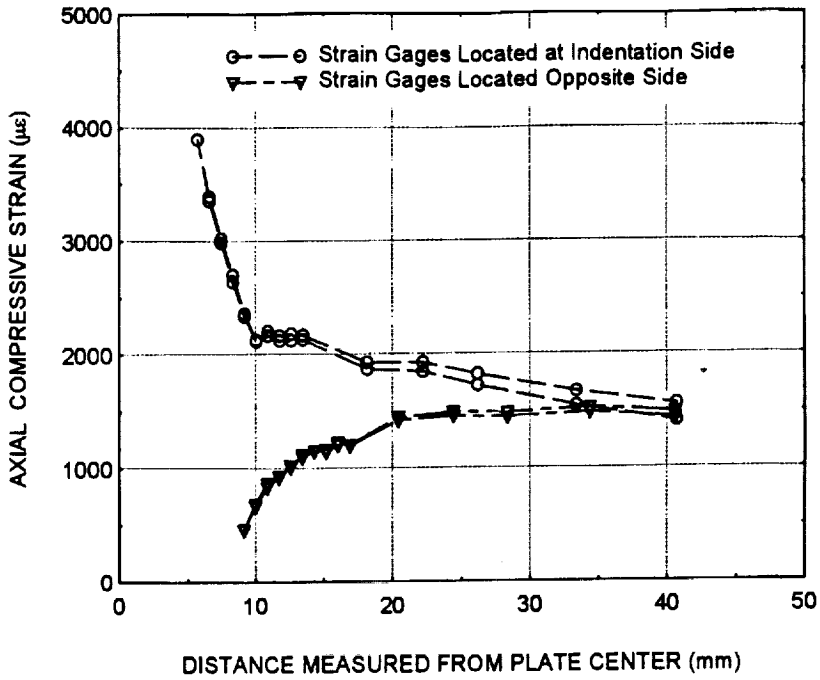

FIG. 12 – *Axial strain distribution in the vicinity of the damaged region for 6.3 mm thick plate specimen at a load of 7.3 kN*

shows the strain variations on the indentation side as well as the backside, for two different specimens. The measured strains for the two specimens agree very well. The figure shows that on the backside (where tension occurs during the transverse indentation) the strains increase away from the damage zone, while on the indentation side, there is a strain concentration due to the damage zone. It can also be noticed that the strains on both sides merge together away from the damage region.

The residual compressive strength (compression after damage) is shown as a function of the back surface crack length for both thicknesses in Fig. 13. It is interesting to note that the curve for the smaller thickness is above that for the larger thickness for relatively short back surface cracks but the two curves cross over around a 20 mm long crack. Earlier, in Fig. 10, it was shown that the thicker composite exhibited a compressive strength closer to that of the thinner composite for relatively larger holes. Thus the 12.7 mm thick composite appears to be more damage tolerant.

The residual compressive strength is shown as a function of the indentation force for both the thicknesses in Fig. 14. The corresponding undamaged compressive strength is also included in the figure. The figure shows that the damaged specimens did not show any degradation of compressive strength unless the threshold indentation force was exceeded. This threshold was 10 kN for the 12.7 mm thickness and about 4 kN for the 6.3 mm thickness.

The compression strength measured for the damaged specimens was used in conjunction with the compression strength of specimens with holes (Fig. 10) to arrive at

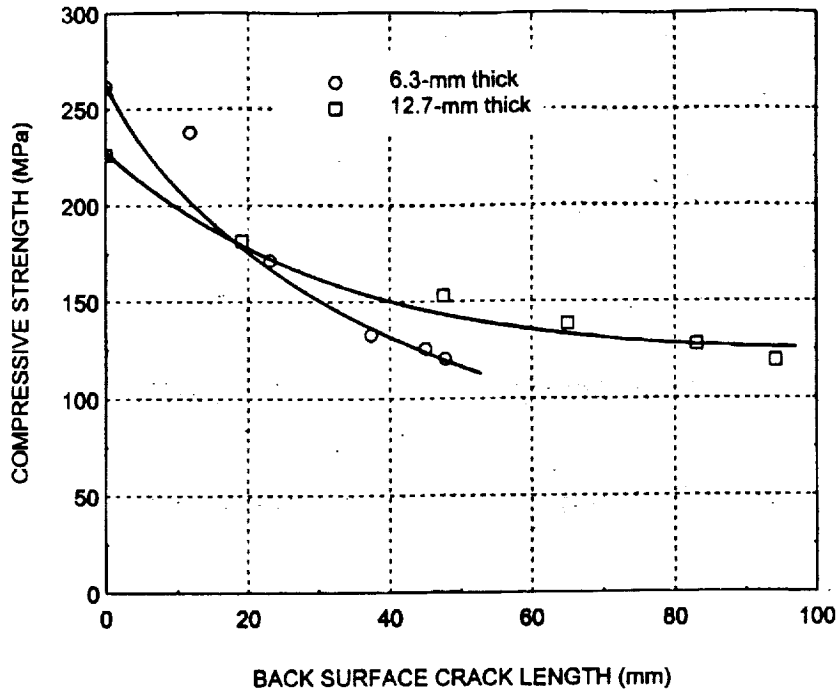

FIG. 13 – *Compressive strength as a function of back surface crack length*

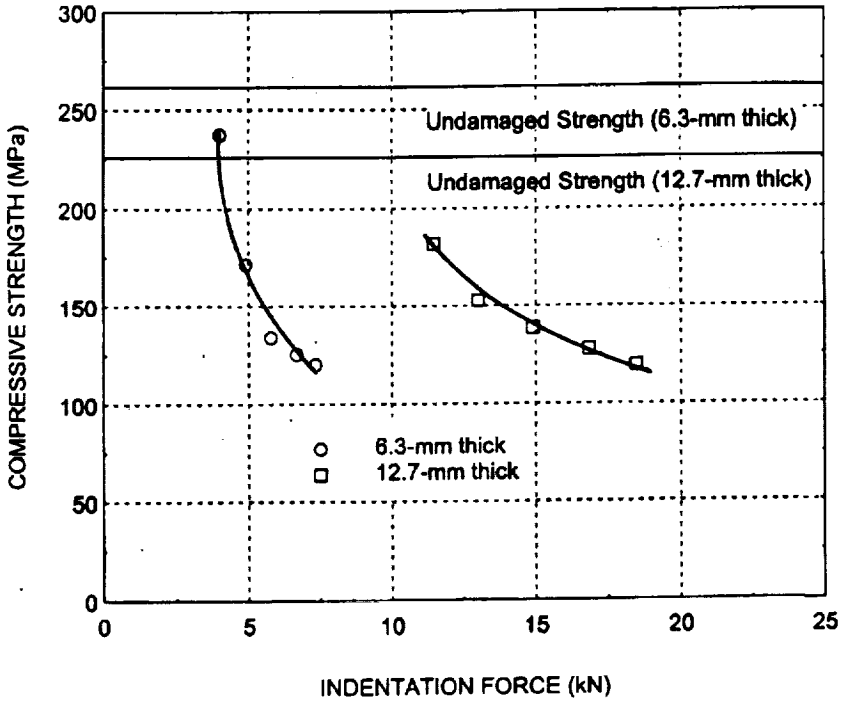

FIG. 14 – *Compressive strength as a function of indentation force*

an 'equivalent hole diameter'. Such an 'equivalent hole diameter', determined for the 6.3 mm and 12.7 mm thicknesses, is shown as a function of the back surface crack length in Fig. 15. Consistent with the results shown in Fig. 13, the 'equivalent hole diameter' for the smaller thickness materials is observed to be larger.

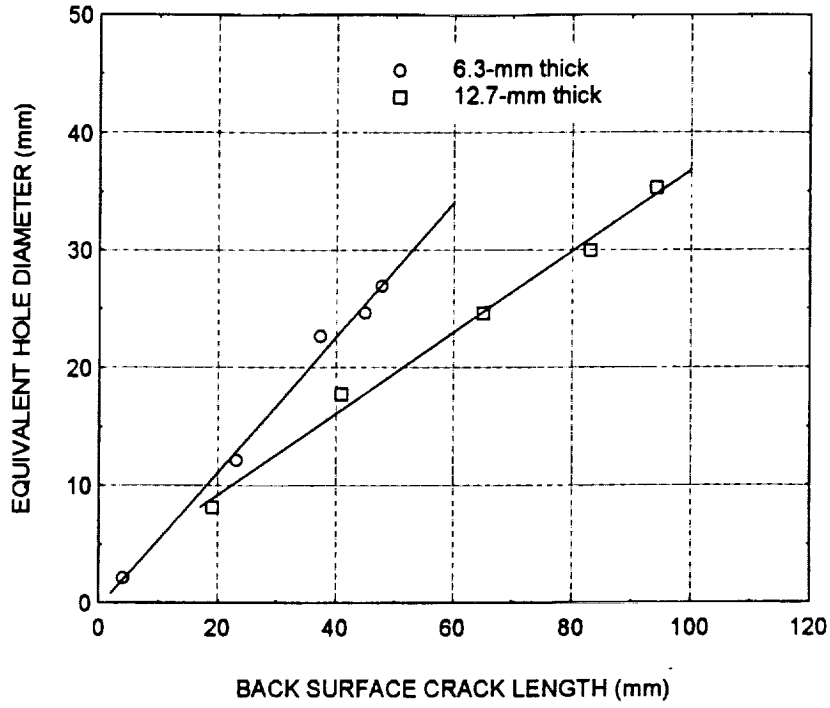

FIG. 15 – *Relationship between the equivalent hole diameter of the damaged specimens and the back surface crack length*

Finally, the variation of the 'equivalent hole diameter' with the damage size (measured from x-radiography images) is shown in Fig. 16 for the two materials. Again, it is seen that the 'equivalent hole diameter' for the smaller thickness composite is larger for a given damage size.

Conclusions

The damage resistance and damage tolerance behavior of a fiberglass-epoxy pultruded composite material, in two thicknesses, has been investigated. The damage parameters were determined from x-radiography, back surface crack length and cross-sectional photomicrographs, after different levels of transverse indentation loads. The repeatability of the experimental results was good, especially in view of the inherent material variability. It may be mentioned here that many investigators have tried, with varying degrees of success, to correlate the results from transverse indentation tests and from low velocity impact tests; most of these investigations have involved aerospace composites containing carbon fibers.

The second phase of this investigation parallel the compression after impact (CAI) studies aerospace composites. Specimens with damage caused by different levels

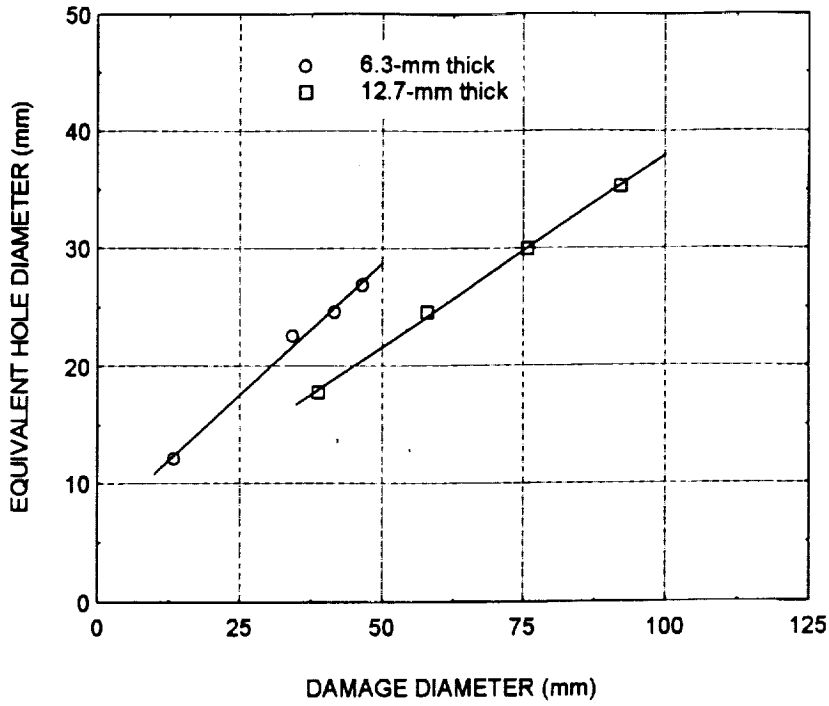

FIG. 16 – *Relationship between the equivalent hole diameter of the damaged specimens and the average damage diameter*

of transverse indentation force were subjected to compression. The compressive strengths and the strain distributions were compared with the corresponding characteristics of specimens with circular holes. Based on this comparison, 'equivalent hole diameters' were determined for some of the damage parameters such as the back surface crack length and the damage area (given by x-radiography).

Acknowledgement

This work was supported by NASA grant number CA NCC-1-389.

References

[1] Lee, S. M. and Zahuta, P., "Instrumented Impact and Static Indentation of Composites," *Journal of Composite Materials*, Vol. 25, 1991, pp. 204-222.

[2] Wu, E. and Shyu, K., "Response of Composite Laminates to Contact Loads and Relationship to Low-Velocity Impact," *Journal of Composite Materials*, Vol. 27, 1993, pp.1443-1464.

[3] Jackson, W. C. and Poe, C. C., "The Use of Impact Force as a Scale Parameter for the Impact Response of Composite Laminates," NASA Technical Memorandum 104189, 1992.

[4] Kaczmarek, H. and Maison, S., "Comparative Ultrasonic Analysis of Damage in CFRP Under Static Indentation and Low-Velocity Impact," *Composites Science and Technology*, Vol. 51, 1994, pp. 11-26.

[5] Sjoblom, P. O., Hartness, T. J. and Cordell, T. M., "On Low-Velocity Impact Testing of Composite Materials," *Journal of Composite Materials*, Vol. 22, 1988, pp. 30-52.

[6] Lagace, P. A., Williamson, J. E., Wilson Tsang P. H., Wolf, E. and Thomas, S., "A Preliminary Proposition for a Test Method to Measure (Impact) Damage Resistance," *Journal of Reinforced Plastics and Composites*, Vol. 12, 1993, pp. 584-601.

[7] Highsmith, A. L., "A Sudy of the Use of Contact Loading to Simulate Low-Velocity Impact," NASA Contractor Report 97-206121, 1997.

[8] Nettles, A. and Douglas, M. J., "A Comparison of Quasi-Static Indentation to Low-Velocity Impact," NASA Technical Publication 2000-210481, 2000.

[9] Starnes, J. H., Jr., Rhodes, M. D. and Williams, J. G., "Effect of Impact Damage and Holes on the Compressive Strength of a Graphite/Epoxy Laminate," *Nondestructive Evaluation and Flow Criticality for Composite Materials*, ASTM STP 696, American Society for Testing and Materials, 1979, pp. 145-171.

[10] Shuart, M. J. and Williams, J. G., "Compression Behavior of 45° Dominated Laminates with a Circular Hole or Impact Damage," *AIAA Journal*, Vol. 24, 1986, pp. 115-122.

[11] Wisheart, M. and Richardson, M. O. W., "Low Velocity Response of a Complex Geometry Pultruded Glass/Polyester Composite," *Journal of Materials Science*, Vol. 34, 1999, pp. 1107-1116.

[12] Saha, M., "Elastic Properties, Strength and Damage Tolerance of Pultruded Composites," Ph.D. Dissertation, Department of Mechanical Engineering, Old Dominion University, Norfolk, 2001.